R-05-09

Äspö Pillar Stability Experiment

Acoustic emission and ultrasonic monitoring

Jon Haycox, Will Pettitt, R Paul Young
Applied Seismology Consultants Ltd

November 2005

Svensk Kärnbränslehantering AB
Swedish Nuclear Fuel
and Waste Management Co
Box 5864
SE-102 40 Stockholm Sweden
Tel 08-459 84 00
+46 8 459 84 00
Fax 08-661 57 19
+46 8 661 57 19

ISSN 1402-3091
SKB Rapport R-05-09

Äspö Pillar Stability Experiment

Acoustic emission and ultrasonic monitoring

Jon Haycox, Will Pettitt, R Paul Young
Applied Seismology Consultants Ltd

November 2005

Keywords: Deposition hole, Excavation, Confinement, Heating.

Executive summary

This report describes the results from acoustic emission (AE) and ultrasonic monitoring of the Äspö Pillar Stability Experiment (APSE) at SKB's Hard Rock Laboratory (HRL), Sweden. The APSE is being undertaken to demonstrate the current capability to predict spalling in a fractured rock mass using numerical modelling techniques, and to demonstrate the effect of backfill and confining pressure on the propagation of micro-cracks in rock adjacent to deposition holes within a repository /Andersson 2002/. An ultrasonic acquisition system installed by Applied Seismology Consultants Ltd (ASC) has provided acoustic emission and ultrasonic survey monitoring throughout the various phases of the experiment. Results from the entire data set are provided with this document so that they can be effectively compared to several numerical modelling studies, and to mechanical and thermal measurements conducted around the pillar volume, in an 'integrated analysis' performed by SKB staff. This document provides an in-depth summary of the AE and ultrasonic survey results for future reference.

The pillar has been produced by excavating two 1.8 m diameter deposition holes 1 m apart. These were bored in 0.8 m steps using a Tunnel Boring Machine (TBM) specially adapted for vertical drilling. The first deposition hole, DQ0066G01, was drilled in December 2003. Preceding this a period of background monitoring was performed so as to obtain a datum for the results. The hole was then confined to 0.7 MPa internal over pressure using a specially designed water-filled bladder. The second deposition hole, DQ0063G01, was excavated in March 2004. Heating of the pillar was performed over a two month period between ending in July 2004, when the confined deposition hole was slowly depressurised. Immediately after depressurisation the pillar was allowed to cool with cessation of monitoring occurring a month later.

At the request of SKB staff this report does not include a summary of the data after July 14th 2004, from the start of depressurisation.

Ultrasonic velocities measured prior to the excavation of the deposition holes give a mean P-wave velocity of 6,051 m.s^{-1}, and mean S-wave velocity of 3,394 m.s^{-1}, in a weakly (1.5%) transversely isotropic rock mass. This has a fast direction orthogonal to the tunnel direction (north west to south east and around to the vertical). The slow velocity direction is thus parallel to the tunnel, orthogonal to the major fracture set and maximum principal stress direction. Ultrasonic velocity surveys were undertaken regularly during the whole of the APSE. Velocity and amplitude results, for every raypath that could be processed, are provided with this document. These include 54 separate P-wave velocity measurements and 23 S-wave velocity measurements on 350 surveys conducted over the monitoring period.

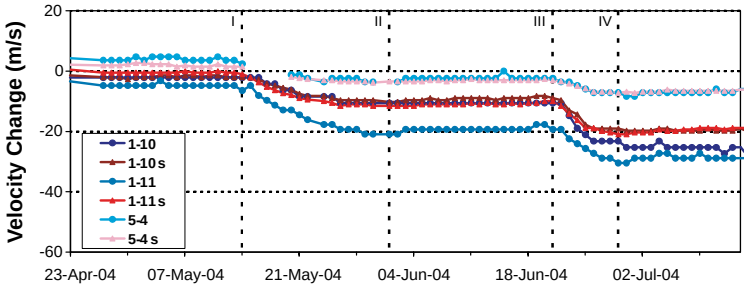

Velocity change graph for a selection of raypaths passing through the centre of the pillar. Markers I to IV represent times when the heater power settings were changed. I and III are times when power was increased.

Skimming ray paths, that pass through excavation damage close to the deposition holes (as imaged by the AE results), often show a significant decrease in velocity during excavation of between 5 to 30 $m.s^{-1}$. Some ray paths also exhibit an increase in velocity of approximately 10 $m.s^{-1}$ over the days following excavation. An increase could be the result of increasing stresses in some volumes of the rock mass acting to close microfractures (the ray paths also pass through the induced zones of high compressive-stress). The velocity increases may counteract any decreases in velocity caused by new fracturing and result in a net increase. During the heating phase there is often a clear decrease in velocity in two stages that correlates very well with the AE activity and known changes in the thermal output of the heaters. Ray paths that travel through the centre of the pillar show a similar response, although of lower magnitude. The velocity decreases could be related to a desaturation of the rock mass, new fracture growth or expansive stresses causing an opening of pre-existing fractures. The latter is unlikely as modelled increasing compressive stresses will act to close preferentially-orientated fractures.

A total of 36,676 AE triggers were recorded over the reporting period between 13th October 2003 and 14th July 2004. Of these 15,198 have produced AE locations. The AE data set shows an intense clustering of events located along the length of the deposition holes to approximately 1 m from their floors. Clustering of events is primarily contained in a damage zone orthogonal to the maximum principal stress, represented by a semi-circle of tightly packed AEs extending from the edge of each hole approximately 20 cm into the pillar. Very few events are situated in the centre of the pillar, although clusters of events occur in the top metre of the pillar volume in two sub horizontal features that cross the pillar. The uppermost feature is believed to be associated with the rock floor of the tunnel, beneath the concrete roadbed, and the lowermost feature is associated with a mapped shear zone.

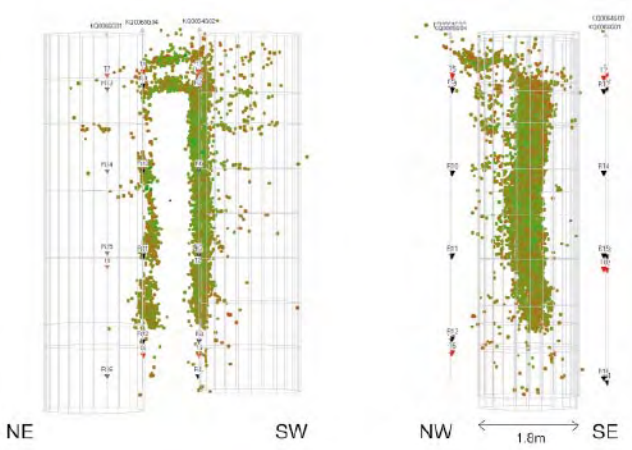

Projections of all AEs located during the APSE. Events are scaled to instrument magnitude.

Plan view of AEs located beneath 446.9m (1m below the tunnelfloor).

Plan view of all AEs.

Acquisition system triggers, channel hit counts and processed locations all show a consistent temporal distribution for the AE activity. During background monitoring, preceding excavation of the first deposition hole, no activity was recorded. Excavation of the two deposition holes produces increased activity. This is much larger for the second deposition hole when the pillar is formed. The activity decays away after excavation over approximately two weeks. Heating of the pillar causes increased activity occurring in two sets between May and July 2004. The sets of activity correspond to two heating periods; the second period being caused by an increase in thermal output by the heaters used.

The clustering of AE locations is observed to migrate along the pillar walls of the two deposition holes during the various phases of the experiment. During excavation of DQ0066G01, the largest amount of activity occurs in a cluster at 3.6 m depth, which qualitatively correlates with spalling observed in the deposition hole. The cluster occurs 1.2 m behind the advancing deposition-hole face and is probably a result of increasing stresses in a weaker part of the rock mass during deeper excavation. During excavation of DQ0063G01, a zone of intense AE activity occurs, extending from close to the top of the deposition hole. and migrating down the hole to a depth of approximately 2.5 m. The highest event rates are observed after excavation is completed. The AE activity correlates well with a zone of breakout damage observed in the open hole after excavation. Similar amounts of high activity are not observed in the confined deposition hole during this phase, suggesting the confinement pressure applied here is sufficient to inhibit breakout occurring.

During heating of the pillar a consistent lag of a few days (3–4) is observed between the heaters being adjusted and when the rock responds to the adjustment. The events initially cluster in previously active regions down the open deposition hole, DQ0063G01. As the temperature increases this cluster grows larger, extending upward to the rock floor of the tunnel and then migrating downward reaching a depth of approximately 5 m below the tunnel floor.

Sammanfattning

Denna rapport beskriver resultaten från den akustiska (AE) och ultraljudsmonitering som gjordes för Äspö Pillar Stability Experiment (APSE) vid SKB:s anläggning Äspö Hard Rock Laboratory. APSE genomfördes för att demonstrera den nuvarande förmågan att med numeriska metoder prediktera spjälkning i en sprucken bergmassa samt för att demonstrera effekten av backfill och dess mothållande tryck på propageringen av mikrosprickor i det berg som ligger i omedelbar närhet till deponeringshålen i ett djupförvar /Andersson 2002/. Ett ultraljudssystem installerat av Applied Seismology Consultants Ltd (ASC) har använts för att inhämta akustisk data och göra ultraljudsmätningar under experimentets olika faser. Det kompletta data setet med resultaten från mätningarna har levererats till SKB. Resultaten används för att göra jämförelser med numeriska modellresultat samt mekaniska och termiska mätningar gjorda i pelarvolymen under experimentets gång. Denna integrerade analys kommer att genomföras av SKB personal. Detta dokument innehåller en utförlig sammanfattning av de akustiska mätningarna och ultraljudsmätningar för att kunna användas som referensmaterial när resultaten beskrivs.

Pelaren har skapats genom att borra två stora borrhål med diametern 1,8 m så att avståndet mellan hålkanterna blev 1 m. Hålen borrades med en tunnelborrmaskin (TBM) som specialbyggts för vertikal borrning. Maskinen borrade i omgångar om 0,8 m innan omtag behövde göras. Det första hålet DQ0066G01 borrades i december 2003. Innan borrningen startade hade akustiska mätningar genomförts för att erhålla områdets bakgrundsnivå innan berget ytterligare störtes med borrningen. Det färdigborrade hålet trycksattes sedan med ett inre övertryck om 0,7 MPa genom en specialutvecklad gummiblåsa. Det andra stora borrhålet, DQ0063G01, borrades i mars 2004. Pelaren instrumenterades sedan och värmdes under en tidsperiod av cirka två månader. I slutet på värmningsfasen, i juli 2004, släpptes sakta det inre trycket i det trycksatta borrhålet. Ett tag efter att trycksänkningen genomförts fick pelaren svalna och moniteringen avbröts efter en månad då den akustiska aktiviteten klingat av.

På begäran från SKB innehåller denna rapport inte en sammanfattning av resultaten efter den 14 juli 2004 vilket var tidpunkten då trycksänkningen startade.

Ultraljudets gångtider före borrningen av hålen gav en medelhastighet för P-vågen på 6 050 m/s, och en medelhastighet för S-vågen på 3 394 m/s i en något (1,5 %) isotrop bergmassa. Isotropin innebar snabbare gånghastigheter vinkelrätt mot tunnelaxeln (nordväst till sydost). Den långsammare gånghastigheten är följaktligen parallell med tunnelriktningen vilket blir vinkelrätt mot dominerande sprickset samt riktningen på den största huvudspänningen. Gångtider för ultraljud gjordes regelbundet under hela APSE:s experimenttid.

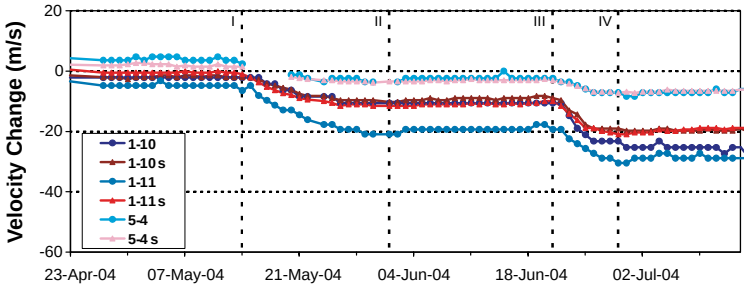

Förändringar i gånghastighet för ett urval av gångvägar som alla passerar genom pelarcentrum. Markeringarna I till IV representerar tidpunkter då effekten till värmarna ändrades. I och III är tidpunkter då effekten ökades.

Hastigheter och amplituder för varje gångväg som var möjlig att analysera är bilagd detta dokument. Detta inkluderar 54 enskilda P-vågshastigheter och 23 S-vågshastigheter på 350 gjorda undersökningar under mätperioden.

Gångvägar som går tätt förbi hålväggarna och passerar genom den störda zonen nära borrhålen (definierad av AE resultat) visar ofta en signifikant lägre gånghastighet, i storleksordningen 5 till 30 m/s, när borrningen skedde. Vissa gångvägar visar även en höjning av gånghastigheten på cirka 10 m/s dagarna efter borrningen. Ökningen kan bero på ökade spänningar i vissa bergvolymer som stänger mikrosprickor (vissa gångvägarna passerar genom områden där stora tryckspänningar skapats). Hastighetsökningarna kan motverka varje reduktion av hastigheten som beror på ny sprickbildning i dessa delar och endast en resulterande nettohöjning uppmäts därför. Under värmningsfasen kunde ofta en klar minskning i hastigheten ses i två skeden som väl kan korreleras med AE aktivitet och förändringar i värmarnas effekt. Gångvägar som går igenom pelarens centrum visar likartade förändringar som dock inte är lika stora. Minskningarna av hastigheten kan bero på uttorkning av bergmassan, bildandet av nya sprickor eller belastningar som öppnar befintliga sprickor. Det senare är osannolikt eftersom de modellerade tryckkrafterna verkar för att stänga dessa sprickor.

Denna rapport sammanfattar tidpunkten mellan 13 oktober och 14 juli, 2004. Under denna tid registrerades totalt 36 676 AE händelser, för 15 198 av dessa har händelsens läge kunnat beräknas. Datasetet visar ett tätt kluster av AE-händelser utefter borrhålens väggar som slutar cirka 1 m över borrhålens botten. Klustret är huvudsakligen belägna i en zon som är vinkelrät mot riktningen på den största huvudspänningen. Detta representeras av tätt packade AE händelser som går från hålkanten och cirka 20 cm in i pelaren. Endast ett fåtal händelser är belägna i pelarens centrum med undantag av pelarens översta meter. Kluster av händelser registrerades där i två subhorisontella band som korsar pelaren. Det övre av dessa band är troligen associerad med tunnelsulan och den undre med den karterade skjuvzonen.

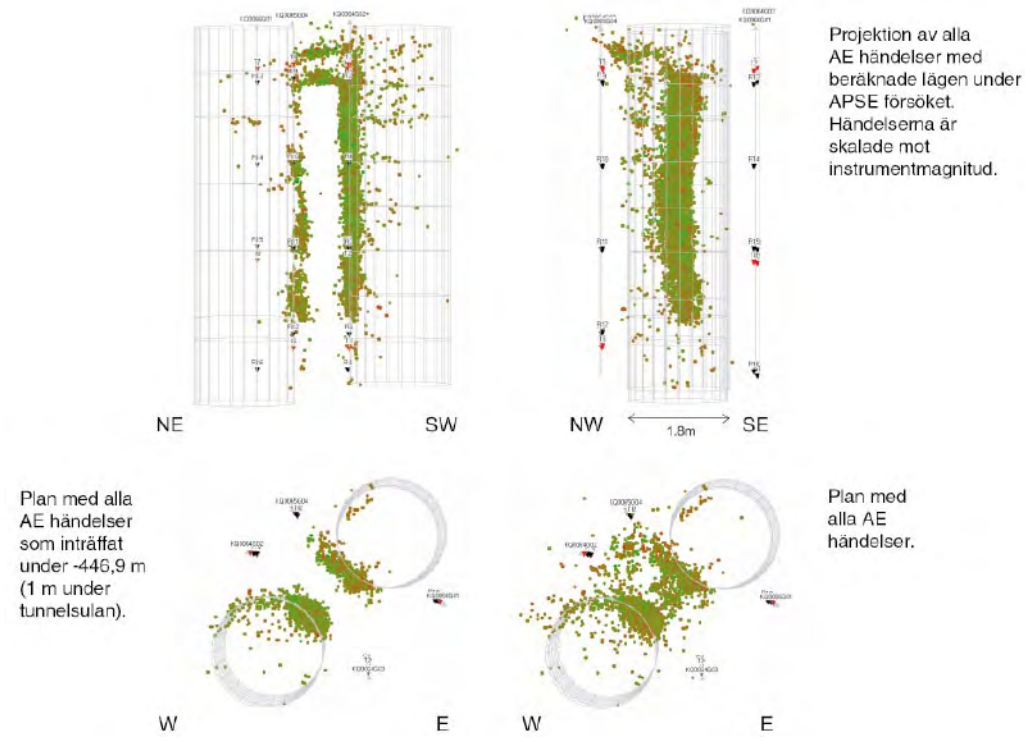

Projektion av alla AE händelser med beräknade lägen under APSE försöket. Händelserna är skalade mot instrumentmagnitud.

Plan med alla AE händelser som inträffat under -446,9 m (1 m under tunnelsulan).

Plan med alla AE händelser.

Triggningar i insamlingssystemet, antalet händelser per kanal och de beräknade lägena visar alla en överensstämmande fördelning av AE händelserna. Under moniteringen av bakgrundsnivån före borrningen av det första hålet hände i princip inget. Borrningen av de två stora borrhålen ökade frekvensen för uppmätta AE händelser. Frekvensen blev mycket högre när det andra hålet som skapade pelaren borrades. AE aktiviteten dog bort under en tvåveckorsperiod efter att borrningen slutförts. Värmningen av pelaren ökade AE aktiviteten i två omgångar mellan maj och juli 2004. Omgångarna är relaterade till starten av värmningen samt då effekten till dem ökades.

Klustren av AE händelser migrerar utefter pelarväggarna i de två deponeringshålen under experimentets olika faser. Vid borrningen av DQ0066G01 skedde den huvudsakliga delen av aktiviteterna i ett kloster vid 3,6 m djup. Detta kluster kunde korreleras till ett område där spjälkning skett. Klustret inträffade då borrningen kommit cirka 1,2 m nedanför det område som spjälkades och är troligen ett resultat av ökande spänningar i en försvagad del av bergmassan då borrningen fortskrider. Under borrningen av det andra hålet, DQ0063G01, bildades en zon med intensiv AE aktivitet. Zonen startade nära toppen av hålet och sträckte sig ned till ett ungefärligt djup av 2,5 m. Frekvensen av uppmätta AE var störst när borrningen slutförts. AE händelserna kan väl korreleras med ett spjälkat område som kunde ses i hålet då borrmaskinen tagits bort. Liknande händelser med hög frekvens av AE aktiviteter observerades inte i det trycksatta hålet. Detta indikerar att det applicerade mothållande trycket var tillräckligt för att hindra att spjälkning skulle initieras.

Vid värmningsfasen uppträdde en tidsförskjutning om tre till fyra dagar mellan de tidpunkter då effekten till värmarna ökades och då AE frekvensen ökade. Händelserna sker initiellt i kluster belägna i redan aktiva regioner i det öppna hålet, DQ0063G01. När temperaturen ökar växer klustren och går först upp mot tunnelsulan för att sedan vända nedåt och nå ett slutligt djup cirka 5 m under sulan.

Contents

1 Introduction

This report describes the results from acoustic emission (AE) and ultrasonic monitoring of the Äspö Pillar Stability Experiment (APSE) at SKB's Hard Rock Laboratory (HRL), Sweden. The APSE is being undertaken to demonstrate the current capability to predict spalling in a fractured rock mass using numerical modelling techniques. It is also designed to demonstrate the effect of backfill and confining pressure (up to 0.7 MPa) on the propagation of micro-cracks in rock adjacent to deposition holes within a repository /Andersson 2002/.

In order to realise these objectives a pillar of rock between two deposition holes has been monitored using an array of ultrasonic transducers. The array geometry (see Section 3.2) has been designed to be sensitive to Acoustic Emissions (AEs) occurring within the pillar volume and to provide ultrasonic surveys with ray paths passing through critical regions of the rock mass. By monitoring for AE activity and undertaking regular, repeated velocity surveys the response of the rock pillar to excavation, heating and variations in confinement pressure can be assessed.

For the purposes of this report, the experiment has been split into four phases described in Table 1-1. In October 2003 an ultrasonic array was installed around the future pillar volume and a high-frequency data acquisition system was connected. The array transducers and installation frames were specially designed for the experiment by Applied Seismology Consultants (ASC) and purchased by SKB. Background monitoring occurred until December 2003 when the first of two 1.8 m-diameter deposition holes were excavated. Confinement of this deposition hole was undertaken in February 2004 using a specially designed bladder pressurised to 0.7 MPa. In March 2004 a second deposition hole was excavated creating a 1 m wide pillar between the two holes (Phase 2). During this period an engineer from ASC was on site to start acquisition immediately after each excavation step, and monitor during an observed quiet period, so as to provide an immediate feedback to SKB staff on the stability of the pillar during this critical stage of the experiment.

The deposition hole was left 'open' after excavation and instrumented with displacement and temperature sensors by SKB. Pillar heating started in May 2004 (Phase 3) and continued for two months until mid July. Confinement removal and cooling occurred in the final phase of the experiment with acquisition ceasing on 16th August 2004. ASC's InSite software has been used underground throughout the experiment to automatically archive the acquired waveform data, and visualise it for data quality purposes. In March 2004 the software was also configured for online processing to provide real-time preliminary AE locations, so as to provide a feedback process to SKB staff on the stability of the pillar during the heating phase.

The entire data set has been collated by ASC and processed for final AE locations and ultrasonic velocity measurements. These results are provided with this document so that they can be effectively compared to results obtained from several numerical modelling studies, and to mechanical and thermal measurements conducted around the pillar volume, in an 'integrated analysis' performed by SKB staff. This document is restricted to presentation of the AE and ultrasonic survey results only up to July 14th 2004. Data from the final phase of the experiment (Phase 4) is to be presented by SKB staff and is not presented in this report.

Table 1-1. Phases in the Pillar Stability Experiment. DQ0066G01 and DQ0063G01 are the two deposition holes. The 'pillar' is the volume between the two holes.

Phase	Name	Description	Dates
1	Background monitoring, DQ0066G01 Excavation and DQ0066G01 Confinement	The first deposition hole was excavated using a Tunnel Boring Machine (TBM) converted to vertical drilling. The deposition hole was excavated in nine 0.8 m steps. No dedicated quiet periods for AE monitoring were performed. The deposition hole is pressurised using a specially constructed bladder filling the hole. Approximately 0.7 MPa of confining pressure is applied.	13 October 2003 to 2 March 2004
2	DQ0063G01 Excavation	The second deposition hole was excavated using a similar method to the first. Dedicated quiet periods were used in AE monitoring.	3 March 2004 to 13 May 2004
3	Pillar Heating	The pillar between the two deposition holes was heated over a period of 2 months.	14 May 2004 to 13 July 2004
4	DQ0066G01 Confinement Removal and Cooling	The confining pressure in the first deposition hole was removed, by de-pressurising the installed bladder, and the pillar was allowed to cool.	14 July 2004 to 16 August 2004

2 Experiment objectives

In a waste repository, vertical, 8 m deep 1.8 m diameter, boreholes will be required to hold copper canisters containing spent nuclear waste. The formation of approximately 4,500 rock mass pillars will be required. SKB is conducting the APSE to 1) demonstrate the current capability to predict brittle failure (spalling) in a fractured rock mass, 2) demonstrate the effect of backfill (confining pressure) on the brittle failure response, and 3) compare the 2D and 3D mechanical and thermal predicting capabilities of existing numerical models /Andersson et al. 2004/.

The rock mass studied in this experiment is a 1 m thick pillar between two vertical boreholes. The design of the pillar has been carefully considered so as to provide a controlled spalling of the rock mass in the damaged zone around the deposition hole. Acoustic emission (AE) and ultrasonic monitoring of the APSE has been conducted in the period 13th October 2003 to 16th August 2004. Data presented in this report detail the results in the first three phases of the experiment (prior to depressurisation) between 13th October 2003 and 14th July 2004.

- Monitor the background AE activity within the deposition hole volume prior to excavation, and perform ultrasonic surveys so as to determine the background ultrasonic velocity in the volume.
- Monitor AE activity after cessation of excavation of each deposition hole step and for a period after completion of each deposition hole. Accurately locate AEs so as to delineate the spatial and temporal extent of brittle microcraking within the rock mass of the pillar and the effect of excavation on pre-existing macroscopic fractures.
- Conduct regular ultrasonic surveys during the excavation period so as to observe the ultrasonic response of the rock mass around the deposition hole as excavation commences. In particular use ray paths that skim the perimeter of the deposition hole so as to have a sensitive measure of the response within the immediate rock mass.
- Analyse the effect of confining pressure on the rock mass around deposition hole DQ0066G01.
- Monitor AE activity and ultrasonic velocities during heating of the pillar.

3 Methodology

3.1 Data acquisition

The ultrasonic array consists of twenty-four ultrasonic transducers mounted on four borehole frames (Figure 3-1). Each frame contains two transmitters and four receivers. The frames are installed in vertical 76 mm diameter boreholes approximately 10 m in length distributed to effectively monitor the pillar between the two deposition holes (see Section 3.2 for a description of the array geometry). The sensors are spring loaded against the borehole wall so as to produce good coupling to the rock (Figure 3-2). The transducers respond to the frequency range 35–350 kHz and are connected to 60 dB pre-amplifiers contained in junction boxes at the side of the tunnel. The boxes are dust tight and protected against water jets with additional silicon sealant around the cables preventing water infiltration. Coaxial cables from the boxes are fed through protective tubing to an instrumentation cabin provided by SKB in the Q-tunnel and connected appropriately to the acquisition system.

The AE acquisition system (Figure 3-2) consists of an *ESG* Hyperion ultrasonic system, a switch-box, a Panametrics pulsing unit, an acquisition computer and an archiving computer (both PC-Pentium type operating Microsoft Windows). The acquisition computer is only used for data acquisition and, by using the switch box, is capable of undertaking automated ultrasonic velocity surveys using each transmitter in turn. Full waveform information is acquired by the hardware and stored to the PC's hard drive. An archiving computer runs ASC's data management and processing software, InSite Seismic Processor. The InSite Leach software utility is used to capture data from the acquisition computer, archive it into a data base and process it 'on-line'. It is possible to remotely dial into the archiving computer to periodically check the data flow and quality. The use of the two computers means that the data acquisition is never disturbed by processing and data examination activities occurring on the archiving computer.

The piezoelectric transducers operate by converting a transient elastic wave into an electric signal or visa versa. The monitoring system is then operated in one of two modes. The first is used to passively monitor AE activity preferentially within the array volume. AEs release elastic energy in the same way as 'earthquakes' but over a very small scale. At these frequencies AEs have a moment magnitude (M_w) of approximately –6. They occur either during the creation process of new fractures within the medium, or on pre-existing fractures due to small scale movements. On the acquisition system an AE is recorded when the amplitude of the signal on a specified number of channels (in this case 6 channels) exceeds a trigger threshold within a time window of 5 ms. The system then records the signals from all 16 transducers. In this case a trigger threshold of 500 mV on all channels was used. This allows the system to have sufficient sensitivity to record high quality data without recording an abundance of activity that cannot be processed (due to low signal to noise on most of the channels). The captured signals are digitised with a sampling interval of 1 µs and a total length of 4,096 data points. Background noise levels of approximately 10 mV were observed giving a good signal to noise. Example waveforms from an AE are given in Appendix 1.

The second operating mode actively acquires ultrasonic waveforms by scanning across the volume. This allows measurements of P- and S-wave velocities and signal amplitudes over a possible 128 different ray paths. By repeating these ultrasonic surveys at increments

in time, a temporal analysis can be obtained for the variation in medium properties. A Panametrics signal generator is used to produce a high frequency electric spike (Figure 3-1). This is sent to each of the 8 transmitters in turn. The signal emitted from each transmitter is recorded over the 16 receivers in a similar fashion to that described above. An external trigger pulse from the signal generator is used to trigger the acquisition system and identifies the transmission start time to an accuracy of one sample point. In order to decrease random noise the signal from each transmitter is stacked 100 times. Example waveforms from an ultrasonic survey are given in Appendix 1.

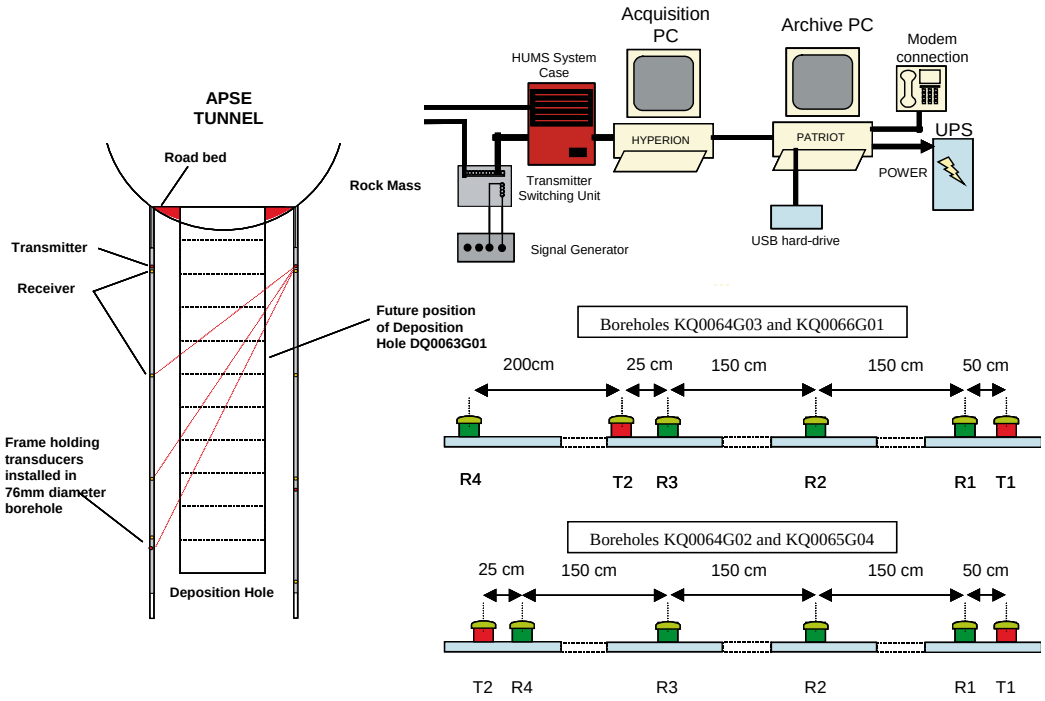

Figure 3-1. *A schematic of the APSE, acquisition system and sensors configuration.*

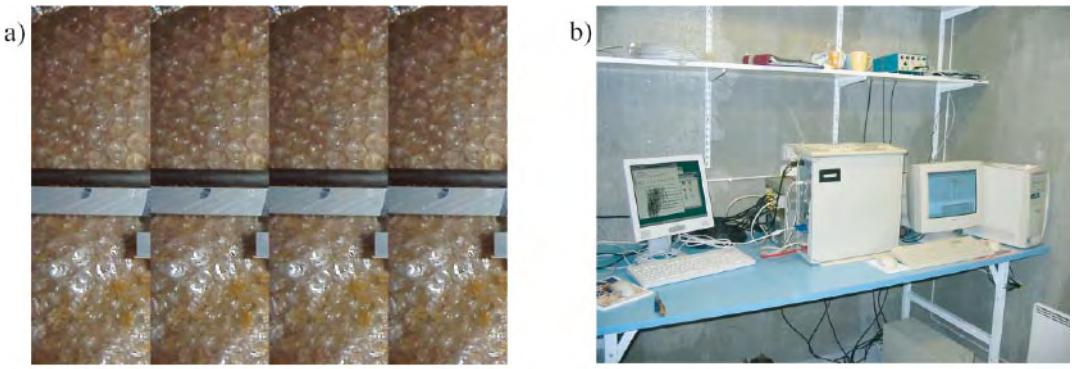

Figure 3-2. *a) A transducer attached to an installation frame. The spring loaded mechanism is adjustable to obtain the best possible coupling. b) Configuration of AE monitoring equipment in the Q-tunnel cabin.*

3.2 Array geometry

The transmitters and receivers contained in each borehole are described in Table 3-1 and Figure 3-3. The array geometry has been designed so as to monitor the pillar between the two deposition holes, enabling accurate AE locations to be determined. Section 5.2.3 discusses the location accuracy obtained by the system. The vast majority of events occurring in the pillar volume will have direct raypaths, not disturbed by any excavation, to all of the instrumentation boreholes. During ultrasonic surveys, 'skimming' ray paths, which travel within centimetres of the deposition wall, are created by the array design.

The instrumentation boreholes have been surveyed by SKB providing the location of all receivers and transmitters (Table 3-2 and Table 3-3). The transducer positions have been corrected for depth and to the borehole edge.

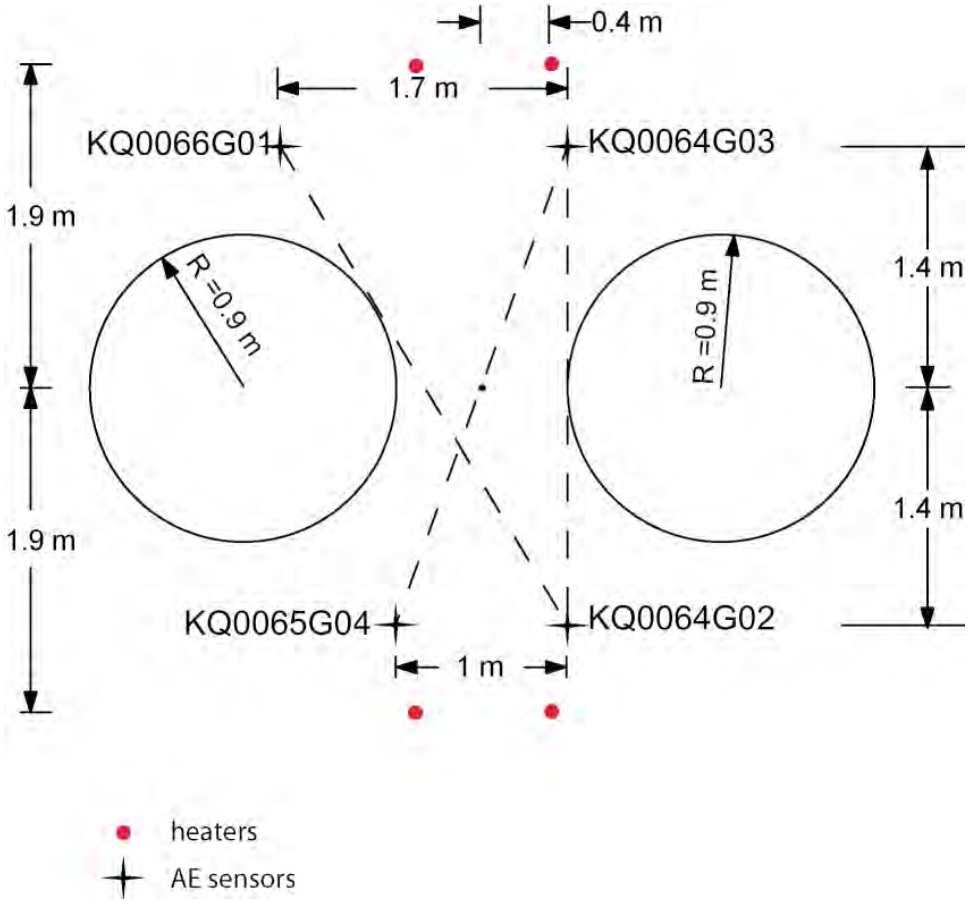

Figure 3-3. *Plan view of the array geometry for the two deposition holes, DQ0063G01 and DQ0066G01 excavated for the APSE. The four instrumentation boreholes are labelled. Red points are locations of the heaters. Dashed lines are direct ray paths between opposing boreholes illustrating the ultrasonic coverage.*

Table 3-1. Location of ultrasonic array for monitoring the pillar. See Figure 3-3 for an illustration of the array geometry.

Sonde #	Borehole ref	Transmitter #	Receiver #
1	KQ0064G03	1, 2	1–4
2	KQ0064G02	3, 4	5–8
3	KQ0065G04	5, 6	9–12
4	KQ0066G01	7, 8	13–16

Table 3-2. Receivers used during and following the excavation of the deposition holes (cable numbers after 08 December 2003).

Corrected receiver parameters									
Receiver #	Acquisition channel #	Cable #	BH Reference	Position N (m)	E (m)	D (m)	Unit vector orientation n	e	d
1	1	2	KQ0064G03	7318.809	2127.944	446.820	0.989	–0.147	0.00
2	9	3	KQ0064G03	7318.809	2127.944	448.320	0.989	–0.147	0.00
3	3	4	KQ0064G03	7318.809	2127.944	449.820	0.989	–0.147	0.00
4	4	5	KQ0064G03	7318.809	2127.944	452.070	0.989	–0.147	0.00
5	5	14	KQ0064G02	7320.787	2126.007	446.820	–0.504	0.864	0.00
6	6	15	KQ0064G02	7320.787	2126.007	448.320	–0.504	0.864	0.00
7	7	16	KQ0064G02	7320.787	2126.007	449.820	–0.504	0.864	0.00
8	8	17	KQ0064G02	7320.787	2126.007	451.320	–0.504	0.864	0.00
9	2	20	KQ0065G04	7321.468	2126.714	446.820	–0.967	0.255	0.00
10	10	21	KQ0065G04	7321.468	2126.714	448.320	–0.967	0.255	0.00
11	11	22	KQ0065G04	7321.468	2126.714	449.820	–0.967	0.255	0.00
12	12	23	KQ0065G04	7321.468	2126.714	451.320	–0.967	0.255	0.00
13	13	8	KQ0066G01	7319.971	2129.127	446.820	0.283	–0.959	0.00
14	14	9	KQ0066G01	7319.971	2129.127	448.320	0.283	–0.959	0.00
15	15	10	KQ0066G01	7319.971	2129.127	449.820	0.283	–0.959	0.00
16	16	11	KQ0066G01	7319.971	2129.127	452.070	0.283	–0.959	0.00

Table 3-3. Transmitters used during and following excavation of the deposition holes (cable numbers after 08 December 2003).

Corrected transmitter parameters								
Transmitter #	Cable #	BH Reference	Position N (m)	E (m)	D (m)	Unit vector orientation n	e	d
1	1	KQ0064G03	7318.809	2127.944	446.570	0.989	–0.147	0.00
2	6	KQ0064G03	7318.809	2127.944	450.070	0.989	–0.147	0.00
3	13	KQ0064G02	7320.787	2126.007	446.570	–0.504	0.864	0.00
4	18	KQ0064G02	7320.787	2126.007	451.570	–0.504	0.864	0.00
5	19	KQ0065G04	7321.468	2126.714	446.570	–0.967	0.255	0.00
6	24	KQ0065G04	7321.468	2126.714	451.570	–0.967	0.255	0.00
7	7	KQ0066G01	7319.971	2129.127	446.570	0.283	–0.959	0.00
8	12	KQ0066G01	7319.971	2129.127	450.070	0.283	–0.959	0.00

3.3 Monitoring procedure

Ultrasonic monitoring commenced immediately after installation of the instrument frames from 13th October 2003. Background monitoring was undertaken between 23:00 and 06:00 each night in an attempt to avoid human noise during the daytime working hours. This regime continued through excavation of deposition hole DQ0066G01. During excavation of deposition hole DQ0063G01, between 4 March and 10 March 2003, monitoring was performed 24 hours a day except during times of high frequency noise in the rock volume (e.g. drilling). An engineer from ASC was on site in order to switch on the acquisition system just before completion of excavation and off when drilling restarted. After each round a one hour quiet period was observed in the tunnel when no maintenance could be performed on the drilling machine. After excavation of both holes and formation of the pillar, automatic monitoring was set between 17:00 and 07:00 from 11 March 2004. From 30 April 2004 the system was set to monitor continuously for the heating phase, and the confinement removal and cooling phase.

Ultrasonic surveys were conducted at 01:00 each night except during excavation of deposition hole DQ0063G01. Between 4 March and 10 March 2004, surveys were undertaken hourly so as to obtain high temporal resolution in the P- and S-wave velocity and amplitude variation along transmitter-receiver raypaths. Surveys were not conducted during the hours when excavation was occurring due to drill noise, and during the first hour of AE monitoring after cessation of drilling.

A calibration survey was performed in deposition hole DQ0063G01 so as to analyse uncertainties in AE locations and to calibrate the location algorithm (Section 5.2.3). A mechanical source (a screwdriver) was used in known locations in the deposition hole interior after the completion of excavation. The source radiates a relatively high energy signal. In order to test the sensitivity of the array to very small signals, pencil break tests were also performed on the interior of each deposition hole.

3.4 Processing procedure

The raw data are stored as ‘events’, each with 16 recorded waveforms. The events contain the following data types.

- Microcrack induced acoustic emissions (AEs).
- Ultrasonic survey recordings.
- Noise events consisting of excavation drill noise, human-related activity and electrical noise spikes.

The first stage of the processing is to split these types into individual data sets. It is highly important that the noise is removed so that spurious ‘AEs’ are not described in the results. The time of completion of each excavation round and any periods of human activity has been logged. Potential erroneous AE triggers have then been removed form the data set. Electrical noise spike are high frequency events with very similar waveforms recorded on every channel. All events have been visually inspected and noise events of this type have been additionally removed from the data set.

AE data and ultrasonic surveys from each deposition hole have then been processed independently. A list of the processing parameters used is given in Appendix 2. Processing for this experiment contains the following steps:

3.4.1 Ultrasonic surveys processing

1. One survey was manually picked for P- and S-wave arrival times where possible. The uncertainty in any P-wave time measurement is approximately ± 3 µs. Velocities were calculated using the time of flight between known transmitter and receiver locations. Uncertainties in the absolute P-wave velocity measurements, from travel times alone, are approximately ± 30 $m.s^{-1}$. This assumes an exact set of transducer positions. A 1 cm position uncertainty on a typical raypath length of 2 m also gives a velocity uncertainty of approximately ± 30 $m.s^{-1}$.

2. P- and S-wave arrival times for each survey during the monitoring period were then measured using a cross-correlation procedure. This gives a much more precise measurement of velocity variation than manual processing allows and thus allowing small (< 30 $m.s^{-1}$) velocity changes to be observed. It also allows the efficient processing of large volumes of data. .Further information on this procedure can be obtained in /Pettitt et al. 2004a/. The manually processed survey acts as a reference survey. The arrivals for every survey are first obtained using an automatic picking algorithm. A data window is then formed around each arrival and the window is then cross-correlated with a similar window from the reference survey. This gives a measurement of the change in arrival time to an accuracy of ± 0.2 µs. The change in time is then used to calculate a change in velocity with an estimated uncertainty of ± 2 $m.s^{-1}$

3.4.2 Acoustic emissions processing

1. Calibration surveys have been used to optimise an automatic picking and source location algorithm, and check location uncertainties, in previous studies (e.g. Prototype Repository). For this experiment a further calibration study was performed and the results were inspected to check the parameters are still applicable in the Pillar Stability Experiment.
2. P- and S-wave arrival times were measured for each AE using an automatic picking procedure.
3. The P- and S-wave arrival times were input into a downhill-simplex location algorithm /Pettitt et al. 2004a/. This has the option of incorporating either a three-dimensional anisotropic velocity structure or an isotropic structure. Velocities calculated from the ultrasonic surveys were used to determine the best input velocity structure to use.
4. Filtering of the data was undertaken to remove events located with large error. The number of independent instruments was set to 10. This means P or S-wave arrivals must be picked on 10 separate instruments in order for the event to be retained. A location error of 0.1 m was also used. This error is calculated from the residuals, knowing the velocity of the structure. A final filter on the location volume removed erroneous events locating too far from the pillar, usually caused by a poorly constrained error minimisation. Further information on these filtering parameters can be found in /Pettitt et al. 2004a/.
5. Spurious AE locations have had their automatic picks manually checked in case these were incorrect or noise interfered with the waveforms.
6. Waveforms of all events were visually inspected to check for noise spikes. These are large amplitude peaks occurring at the same time on all channels, thought to be the result of electrical interference from the heaters.

4 Acoustic emissions and stress conditions at the HRL

The APSE is the latest in a number of ultrasonic monitoring experiments conducted at the HRL in Sweden. The techniques described in this report have also been performed in experiments conducted in the Zone of Excavation Damage Experiment (ZEDEX) /Falls and Young 1996/, the Canister Retrieval Tunnel at the 420 m level /Pettitt et al. 1999a/ and the Prototype Repository at the 450 m level /Pettitt et al. 1999b/. The results from the latter two experiments will be summarised here. It is important when investigating the response of a particular rock mass to excavation to consider the in situ stress conditions and the overall rock mass stability. These are also summarised for the APSE here.

4.1 Acoustic emission in the Canister Retrieval Tunnel

In the Canister Retrieval tunnel, two deposition holes (DD0092G01 and DD0086G01) were excavated. The tunnel was excavated using a Drill and Blast technique to a height of approximately 6 m. An ultrasonic array was installed around each deposition hole to investigate the response of the rock mass to the excavation /Pettitt et al. 1999a/. During the entire monitoring period there were a total of 2,746 AE triggers. The AE results showed regions of intense fracturing located in clusters down the deposition hole wall (e.g. Figure 4-1). These regions were orientated orthogonal to the maximum principal stress at the 420 m level. The damaged zone was restricted to approximately 20 cm from the deposition hole wall and the activity decayed rapidly within the first few hours after excavation. The clusters are probably a result of the interaction of induced stresses with excavation through pre-existing features. A linear macroscopic fracture was also imaged. AEs were observed to be strongly time-dependent with fracturing being reinitiated around previous rounds when excavation of the deposition hole continued. AEs occurred at a much reduced rate (< 10 triggers per night) after completion of excavation.

Ultrasonic surveys gave velocities for the pre-disturbed rock mass as approximately 5,900 $m.s^{-1}$ for P-waves and 3,350 $m.s^{-1}$ for S-waves. A 3% anisotropy was imaged. These results are consistent with those obtained in the ZEDEX experiment, e.g. /Falls and Young 1996/. The surveys generally described a drop in velocity during excavation (e.g. Figure 4-2). Observed changes vary from 4 $m.s^{-1}$ for ray paths at distance from the deposition hole to sharp drops of 20–30 $m.s^{-1}$ for ray paths skimming the deposition hole wall. These variations were explained using a disturbed and a damaged zone model. As ray paths travel through the disturbed zone, in which induced stresses have preferentially opened or closed pre-existing microcracks, then the ray experiences small increases or decreases in velocity. This results in, for example, a 4 $m.s^{-1}$ change observed at distance from the deposition hole. However, ray paths skimming the deposition hole perimeter at 2–3 cm distance pass through a region of accumulated damage close to the wall. These then experience a much sharper change in velocity of the order –15 $m.s^{-1}$ measured over the entire ray path. This velocity change can be used to estimate the change in elastic moduli in the damaged zone.

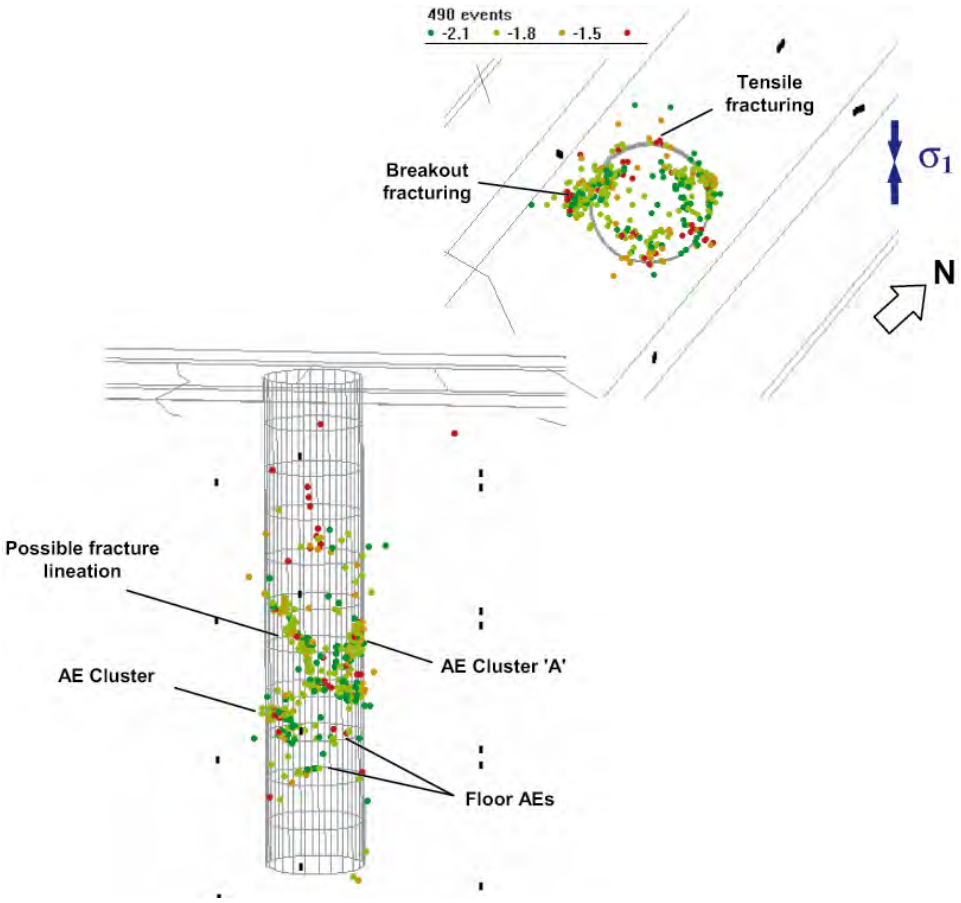

Figure 4-1. *AE locations from excavation of deposition hole DD0092G01 in the Canister Retrieval tunnel.*

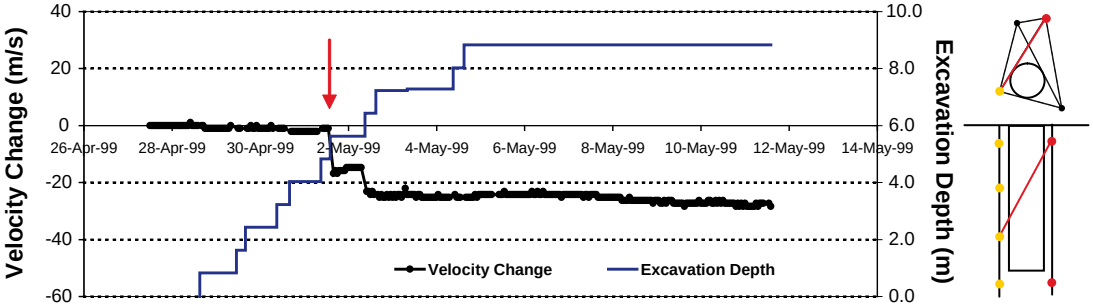

Figure 4-2. *Velocity change for deposition hole DD0092G01 in the Canister Retrieval tunnel measured on the ray path illustrated in the right-hand margin. The red arrow shows the time at which excavation passed the ray path.*

The velocity of the rock in the damaged zone alone is given by Equation 1 /Pettitt et al. 2002/. This assumes the remainder of the rock mass outside of the damaged zone has an average velocity that is unchanged by the excavation, and that the ray path remains a direct ray path.

$$(v_R - v_D) = \frac{\Delta v_m . v_R . d}{d_D v_R + \Delta v_m d_R}$$ Equation 1

Assuming that the measured velocity change is small compared to the reference velocity and that the ratio d_D/d_R is not << 1, then Equation 1 approximates to Equation 2 /Pettitt et al. 2002/. That is, the difference between the velocity in the damaged zone and the velocity outside it is a simple function of the relative ray path lengths, d and d_D (how much of the ray path is damaged).

$$(v_R - v_D) \approx \Delta v_m . \frac{d}{d_D}$$ Equation 2

/Pettitt et al. 2002/ undertake calculations to determine the decrease in velocity through the damaged zone for the deposition hole. They estimate 5% of the skimming ray path typically passes through the damaged region. Ray path lengths average 4 m in length, and the damage zone is approximately 20 cm of the ray path as defined by AE observations. Hence, using Equation 2, the *decrease* in P- and S-wave velocities in the damaged zone is determined as $(v_R – v_D)$ = 300 m.s^{-1} i.e. a drop of 20x the measured velocity change. Using a rock mass density of ρ = 2,650 kg.m^{-3} then dynamic elastic moduli can be calculated for the intact and damaged rock. This results in Dynamic Young's moduli, E_R = 75 GPa and E_D = 64 GPa respectively. The damaged region hence experiences a reduction in Young's modulus of approximately 15%.

4.2 Acoustic emissions in the Prototype Repository

Two deposition holes, DA3551G01 and DA3545G01, were monitored in the Prototype Repository in a similar manner to the Canister Retrieval tunnel /Pettitt et al. 1999b/. The Prototype Repository consists of a 90 m long, 5 m diameter sub-horizontal tunnel, excavated with a Tunnel Boring Machine (TBM). An ultrasonic array was installed to monitor the excavation of both deposition holes, and monitor the effect of heating the canister in deposition hole DA3545G01. 2,467 events were located in total during the excavation of the deposition holes. The events locate down the whole of the deposition holes in clusters (Figure 4-3), similar to the pattern experienced in the Canister retrieval tunnel. In plan view there is a clear clustering of events in the NE-SW quadrant. This distribution is shown to be orthogonal to the maximum principle stress and hence represents a region of high compressive stresses. Events were subsequently recorded during heating of the deposition holes, locating around the deposition hole wall and along a semi-horizontal macroscopic fracture /Pettitt and Haycox 2003/. The mechanism for producing the AEs could be associated with movement around the pre-existing macrofractures, or microcracking in the immediate vicinity of the fractures.

Unlike in the Canister Retrieval tunnel, the rock at the Prototype Repository was found to be ultrasonically isotropic and homogeneous. A mean P-wave velocity of 6,013 m.s^{-1} and S-wave velocity of 3,397 m.s^{-1} was determined prior to excavation. Drops in velocity were observed during excavation of the deposition holes. In particular, raypaths skimming very close to the deposition hole displayed large decreases. However, the orientation of the raypaths was important in determining the extent of the decrease. Stress effects around the deposition hole caused certain areas to display a high compressive stress, in which an increase in velocity is observed, or a low compressive stress, in which a decrease in velocity occurs. Consequently, average velocities between instrumentation boreholes varied between

–27.4 m.s^{-1} and –0.5 m.s^{-1} during excavation. During heating, thermal stresses induced by temperature caused many raypaths to exhibit an increase in velocity /Pettitt and Haycox 2003/. This is interpreted as the result of compressive stresses which lead to closure of microfractures and pore spaces. Examples of velocity changes on a skimming raypath are shown in Figure 4-4 showing a decrease occurring during excavation and an increase occurring during heating.

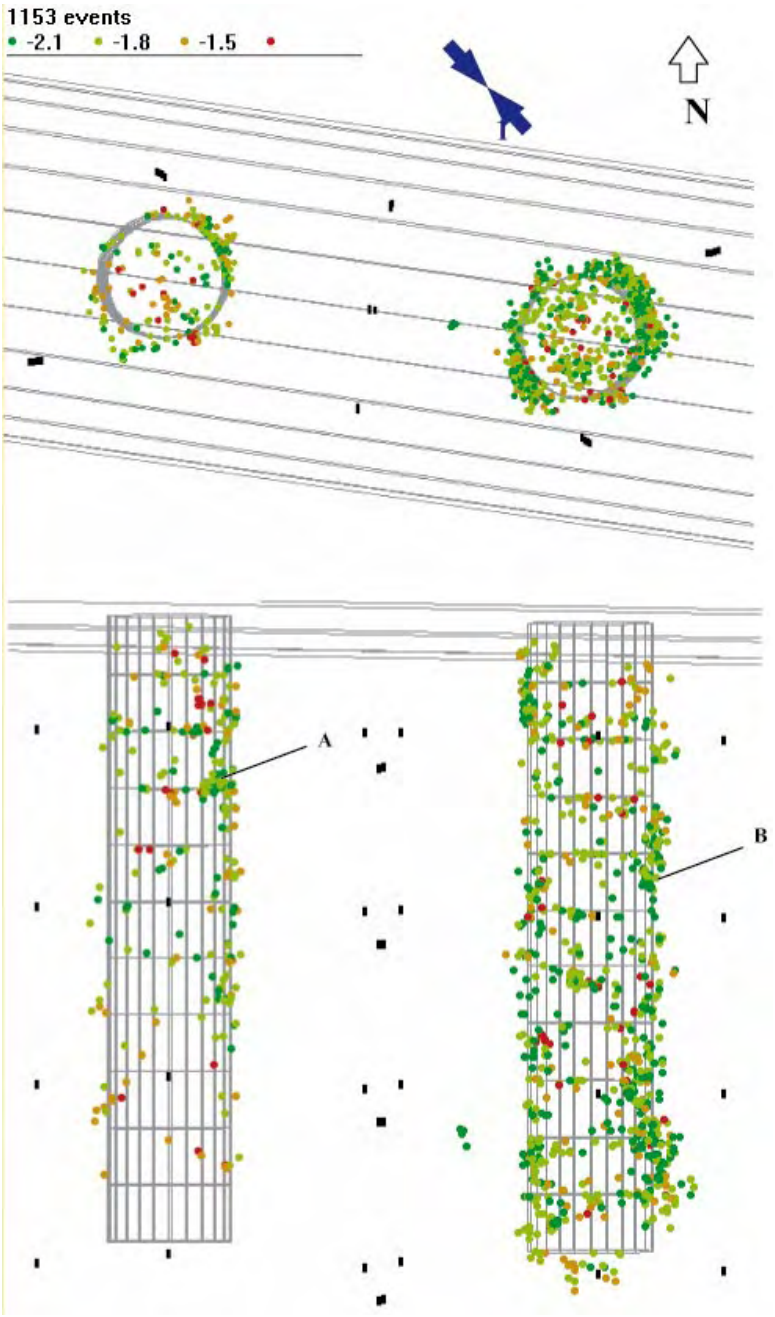

Figure 4-3. *Acoustic emissions during excavation of deposition holes DA3551G01 and DA3545G01.*

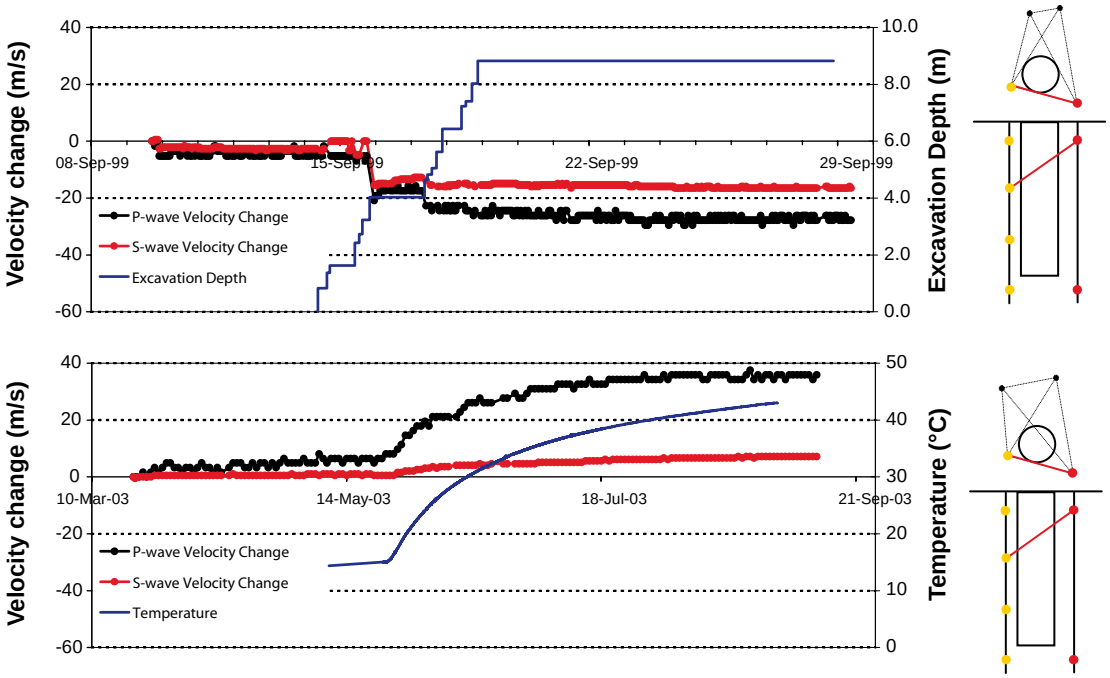

Figure 4-4. *Velocity change for deposition hole DA3545G01 during excavation and heating on the same raypath, illustrated in the right hand margin.*

4.3 Stress conditions for the APSE

/Staub et al. 2004/ present detailed geological mapping of the TASQ tunnel in which the APSE has been undertaken. The fracture sets identified are found to coincide well with the geological data set of the Äspö Hard Rock Laboratory. Figure 4-5 shows the structures identified in the TASQ tunnel and the three dominant orientations.

Extensive stress measurements have been undertaken around the site of the experiment /Staub et al. 2004/. When complemented with convergence measurements obtained during excavation of the deposition holes, back calculations were performed to find the best fit stress field (Table 4-1). The second principle stress is vertical and approximately 25% higher than the weight of the overburden. The principal stress field agrees well with the dominant orientations of the mapped geological structures.

In the case of the APSE, the Q-tunnel's orientation is orthogonal to the maximum principle stress. JobFem stress modelling at 1.5 m below the tunnel rock floor shows stress magnitudes at the hole walls of greater than 150 MPa /Andersson et al. 2004/. This is the level of stress that is predicted to be required to initiate spalling. Anticipated stresses in the rock range from approximately 100 MPa in the centre of the pillar to 170 MPa by the deposition hole walls. Near the tunnel rock floor, the whole of the pillar will be subjected to stresses higher than the crack initiation strength. After the heaters are turned on, the total major stress could be increased by 30 MPa after 120 days.

The rock into which the deposition holes are drilled is Äspö Diorite. This is the same as throughout the HRL, however in the Q-tunnel the diorite is not as fresh as in the rest of the laboratory, containing volumes with some oxidized bands /Andersson et al. 2004/. A number of fractures have been mapped and a near-horizontal shear zone cuts through the pillar volume at approximately 0.5 m below the rock floor. Figure 4-6 shows the location of the fractures as determined by /Staub et al. 2003/. Fract_1 passes through deposition hole DQ0066G01 with a strike of approximately 133° East of North and a dip of 86° SW.

Table 4-1. Principal stress values for the TASQ tunnel from /Staub et al. 2004/.

Stress component	Magnitude (MPa)	Trend (°)	Plunge (°)
σ_1	30	310	0
σ_2	15	90	90
σ_3	10	208	0

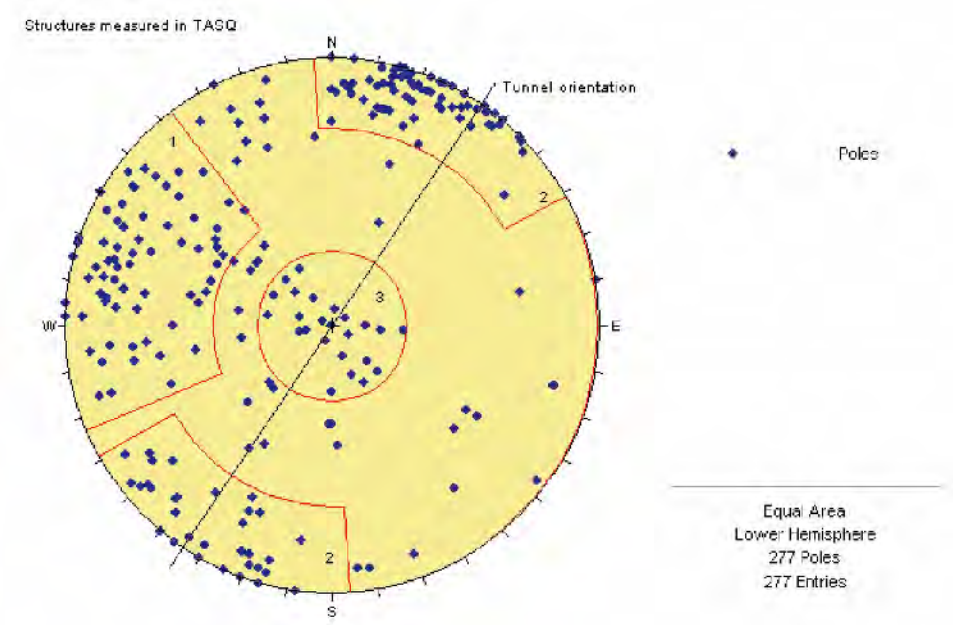

Figure 4-5. *Projection of poles to fracture planes to all structures measured in tunnel TASQ from /Staub et al. 2004/. Three groups of structures are identified; Group1 include shear zone parallel structures, Group 2 are a brittle sub vertical set striking parallel to the tunnel and Group 3 are a set of sub horizontal brittle fractures.*

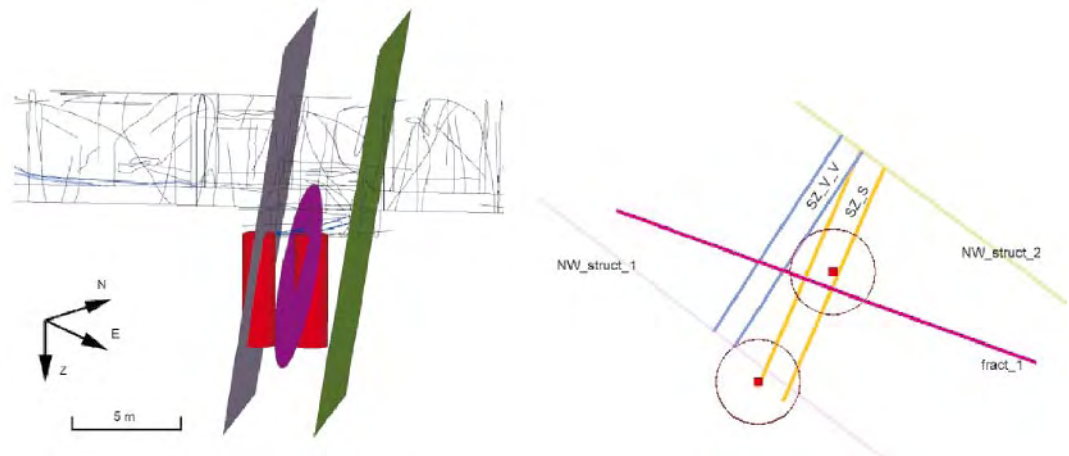

Figure 4-6. *Location of principal fractures in the pillar volume determined by /Staub et al. 2003/.*

5 Results from acoustic emission monitoring

5.1 Ultrasonic velocity and amplitude structure

An ultrasonic survey has been chosen (28 November 2003) from the period before excavation began so as to obtain a measure of the background velocity structure for input to the AE source location algorithm. P- and S-wave velocity measurements for the array are shown in the lower-hemisphere stereonets of Figure 5-1. The mean P-wave velocity is 6,051 $m.s^{-1}$ and the mean S-wave velocity is 3,394 $m.s^{-1}$. Estimated uncertainties, resulting from travel-time picking errors between measurements, are 30 $m.s^{-1}$ and 19 $m.s^{-1}$ respectively for P- and S-wave velocities (Section 3.4). Similar magnitude velocity uncertainties also exist for every 1 cm error in raypath length – caused by uncertainties in the surveyed locations of the borehole collars, which are believed to have millimetre accuracy.

The P-wave velocities suggest a weakly transversely isotropic rock mass with a fast direction orthogonal to the tunnel direction (north west to south east and around to the vertical). The slow velocity direction is thus parallel to the tunnel, orthogonal to the major fracture set and maximum principal stress direction. This velocity difference is approximately 90 $m.s^{-1}$, or 1.5%. When taking account of the uncertainties in the measurements, this is not a significant anisotropy. Therefore, a homogeneous-isotropic velocity model has been used in acoustic emission processing.

The measured velocities are consistent with those obtained at the Prototype Repository, where average P-wave velocities of 5,988 $m.s^{-1}$ and 6,013 $m.s^{-1}$, and S-wave velocities of 3,392 $m.s^{-1}$ and 3,397 $m.s^{-1}$, were recorded prior to excavation. Results from the Canister Retrieval Tunnel showed 3% anisotropy and velocities were lower than the Prototype Repository. Small variations in the observed velocities between the experiments (< 100 $m.s^{-1}$) are likely to be the result of small variations in rock type between the different regions of the HRL. Litholigical differences in the Äspö Diorite are recognised to be the result of different mixtures of dioritic compositions, varying in chemistry and grain sizes.

It has been observed that low amplitude signals are systematically received on borehole KQ0066G01. Figure 5-2 compares signal amplitudes recorded on raypaths using KQ0066G01 with amplitudes recorded on raypaths using the other three boreholes. Only two raypaths involving borehole KQ0066G01 have amplitudes greater than 100 mV. Close to half of the raypaths involving the other 3 boreholes have amplitudes greater than this value. Sensor coupling with the borehole wall can cause small variations in signal amplitude between individual sensors, however, in this experiment all four boreholes have the same instrumentation configuration and are installed in exactly the same manner. Variations in sensor coupling should therefore be similar across the array. Hence, the reduction of signals on KQ0066G01 must be a result of the rock mass. The observed response has been interpreted as due to the water-bearing fracture (fract_1) observed by /Staub et al. 2003/ and shown in Figure 4-6. Assuming that this fracture is reasonably linear over a few metres then borehole KQ0066G01 is positioned on the opposite side of the fracture to the other boreholes, and thus raypaths travelling to this borehole will have to pass through it. The fracture may also intersect borehole KQ0065G04, but considerable effects are not observed on raypaths here. Waves at the high frequencies used here will lose energy as they cross the interface between the fracture faces and hence the amplitude of the recorded signal will decrease. Velocity measurements are not observed to be effected by the fracture.

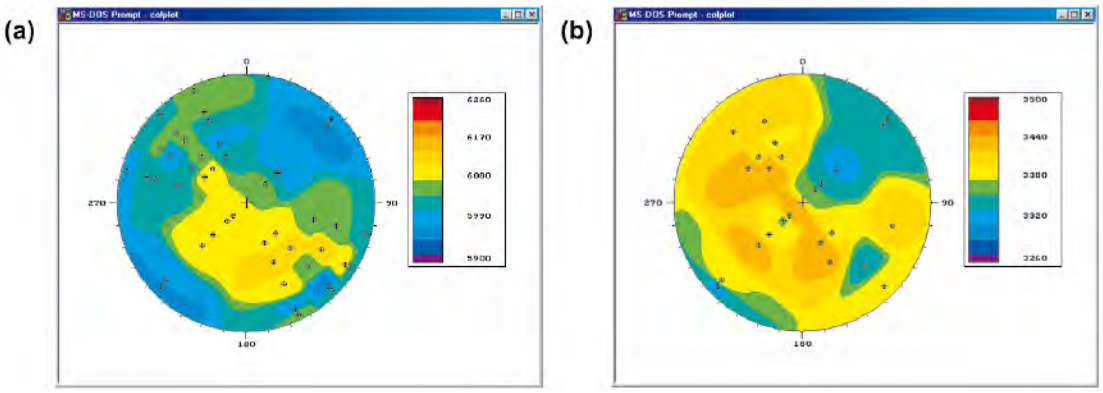

Figure 5-1. *Measured ultrasonic velocities from a survey during background monitoring, shown on lower-hemisphere stereonets. The survey was performed on 28th November at 01:00. a) P-wave velocities. b) S-wave velocities. One colour increment represents the estimated velocity uncertainty.*

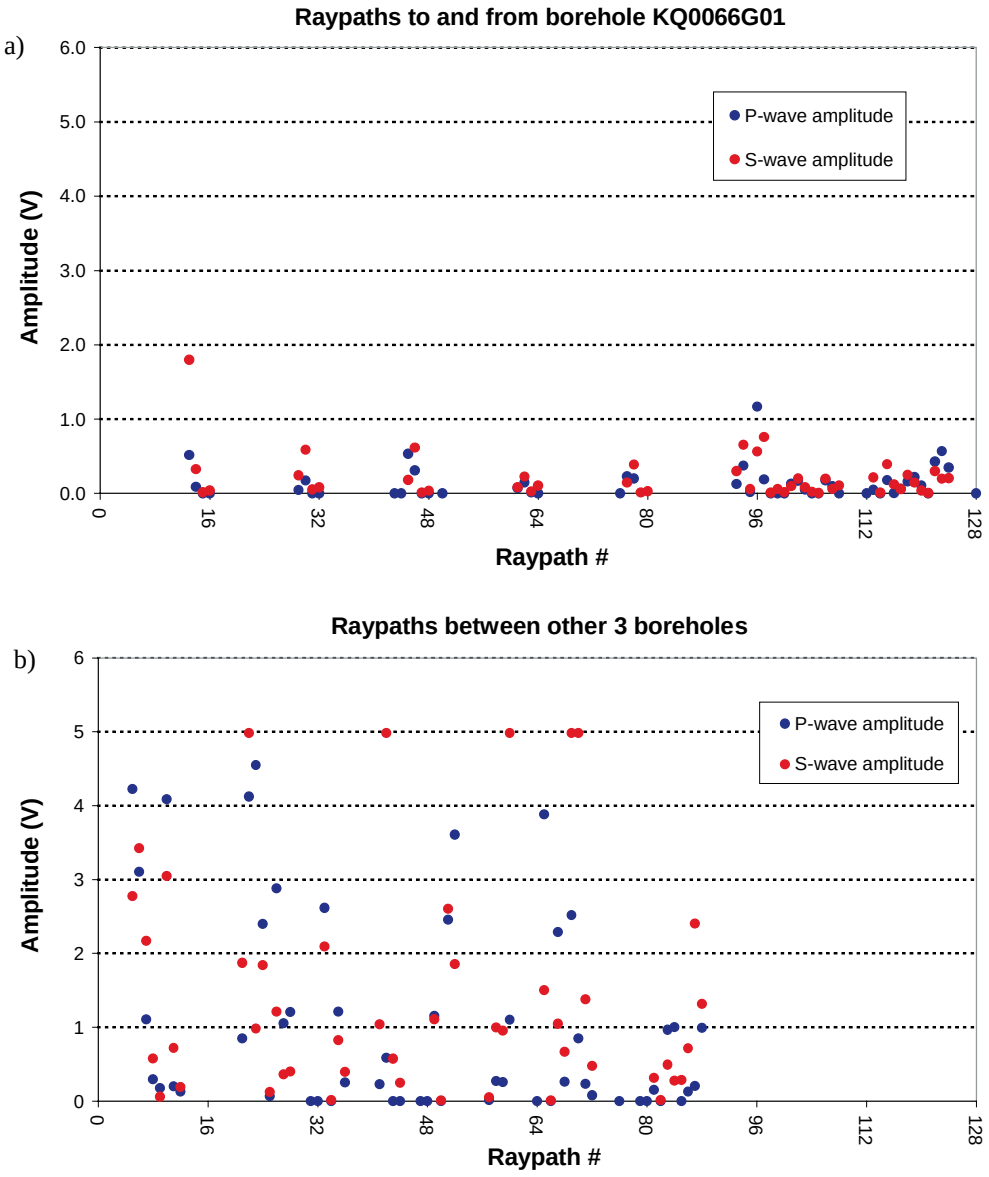

Figure 5-2. *Signal amplitude recorded on a survey before excavation separated into (a) raypaths to and from KQ0066G01 and (b) raypaths between the other three instrumentation boreholes.*

This is consistent with full-waveform modelling of synthetic fractures by /Hildyard and Young 2002/ where velocity measurements are observed to be sensitive to a bulk change in rock properties (i.e. a large population of smaller fractures) rather than travelling through a single large fracture.

5.2 Overview of acoustic emission locations

5.2.1 Spatial and temporal distribution

AE locations from the reporting period between 13th October 2003 and 14th July 2004 are shown in Figure 5-3. The pillar has been produced by excavating two 1.8 m diameter deposition holes 1 m apart (Section 2). These were bored in 0.8 m steps using a Tunnel Boring Machine (TBM) specially adapted for vertical drilling. Each step took approximately 3 to 5 hours to complete. The first deposition hole, DQ0066G01, was drilled between 2 December 2003 and 8 December 2003. This was then confined to 0.7 MPa internal pressure using a specially designed water-filled bladder /Andersson et al. 2004/. The second deposition hole, DQ0063G01, was excavated between 4 and 11 March 2004.

The monitoring system recorded a total of 36,676 triggers over the monitoring period, of which 15,198 events have been located. These are shown with colours scaled to magnitude. A vast majority of events locate in the pillar volume, between the two deposition holes. Figure 5-3a is a view orthogonal to the tunnel and displays the close proximity of the AEs to the deposition hole walls (< 20 cm). Figure 5-3b shows how the events are clustered when viewed parallel with the tunnel. Few events locate outside a tightly constrained damaged region, which extends down the length of the deposition holes to approximately 1 m from their floors. Figure 5-3c is a plan view. This shows clustering of events in a damage zone orthogonal to the maximum principal stress, represented by a semi-circle of tightly packed AEs extending from the edge of each hole approximately 20 cm into the pillar. Some AEs close to the first deposition hole may be constrained by Feature 1 (Fract_1 from /Staub et al. 2003/) highlighted in Figure 5-4. Very few events are situated in the centre of the pillar, although clusters of events occur in the top metre of the pillar volume in two sub horizontal features that cross the pillar. The uppermost feature is believed to be associated with the rock floor of the tunnel, beneath the concrete roadbed, and the lowermost feature is associated with a mapped shear zone /Andersson 2004/. These events also delineate a single plane (named Feature 2 in Figure 5-4), and orientated with a dip of approximately 20° in a NE direction.

Figure 5-5 shows the temporal distribution of the located events. This shows a similar pattern to that described for the hit counts (Section 5.2.2). There are a number of groups of events that occur at different stages of the experiment. These are associated with the experiment phases described in Table 1-1. The first two groups relate to events occurring during excavation of the deposition holes. The number of events during drilling of DQ0066G01 (December 2003) peaks at 120 events per day. This is far less than the peak of 820 events per day when DQ0063G01 is excavated in March 2004. Events are observed to locate on both deposition holes during drilling of the second hole (Section 5.4), despite confinement on DQ0066G01 with the bladder. This is likely to be the result of the increased stresses induced during the formation of the pillar.

Two stages of increased heating rate are apparent during May and June. In the first stage a peak of 807 events per day is reached and in the second a peak of 863 events per day is achieved. The cumulative events line shows two sharp increases, each followed by a period of slow increase. These correlate well with the start of heating and a change in the heating intensity respectively.

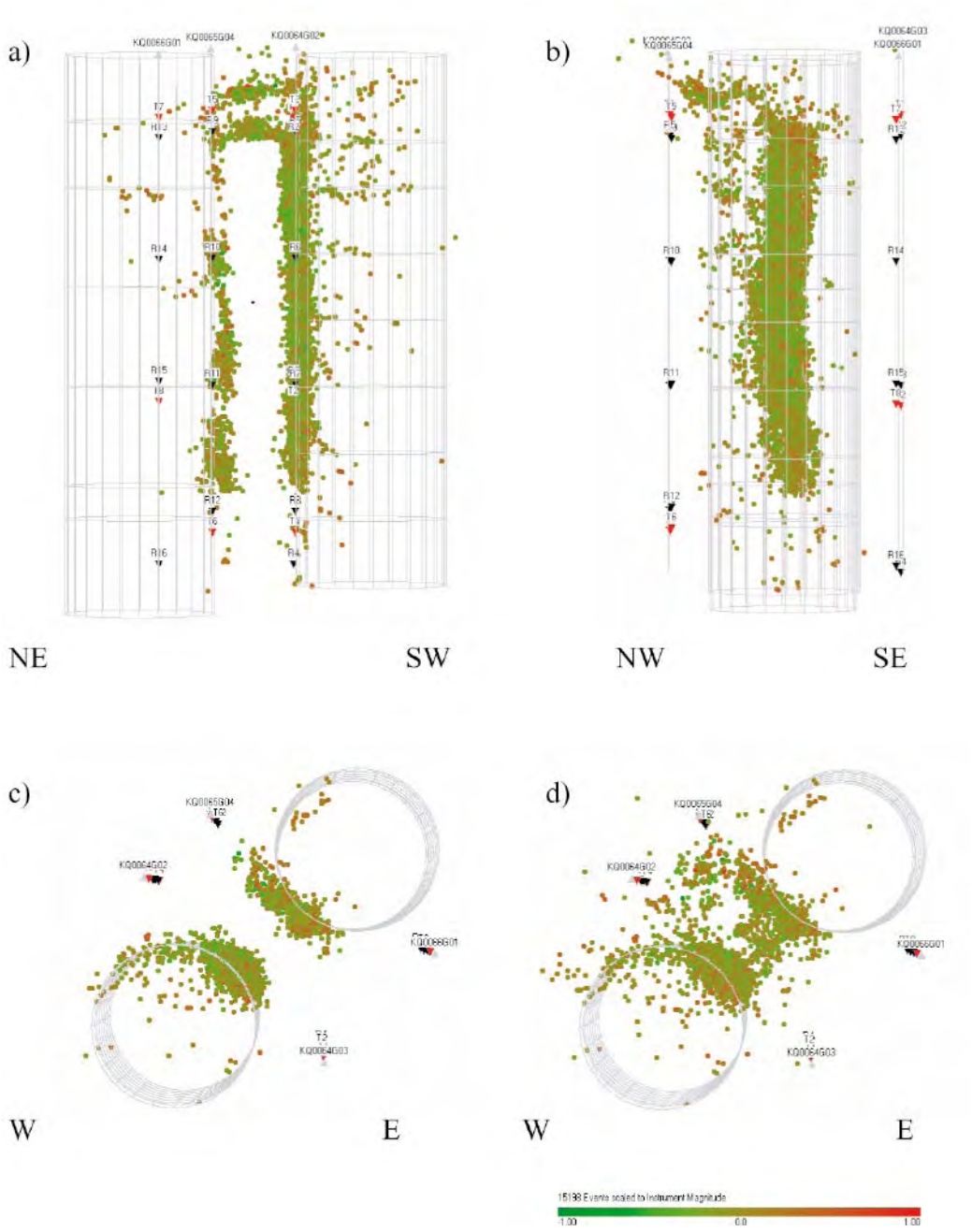

Figure 5-3. *AE locations of all 15,198 events between 13 October 2003 and 14 July 2004. a) View orthogonal to tunnel, b) View parallel to the tunnel, c) Plan view of events below 446.9 m (1 m below tunnel floor), d) Plan view of all events.*

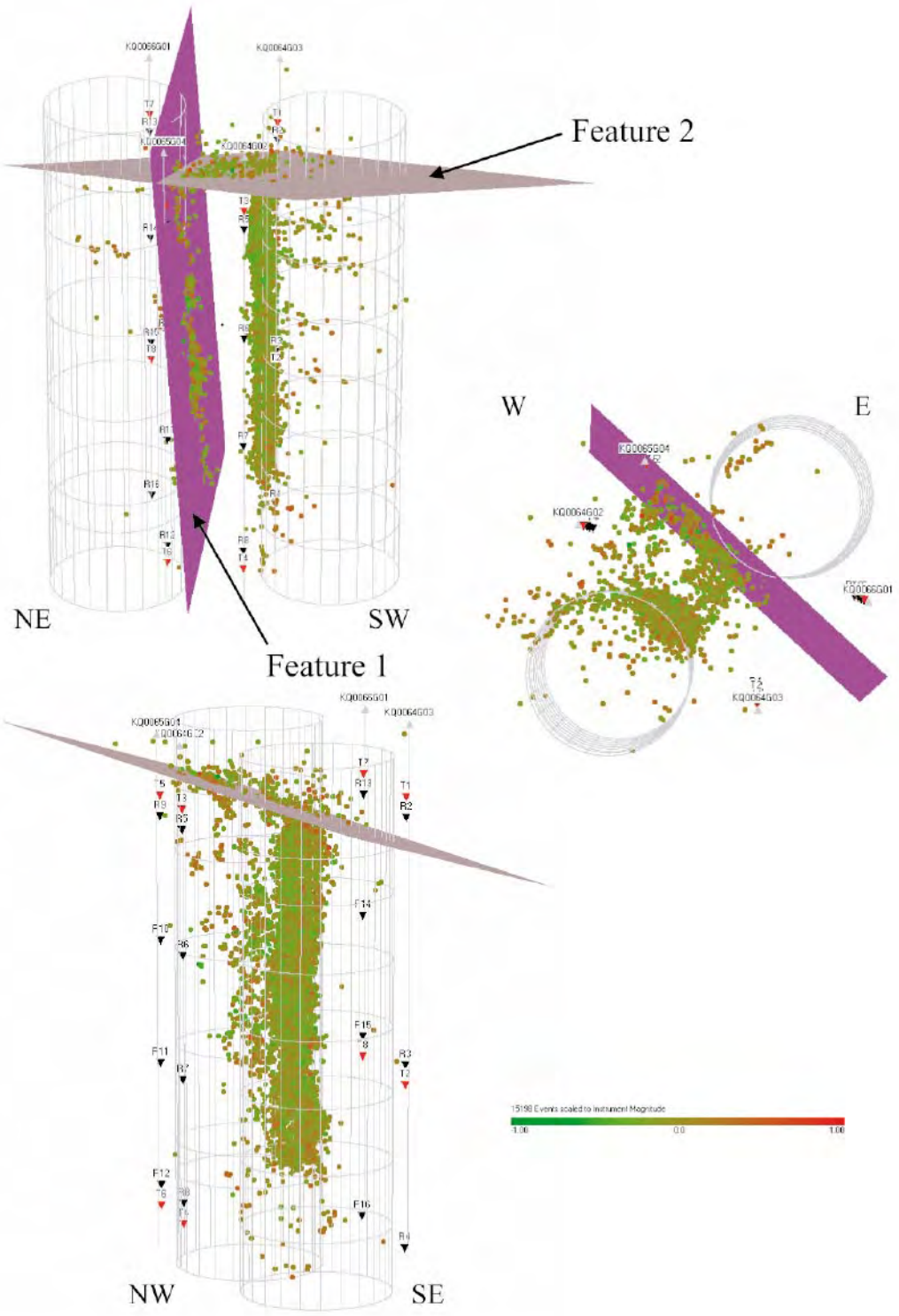

Figure 5-4. *Position of two interpreted features from the data obtained during the whole of the APSE.*

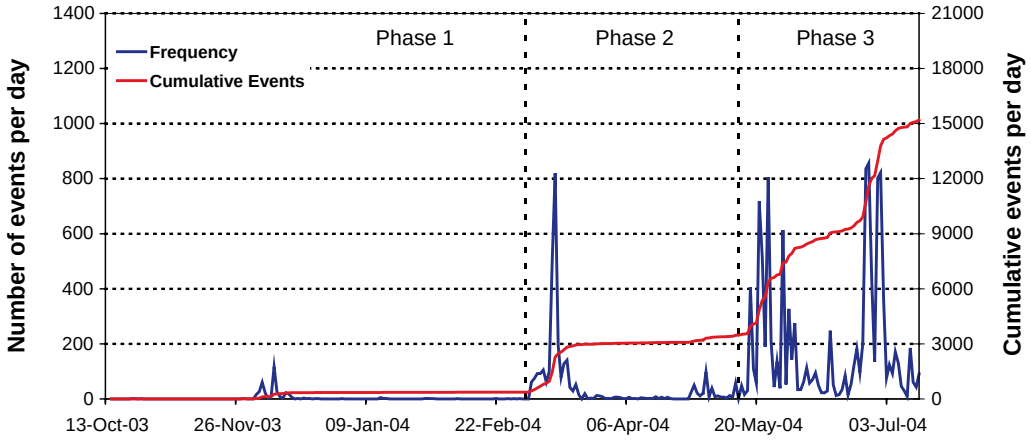

Figure 5-5. *Temporal distribution of AE events located at the APSE between 13 October 2003 and 14 July 2004. Phases of the experiment, described in Table 1-1, are also indicated.*

Figure 5-6 shows the number of triggers per day. This is a measure of the total number of events captured by the system, rather than the subset produced by location processing. Noise events have been removed from this data. The pattern is very similar to the number of located events suggesting that the location processing has provided a well distributed subset of all the events captured and that there is no biasing of the results. Over 2,000 triggers occur in a single day during excavation of deposition hole DQ0063G01.

Figure 5-7 shows how the depth of events in three volumes changes with time. Events in the upper metre of the pillar (Figure 5-7a) occur through all the phases in the experiment. In particular, events are observed during excavation of the deposition holes and heating of the pillar. The other plots (Figure 5-7b–c) show events at depths exceeding 446.9 m in the damaged zones of the two deposition holes. Most events are observed in deposition hole DQ0063G01 (Figure 5-7c), the majority occurring during excavation of the deposition hole and pillar heating. Events on DQ0066G01 occur down to 452 m during excavation of both deposition holes. AEs occur in clusters over short time frames for DQ0066G01 in contrast to DQ0063G01 in which events occur in regions over long periods and slowly migrate along the length of the deposition hole.

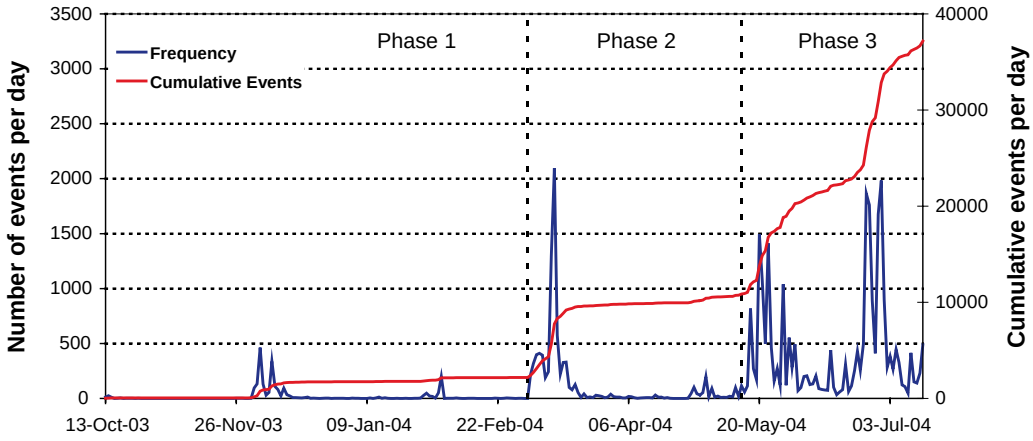

Figure 5-6. *Temporal distribution of AE triggers at the APSE between 13 October 2003 and 14 July 2004. Noise events have been removed from the data. Phases of the experiment, described in Table 1-1, are also indicated.*

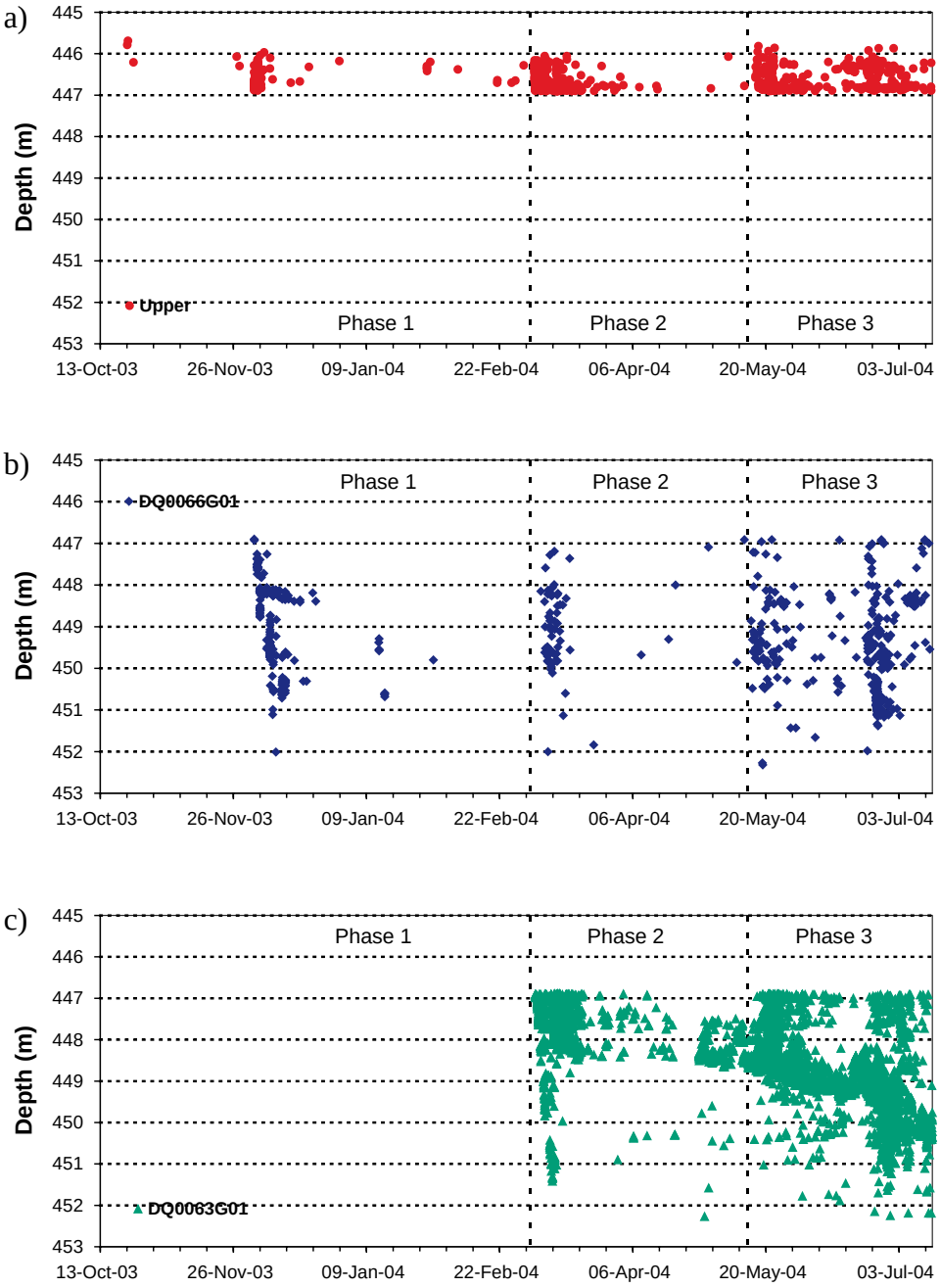

Figure 5-7. *Chainage plots of (a) 1,154 events in upper region near tunnel (above 446.9 m); (b) 918 events in lower region (deeper than 446.9 m) in damaged zone adjacent to deposition hole DQ0066G01; (c) 13,143 events in lower region (deeper than 446.9 m) in damaged zone adjacent to deposition hole DQ0063G01.*

5.2.2 Acoustic emission hit counts

Hit counts are measured per recording channel on the Hyperion Monitoring System. A 'hit' occurs on a channel when the observed amplitude goes above a pre-set voltage threshold on that channel. Therefore, interpreting the number of hit counts is a way of determining activity rates close to each sensor that may not be represented in triggers or located events.

Appendix 3 contains histograms of hit counts for all receivers over the whole experiment. Figure A3-1 uses a maximum scale range of 10,000 counts per day on the y-axis in order to compare all channels. Figure A3-2 uses an automatic y-axis scale range so as to visualise smaller variations on individual channels.

An example plot showing the hit counts for receiver 9 is displayed in Figure 5-8. This receiver is positioned at the top of borehole KQ0065G04 close to deposition hole DQ0066G01. During background monitoring no activity was recorded. There is then a relatively small increase in the number of events during excavation of deposition hole DQ0066G01 reaching a maximum of 751 counts per day. A much larger increase is observed during excavation of deposition hole DQ0063G01 where a peak of 8,705 events per day is reached. This decays away over approximately two weeks. An increase in the number of counts is also observed between 24 January and 4 February 2004, during what is believed to be the pressurisation phase of DQ0066G01 prior to excavation of DQ0063G01.

Heating of the pillar causes increased activity occurring in two sets between 16 May and 1 June and 17 June and 17 July. The sets of activity correspond two heating periods; the second period being caused by an increase in thermal output by the heaters used. Peak levels of activity are very similar, being 5,349 in the first phase and 5,418 in the second phase.

Channels 13–16 show consistently low hit counts believed to be due to the fracture noted in Section 5.1. Channel 14 is consistently active throughout much of the experiment.

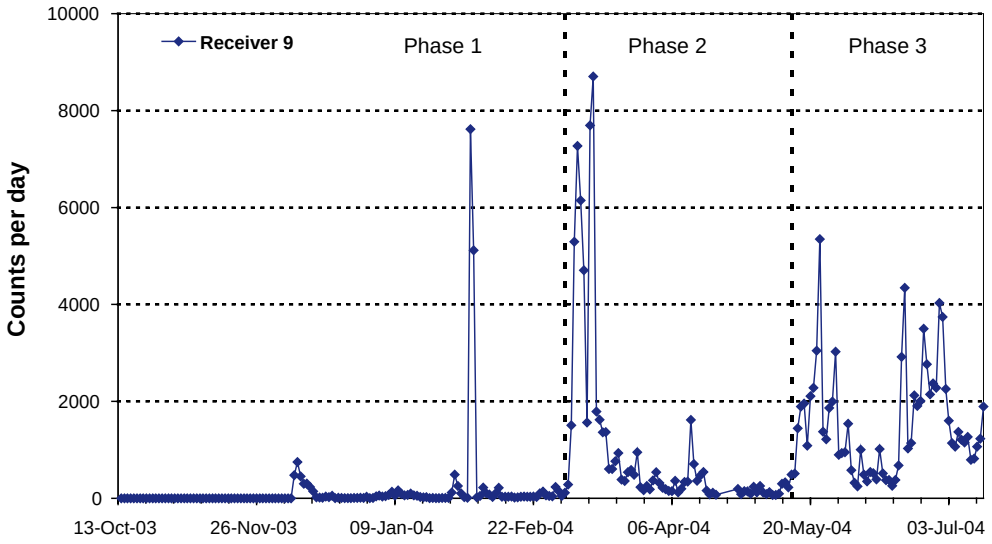

Figure 5-8. *Count rate per day for receiver 9. Day is set to between 21:00 and 06:00 in order to avoid noise. Values were manually checked for large numbers signifying some form of noise.*

5.2.3 Accuracy of acoustic emission locations

To test the source location accuracy of the array geometry a set of calibration shots were performed down deposition hole DQ0063G01. The shots used both pencil-lead breaks and screwdriver hits as ultrasonic sources.

Locations for the screwdriver hits are shown in Figure A4-1 in Appendix 4. A 'screwdriver hit' is produced by manually applying a sharp tap on the rock with the metallic operational end of the screwdriver. Each hit results in an event being recorded on the acquisition system. These have then been located using exactly the same parameters as used in the acoustic emission (AE) processing. The shot positions are well clustered. Each set of calibration hits varies on average only 0.05 m from the mean of those points (Table A4-1 in Appendix 4). The standard deviation for all the shot locations from the average in each cluster is only 0.04 m. This is believed to be a good representation of the location accuracy for the acoustic emission processing.

From experience gained in other experiments it was observed that this source is lower frequency and much higher magnitude than the real AEs recorded around the deposition hole. In order to also test the sensitivity of the array to very small magnitude events a pencil lead source was also used at points within the borehole. Pencil lead breaks are often used as standard calibration sources for ultrasonic transducers in the laboratory /e.g. Breckenridge et al. 1990/. The method uses a breaking 0.5 mm HB lead from a Pentel ratchet pencil orientated at approximately 45° to the deposition hole surface. In a laboratory sample of a few centimetre dimensions such a source is regarded as high magnitude. In the case of deposition hole monitoring however, where source-receiver distances are often > 2 m, it is a very low magnitude source. Therefore, manual picks of P- and S-wave arrivals were undertaken for the pencil lead breaks.

The pencil lead tests allow an estimate of the scale of cracking that AEs represent. Although at present it is not possible to directly compute AE source dimension from recorded waveforms, the fact that pencil lead tests can be recorded at all indicates that the array can record cracking down to millimetres in dimension. Instrument Magnitudes /Pettitt et al. 2004a/ have been calculated for all located events in this study (see Section 5.2.1). This scale is not calibrated to a seismological scale such as moment magnitude (M_w). AE magnitudes computed around the deposition holes are in the range $-0.7 < M_I < 0.8$. The pencil lead tests are at the lowest end of this scale in the range $-0.5 < M_I < -0.4$ and represent failure on a source region of approximately 1 mm. The ultrasonic system is hence able to record AEs from fractures that are of the order of millimetres; approximately the grain size of the rock.

5.2.4 Outlying events

There are four regions of events which lie a significant distance from the pillar volume between the deposition holes. Figure 5-9 shows all AEs located, including these outliers, and four regions are identified. Manual checks have been performed on the arrival picks of these AEs and have been found to be accurate. Figure 5-9 also gives some example waveforms. It is believed that the development of breakout zones during and after excavation of the second deposition hole results in some of these events being mis-located by a heterogeneous velocity zone.

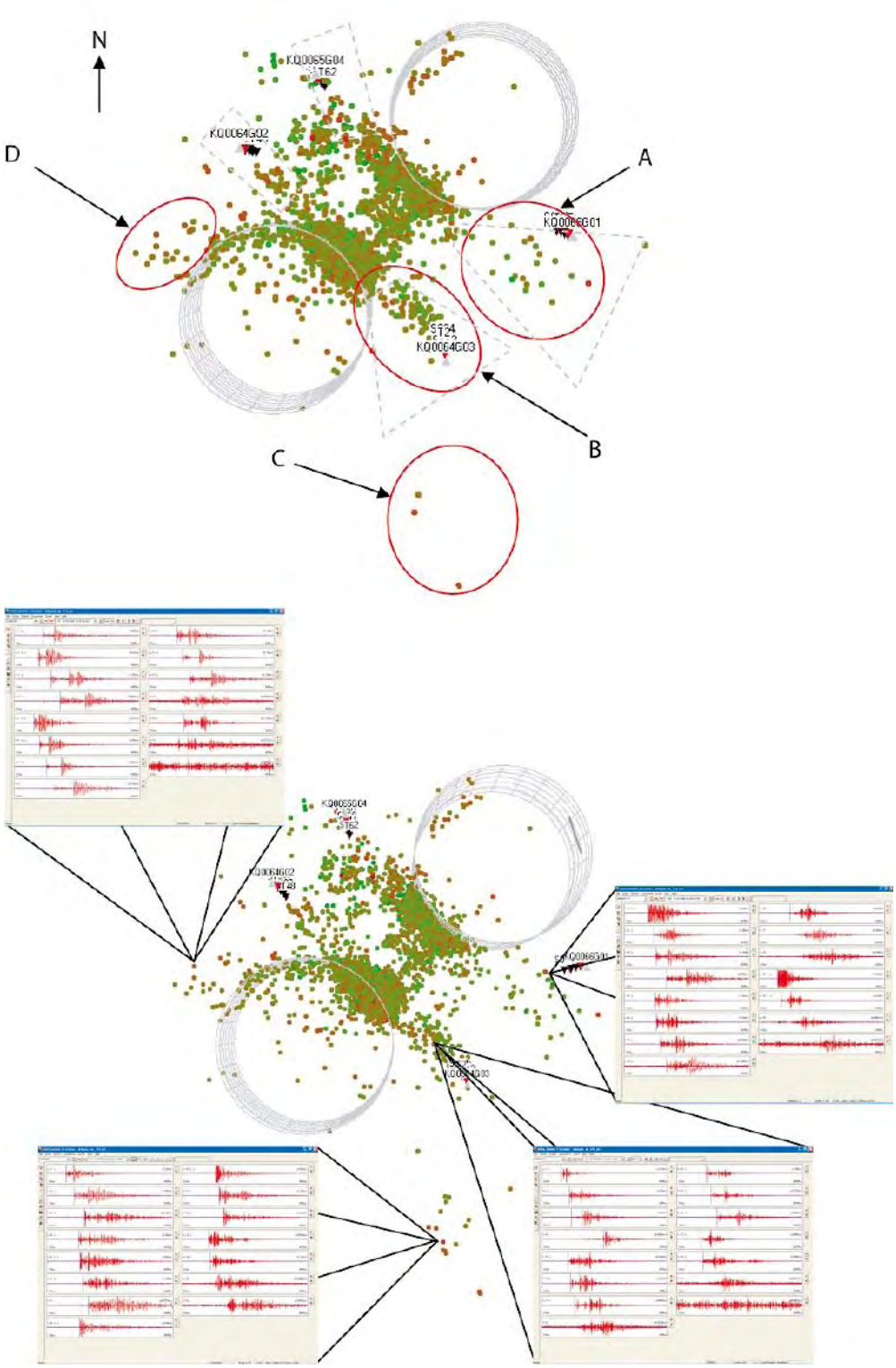

Figure 5-9. *Plan views of AE locations, including observed outlying events. Top view shows four regions of outliers circled in red. Bottom view has example waveforms demonstrating accuracy of picks.*

- Group A are a scatter of diffuse events that may locate along a sub-vertical feature (Feature 1), described in Section 5.2.1. These events may also not be located correctly and may actually be closer to the deposition hole (DQ0066G01) wall and damage zone. They occur predominantly in the later stages of the experiment (after May 2004) during heating. Raypaths from these events to the instrumentation boreholes on the opposite side of the deposition holes travel through the breakout zone resulting in a heterogeneous velocity structure along the ray path. When the events are located the algorithm assumes straight raypaths and a homogenous-isotropic velocity structure resulting in the AE locations being pushed outwards.

- Group B events locate down the full length of deposition hole DQ0063G01 and are equivalent to the Group A events above.

- Group C events are located a relatively long distance from the pillar volume (4 m) close to the floor of the tunnel, or perhaps around a borehole at this position.

- Group D events predominantly occur during excavation of deposition hole DQ0063G01 and may locate in a tensile zone induced by excavation. These events are also located close to Feature 2 near the tunnel floor. These locations may be mis-located further into the rock volume as ray paths to some of the instruments have to bend around the deposition hole volume.

For Groups A and B, volumes of increased location uncertainties have been estimated (dashed volumes on Figure 5-9) where ray paths are believed to be significantly effected by passing through the entire damaged zones, across to instrumentation boreholes on the opposite side of the pillar volume. Events that lay within these volumes have been removed from the data set if they occur after 3rd March 2004 (start of excavation of DQ0063G01), and beneath 1 m depth below the tunnel floor (i.e. outside of induced damage observed immediately below the tunnel). Group C events have been removed from the data set as they occur in a volume not associated with the pillar. Group D events have been retained as they are believed to be relevant to the data interpretation.

5.2.5 Magnitudes and b values

Instrument Magnitudes /Pettitt et al. 2004a/ have been calculated for all located events. The range of magnitudes during the experiment is between –0.712 and 0.778 (the screwdriver hits and pencil breaks described in Section 5.2.3 have mean magnitudes of approximately 0.05 and –0.4 respectively). Figure 5-10 shows four plots of AE events, grouped according to instrument magnitude. ‘Quartiles’ were used to define the limits; therefore there is approximately the same number of events in each plot. The plots show a very similar distribution of AE locations for all magnitude ranges. This result indicates that the AE locations presented here are unbiased by array sensitivity, as sensitivity variations would result in larger numbers of smaller magnitude AEs being recorded in different parts of the rock mass. The plots also highlight that there is no preferred spatial distribution to the largest events, but instead these are distributed throughout the regions of high activity. This suggests that there is no intense focus of high stresses in the volume.

Figure 5-11 is a histogram of instrument magnitude. The mode value of instrument magnitude is –0.19 with 689 events between –0.18 and –0.20. There is a consistent high frequency in the range –0.18 and –0.08. In Figure 5-12 the b-value for the located events at the APSE has been determined. The inset graph shows a plot for the whole range of magnitudes. The slope of the graph between $M_I = 0$ and 0.7 gives a b = 4.381. This is much higher than earthquake seismology where b-values are usually around 1.0. However, it is a similar magnitude

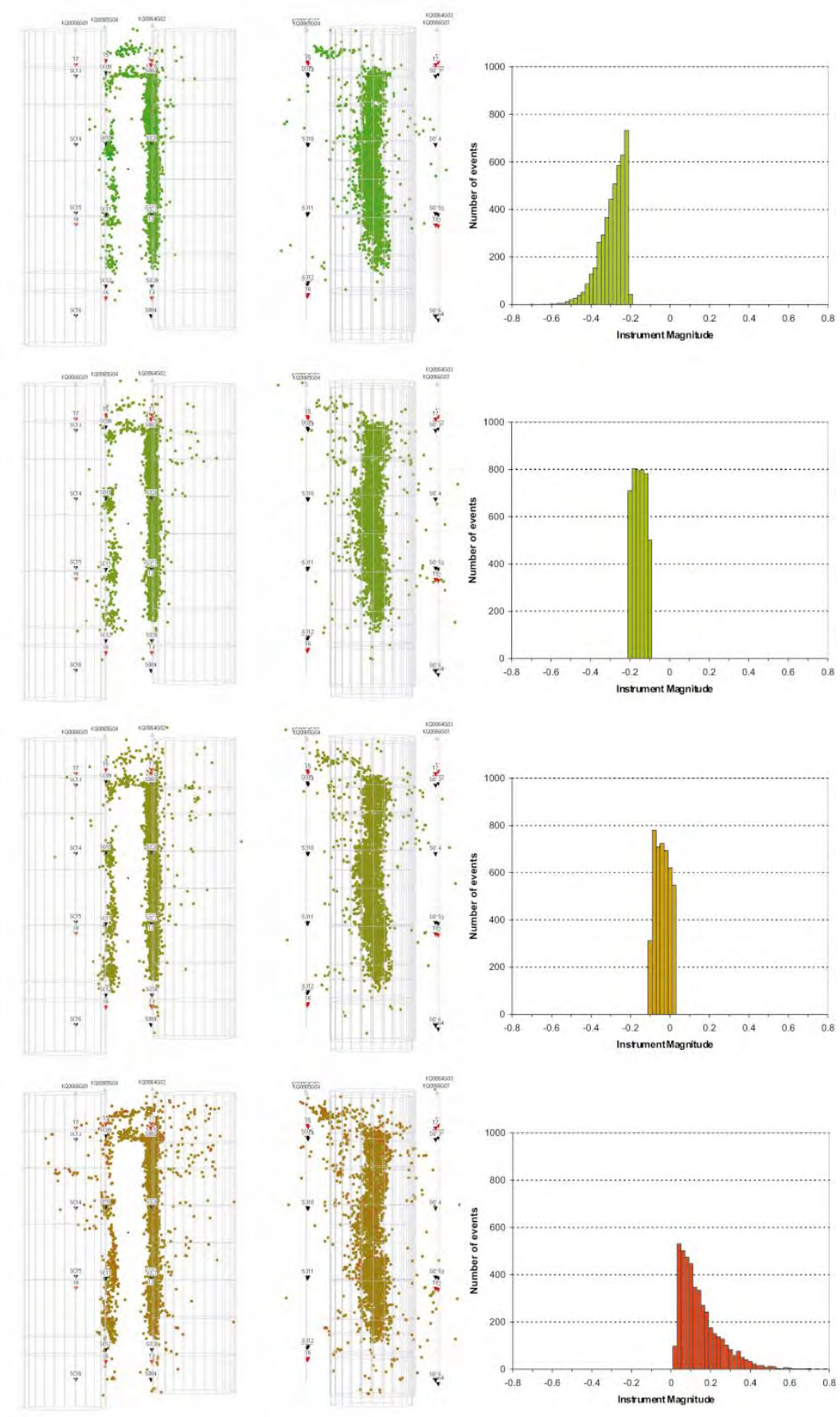

Figure 5-10. *AE locations and histograms in groups according to instrument magnitude. (a) 1st Quartile: Mi < –0.2184; (b) 2nd Quartile: –0.2184 < Mi < –0.1064; (c) 3rd Quartile: –0.1064 < Mi < 0.01844; (d) 4th Quartile: 0.01844 < Mi.*

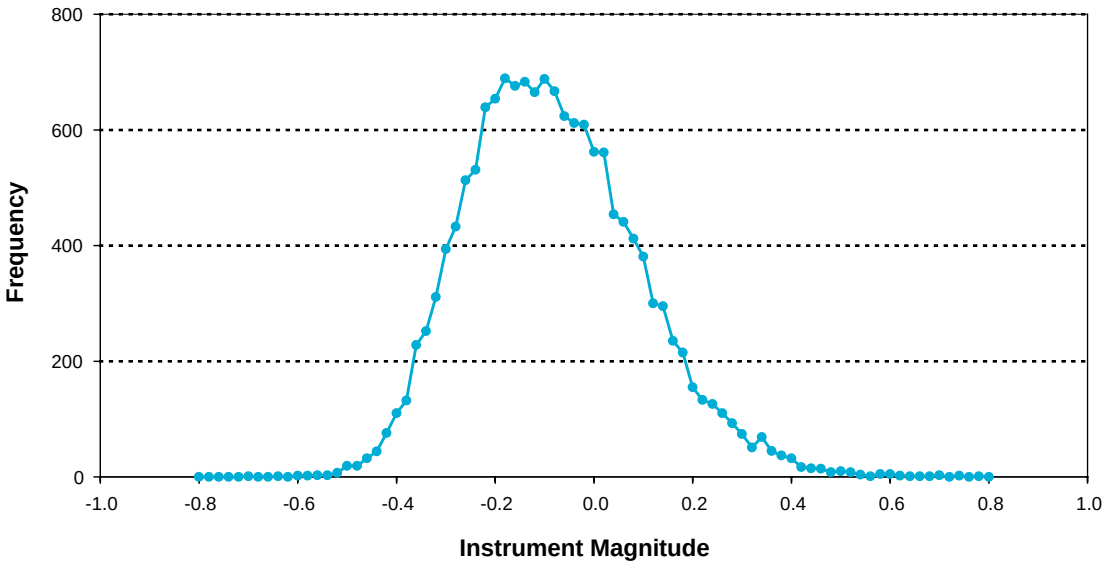

Figure 5-11. *A frequency histogram of instrument magnitudes for 15,198 located events.*

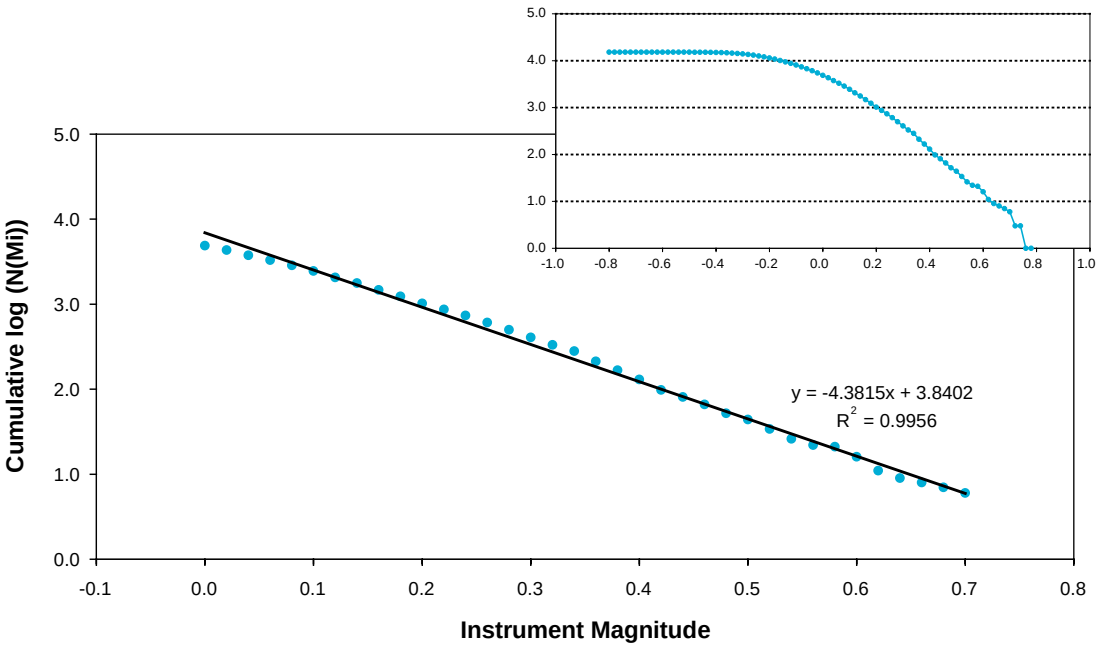

Figure 5-12. *b-value plot of instrument magnitudes for all 15,198 located events.*

to b-values recorded in other high-frequency AE experiments /Pettitt 1998/ and in dynamic numerical models of rock fracture /Hazzard 1998/. Research is currently on-going regarding why b-values recorded during rock fracture are much higher than earthquake seismology /Young et al. 2004/. The data set recorded here represents a good opportunity for this type of research.

5.3 Phase 1: Excavation of deposition hole DQ0066G01 and confinement

Figure 5-13 displays cumulative plots of the 282 AEs located from excavation of deposition hole DQ0066G01. In the first 3 m of excavation (Figure 5-13a–c) events locate sparsely down the pillar side of the deposition hole wall and beneath each excavation step. There is one relatively tight cluster of events at approximately 1 m depth (I). This corresponds to the intersection of a near horizontal feature that is mapped by the AE results throughout the experiment. There is also a cluster of events at approximately 1 m distance from the deposition hole wall and 0.5 m depth (II). These are believed to locate close to the tunnel rock floor (beneath the concrete roadbed).

The number of events recorded gradually increases during the first 3 m of excavation, however there is then a period of quiescence during excavation of the following 1.6 m (Figure 5-13d–e). A large cluster is then observed at approximately 3.6 m from the top of the deposition hole (III), when excavation reaches 4.8 m depth (Figure 5-13f). The cluster is hence not close to the region of excavation, but instead 1.2 m behind. This activity is probably a result of spalling as stresses increase in a weaker part of the rock mass. During the final round events occur in regions previously active. Very few events are located in the deepest section of the deposition hole. In the week following excavation, the events predominantly occur in two clusters at approximately 2.8 m and 5 m depth (IV).

The activity observed here qualitatively correlates with spalling observed inside the deposition hole after excavation /Staub et al. 2004/. The lack of activity observed on the opposite side of the deposition hole to the pillar is due to that part of the rock mass being shadowed from the transducer array by the excavation void. The transducer array is focussed on the pillar volume (Section 3.2) so it should be assumed that a pattern of damage similar in style to that observed here is also occurring on the opposite side to the pillar.

Activity decays rapidly after excavation is completed, (Figure 5-14) decreasing to sporadic clusters (of approximately 10 events) after two weeks. An average of only 0.48 events per day were recorded during January 2004. In early February a water-filled bladder was installed in the deposition hole and on 4th February the pressure inside the bladder was increased to 0.7 MPa applying confinement to the deposition hole walls. The average number of events per day between the confinement of DQ0066G01 and excavation of DQ0063G01 on 3rd March is 0.21. There were only 6 events recorded during that period, with a peak of 2 events on 21 February 2004. This demonstrates that a drop in event rate followed confinement of the first deposition hole, although the event rate was already quite low in the month prior to confinement.

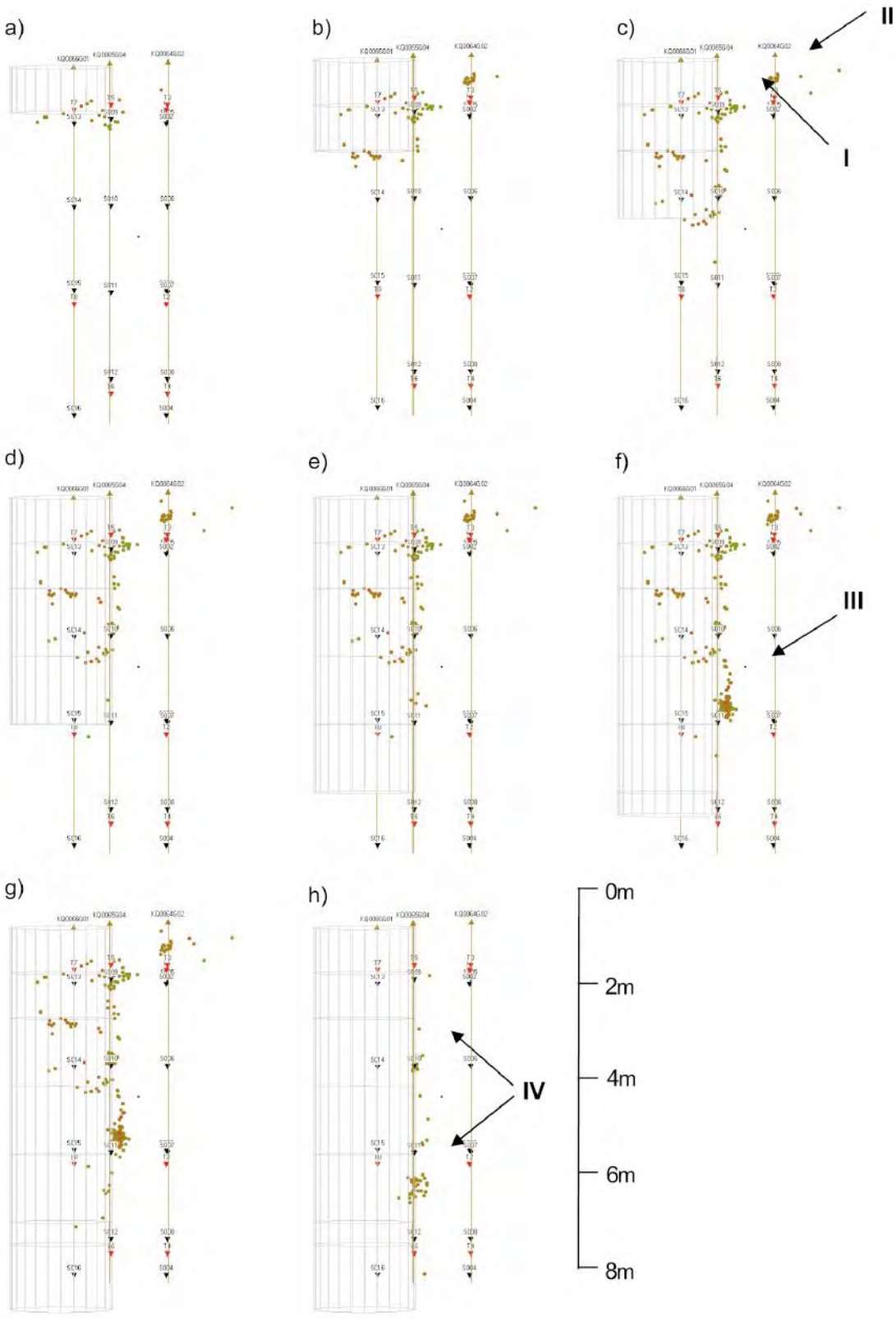

Figure 5-13. *Located events during excavation of deposition hole DQ0066G01. Views a to g show cumulative events recorded for each round from 02-12-2003 20:20 to a) 03-12-2003 08:29; b) 04-12-2003 07:44; c) 05-12-2003 07:19; d) 06-12-2003 09:24; e) 07-12-2003 09:37; f) 08-12-2003 10:21; g) 09-12-2003 10:21. The last view, h, is for one week after excavation between 09-12-2003 10:21 and 16-12-2003 10:21.*

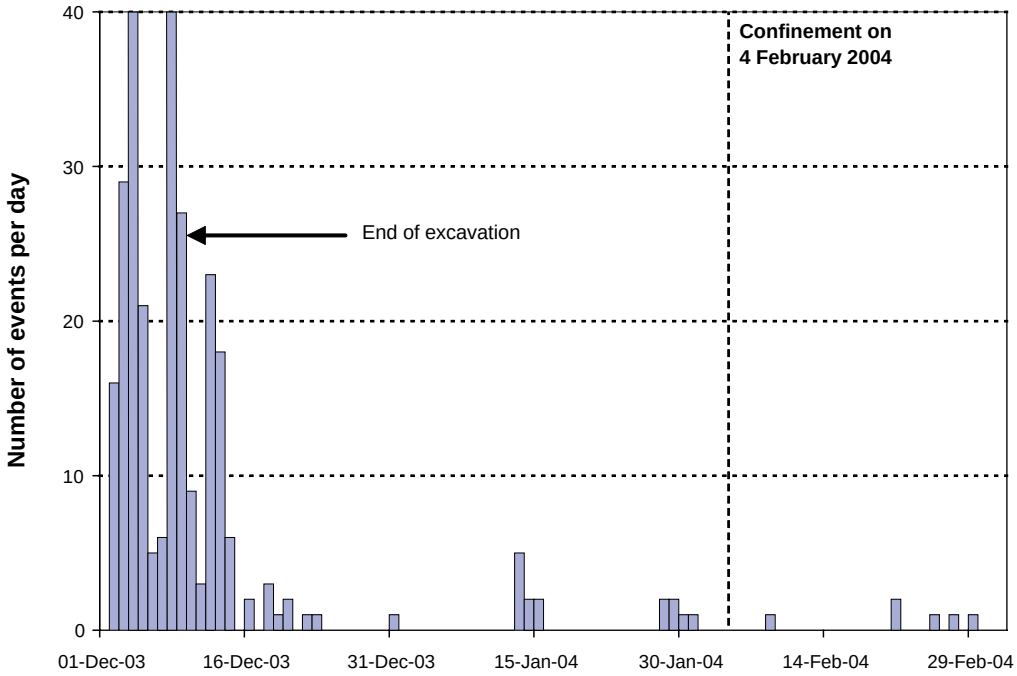

Figure 5-14. *AE located event rate for the period between 1 December 2003 and 29 February 2004. The time of confinement of DQ0066G01 to 0.7 MPa is shown.*

5.4 Phase 2: Excavation of deposition hole DQ0063G01

Figure 5-15 shows cumulative plots of AEs located during drilling of the second deposition hole, DQ0063G01. The development of two features in the pillar, close to the tunnel floor, can be observed creating a 'bridge' of activity crossing between the two deposition holes (V). The AEs are either located on two sub-horizontal features or on a single plane with a dip of approximately 20° in a NE direction. The uppermost events correlate with the rock floor of the tunnel, beneath the concrete roadbed. The lowermost events correlate with a 'shearzone' mapped in the sidewalls of the deposition holes /Staub et al. 2004/. The AEs located here are an extension of activity observed during excavation of the first deposition hole, DQ0066G01 (Section 5.3). During the first 2.4 m of excavation (Figure 5-15a–c) AEs are also observed to locate sparsely down the pillar side of the deposition hole and beneath each excavation step, in a similar pattern to that observed during the upper few metres of the first deposition hole. Events are also observed to locate on the first deposition hole during excavation of the second one. AEs on DQ0066G01 follow the depth of the excavation steps during excavation of DQ0063G01. This result indicates that a disturbance of the stress field around deposition hole DQ0066G01 is occurring, caused by excavation of the second hole. The 0.7 MPa of confinement pressure in the that hole probably acts to reduce the amount of damage, and hence AEs, created.

After 9th March (Figure 5-15g–i) a zone of intense AE activity is observed (VI), extending from close to the top of the deposition hole, at the rock floor level. As the excavation progresses the zone is observed to migrate down the hole. When the deposition hole has been completed the events extend from the surface to 2.5 m (below the level of the concrete roadbed). This pattern of activity is not matched on the confined hole where induced stresses would be expected to be of similar magnitudes. This result therefore suggests that the confinement pressure applied is sufficient to inhibit breakout occurring. The AE activity correlates well with a zone of breakout damage observed in the open hole after excavation /Andersson 2004/

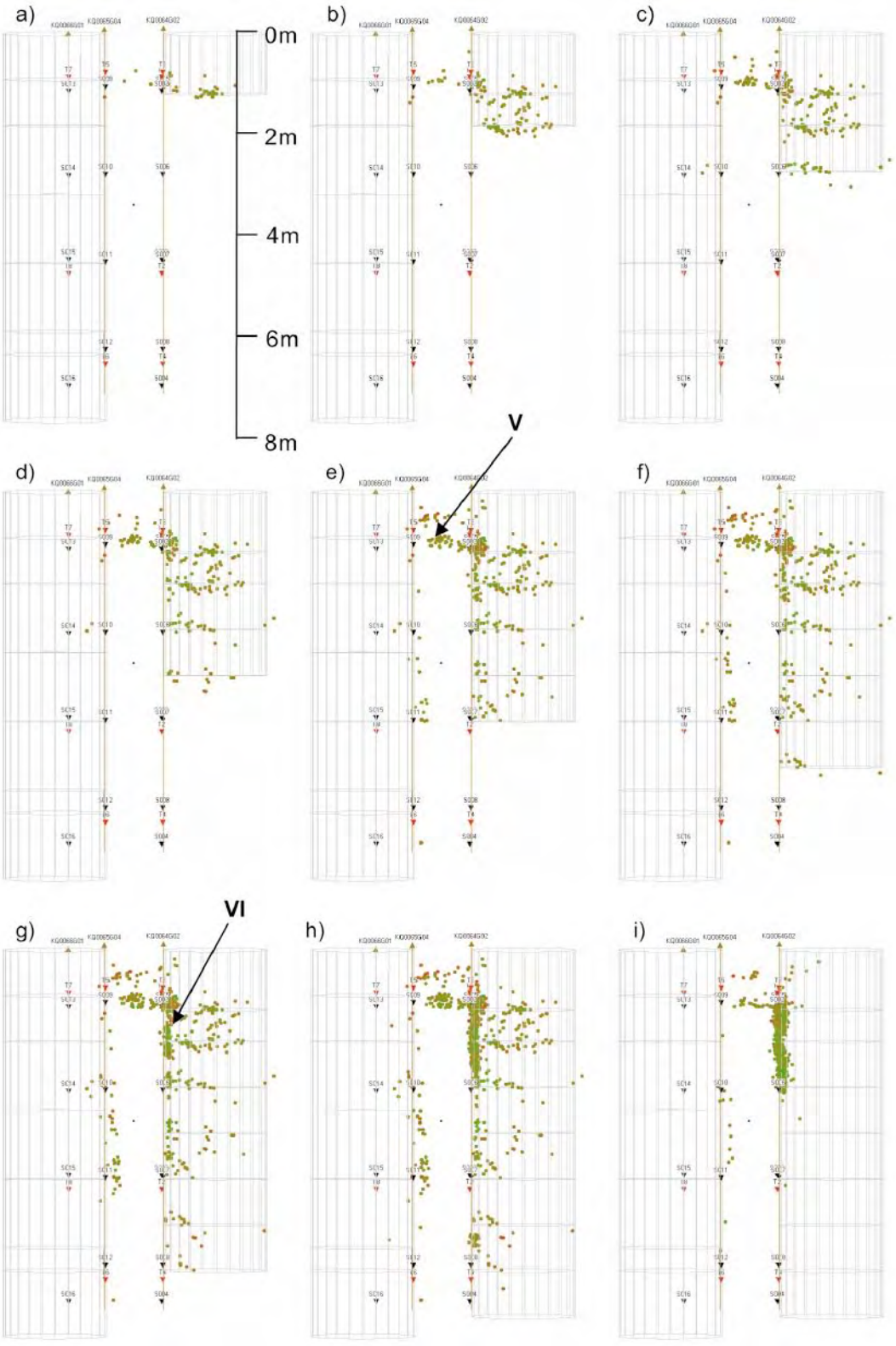

Figure 5-15. *Located events during excavation of deposition hole DQ0063G01. Views a to h show cumulative events recorded during each stage of drilling between 04-03-04 19:30 and a) 05-03-04 08:00, b) 06-03-04 08:00, c) 07-03-04 08:00, d) 07-03-04 16:00, e) 09-03-04 08:00, f) 09-03-04 19:00, g) 10-03-04 15:00, h) 12-03-04 00:00. The last view, i), is for one week after excavation between 12-03-04 00:00 to 19-03-04 00:00.*

Figure 5-16 shows the AE event rate during the period of excavation for each of the deposition holes. In the first deposition hole the greatest event rate is observed close to the end of excavation at 5.5 m depth, where the rate reached approximately 120 events per hour. In the second deposition hole the event rate reaches its peak after excavation has been completed (224 Events per hour at 05:00 on 12 March 2004). This activity is observed in the breakout zone discussed above. The event rate decays rapidly after excavation is completed for the second deposition hole reducing to sporadic clustering after two weeks. This behaviour is similar to that observed in the first hole.

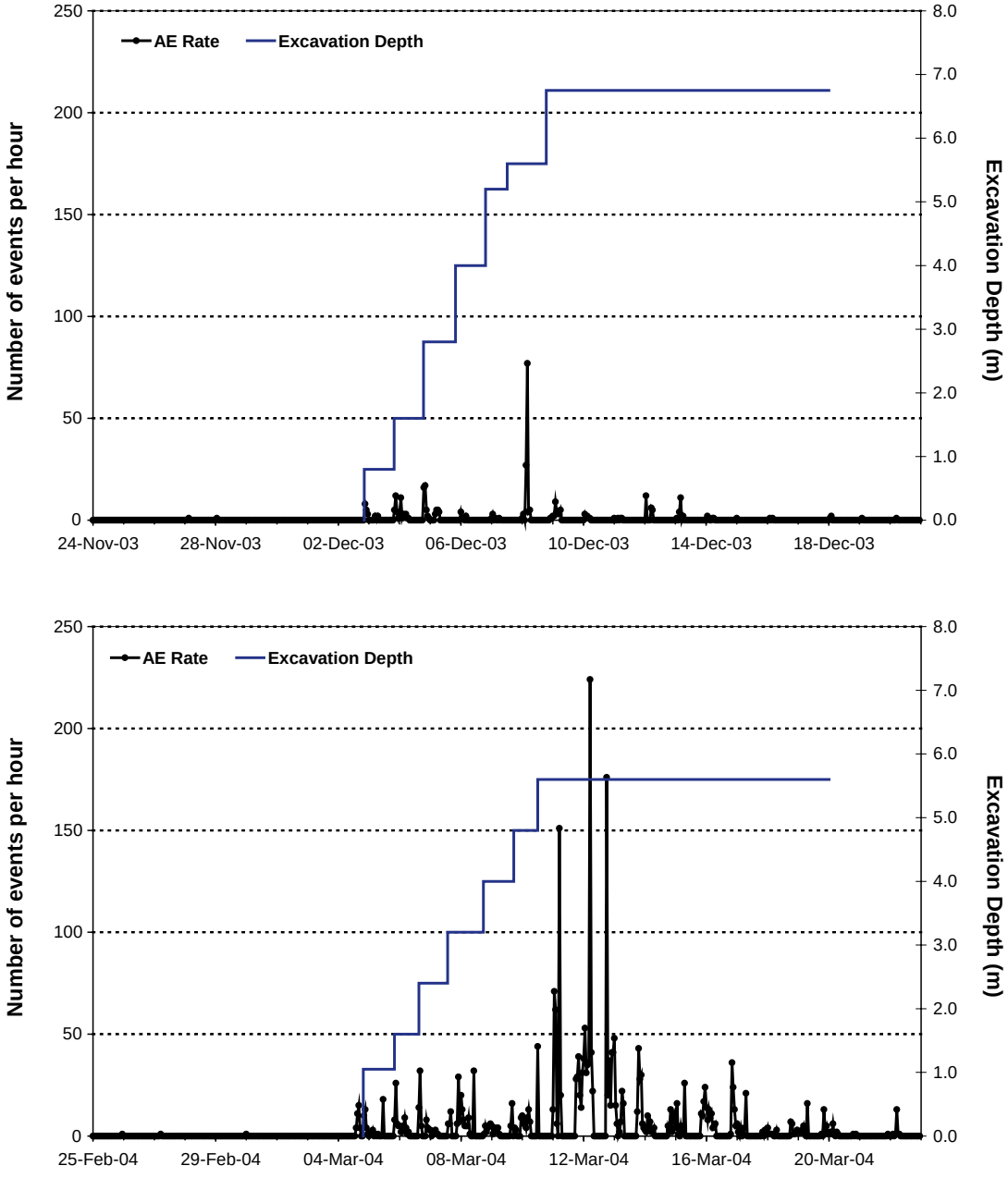

Figure 5-16. *AE located event rate during excavation of the deposition holes: a) DQ0066G01 and b) DQ0063G01. Also shown is the excavation depth of each deposition hole.*

The spatial-time dependency of the AE locations is displayed in Figure 5-17. During the first 3 m of excavating deposition hole DQ0066G01 (to 5th December) the majority of the events locate at the depth at which excavation is occurring. After this point, events are delayed in time with respect to the excavation period and locate down the length of the hole some days after excavation. This occurs in clustered regions indicating a slow degradation of the rock mass. This pattern of continued clustering has been observed in previous monitoring experiments in the Prototype and Retrieval tunnels /Pettitt et al. 1999ab/.

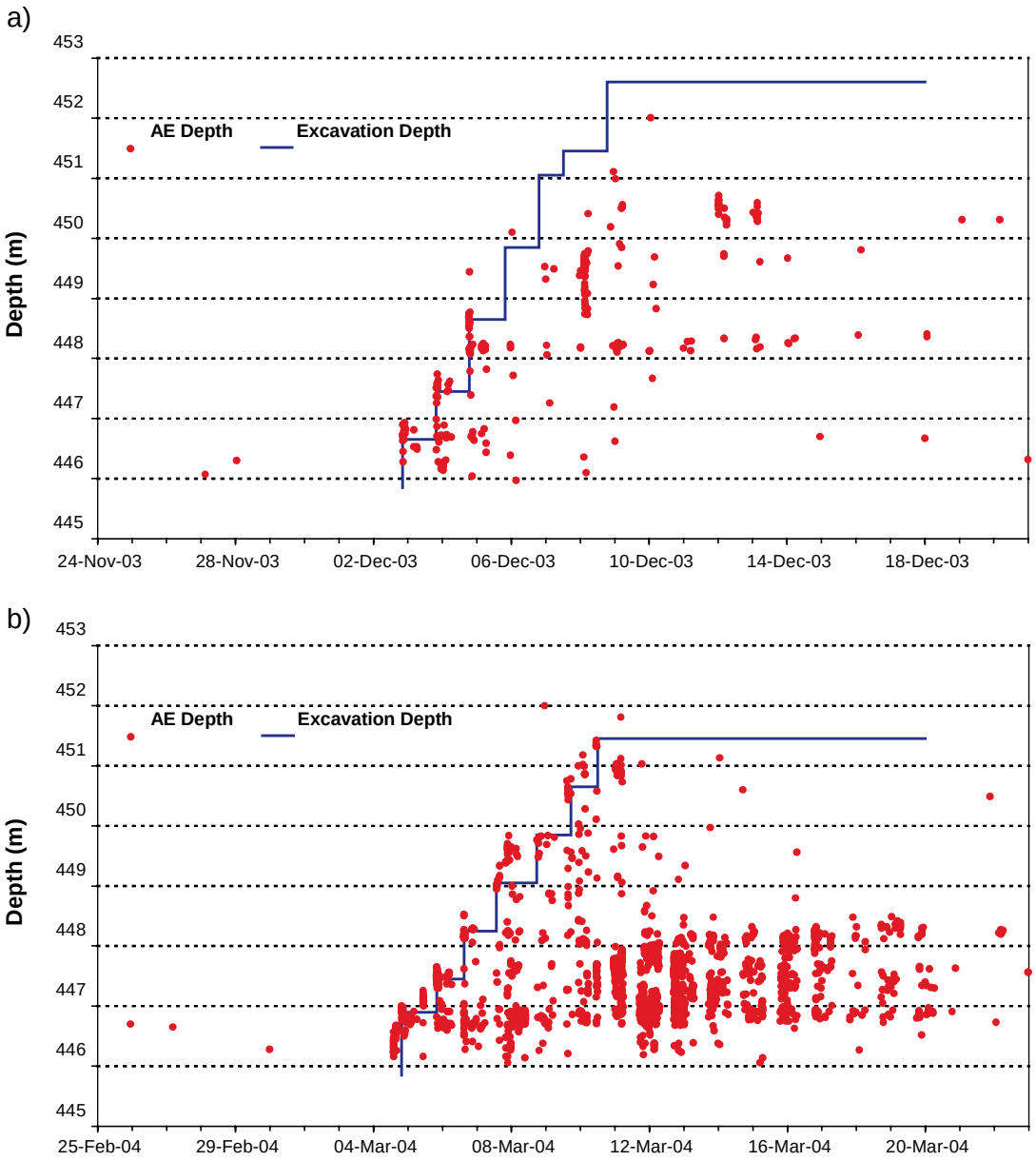

Figure 5-17. *Acoustic emission time dependency for a) DQ0066G01 and b) DQ0063G01. Red markers are AE depth with time. The solid blue line is the excavation depth with time. Note that depth is increasing in the vertical axis.*

Deeper rounds (> 451 m – or 5 m below the concrete floor) do not show this pattern as few events occur during excavation, or in the following days. The largest concentration of events (196) is positioned between 448.35 m and 448.85 m (2.5–3 m depth) shown by Figure 5-18a with activity occurring throughout the excavation period. This coincides with the cluster of events observed at 3 m depth in Section 5.3. The cluster of activity observed at 3.6 m depth occurs almost completely on 8 March between 02:00 and 04:00, and is represented by a peak of 168 events between 449.85 m and 450.35 m (4–4.5 m depth).

Unlike in the first deposition hole, events in the second deposition hole occur down its length as excavation progresses (Figure 5-17b) indicating that induced stresses must have increased due to the neighbouring void. The histogram in Figure 5-18b shows most events occur between 446.85 m and 448.35 m, nearly 2,000 AEs locating in a 1.5 m depth. The AE's occur in large numbers several days following excavation and are almost exclusively in the top 2.5 m breakout zone discussed above. Many events continue to be located in this zone a week after drilling ceases. Figure 5-19 shows how the acoustic emission locations build up during 4 rounds of drilling. During excavation of round 3 most events occur in the top 2 m of the deposition hole. When Round 5 is excavated, many events still locate in the top 2 m but some are occurring at greater depths.

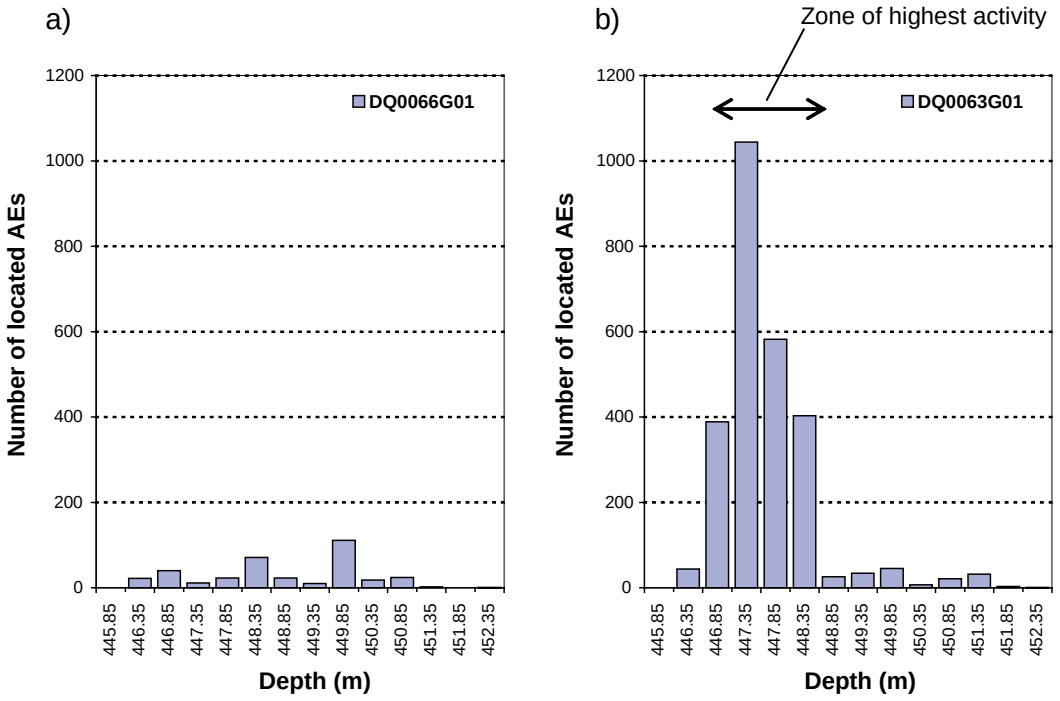

Figure 5-18. *Distribution of AE locations with depth for: a) deposition hole DQ0066G01; b) deposition hole DQ0063G01. Each depth increment represents 0.5 m.*

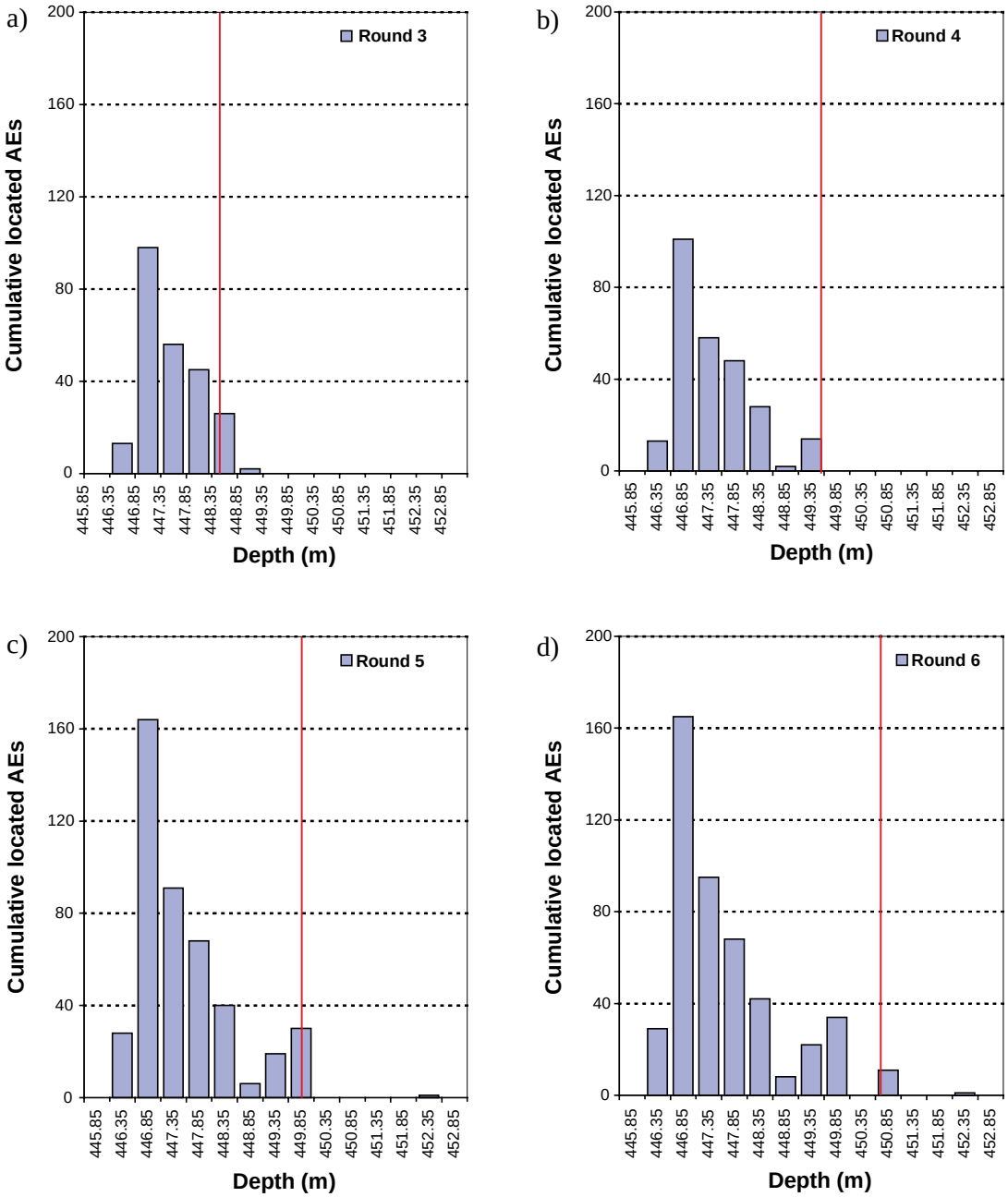

Figure 5-19. *Four histograms showing the cumulative development of acoustic emissions along deposition hole DQ0063G01. (a) Events up to excavation of Round 3; (b) Events up to Round 4; (c) Events up to Round 5; and (d) Events up to Round 6. The plots correspond to locations (c), (d), (e), and (f) respectively in Figure 5-15. Red vertical lines indicate the depth reached after excavation of each round.*

Phase 3: Pillar heating

Heating of the pillar has used two pairs of boreholes located to the North-west and South-east of the deposition holes (Figure 3-3). The temperature in the rock has been measured by thermocouples in protective cuprum-nickel tubes, placed at the hole walls and in adjacent core boreholes. Symmetry of the layout means that it is possible to evaluate the contribution of each heater to any point in the pillar /Andersson et al. 2004/. Power supplied to the heaters was changed at various times during the experiment, given in Table 5-1.

Figure 5-20 shows the event rate during heating of the pillar. Red dashed lines show dates of changes to the heater settings, from Table 5-1. Relatively few events are recorded before the heaters are switched on (the analysis starts two weeks after excavation of deposition hole DQ0063G01 has been completed). Only about 3 events per day are recorded during this time. There is an initial increase in the event rate after 27th April 2004, however it is not until 17th May that the number of located events increases dramatically. This is three days after the heaters are switched on. It is not certain why the event rate increases at the end of April, but it may be associated with installation or testing of the heaters. On 23rd May a peak of 807 events are located. The high rate of activity continues until 2nd June 2004 when the number of events per day falls below 250 after a decrease in heater power. The final phase of high activity begins on 25th June 2004 as over 800 events are located. This is four days after the heaters are increased to maximum power. On the 2nd July 2004, the event rate reduces to below 200 events per day after a decrease in heater power. There is a consistent lag of a few days (3–4) between when the heaters are adjusted and when the rock responds to the adjustment.

AE locations are displayed in six periods (a–e) in Figure 5-21. The periods shown relate to observed changes to the cumulative number of events in Figure 5-20. Figure 5-22 gives ‘chainage’ plots for the three volumes discussed in Section 5.2.1; in the upper 1 m and around each of the deposition holes.

a) During the period 23rd March to 28th April the events that occur on the open deposition hole (DQ0063G01) are primarily located in the breakout zone created during excavation and extending to approximately 2.5 m depth beneath the tunnel floor[1] (see the previous section). Only a few events occur on the confined deposition hole (DQ0066G01).

b) After heating commences (in the period up to 17th May) a tight cluster of events forms on DQ0063G01. This extends approximately 0.5 m below the previous level of breakout.

c) As the temperature increases (17th May to 2nd June) this cluster grows larger, extending upward to the rock floor of the tunnel and downward to approximately 449.5 m depth (3.5 m below the tunnel floor). See Figure 5-22c. A large number of events also locate on the features crossing the pillar in the first 1 m beneath the tunnel floor. The event rate on the other deposition hole (DQ0066G01) increases.

d) After the heaters are reduced in power (2nd June to 25th June) the majority of events are situated in a cluster approximately mid way down deposition hole DQ0063G01. They do not extend as far up the deposition hole as during the previous phase but loose clustering is observed at greater depths. Events also locate in the wall of DQ0066G01, approximately positioned in the original clusters developed during excavation of this hole (Section 5.3).

[1] The tunnel floor is defined as the level of the concrete roadbed (a depth of 445.85 m).

e) When the heaters are increased (25th June to 3rd July) the events migrate down deposition hole DQ0063G01 reaching 451 m depth (5 m below the tunnel floor). Clustering has also developed on deposition hole DQ0066G01.

f) After 3rd July, leading up to the depressurisation phase, the events are occurring sporadically up the length of the open deposition hole, but in particular there is a cluster at around 450 m depth (4 m below the tunnel floor).

Table 5-1. Heating log for the APSE with dates and times of changes /Andersson 2004/. Location of heaters is shown in Figure 3-3.

Label	Date	Time	Left heaters (W/heater)	Right heaters (W/heater)
I	14 May 2005	09:40	1,300	1,300
II	1 June 2004	15:00	1,100	1,300
III	21 June 2004	10:30	2,300	2,600
IV	29 June 2004	10:30	1,700	2,600
V	19 July 2004	14:05	OFF	OFF

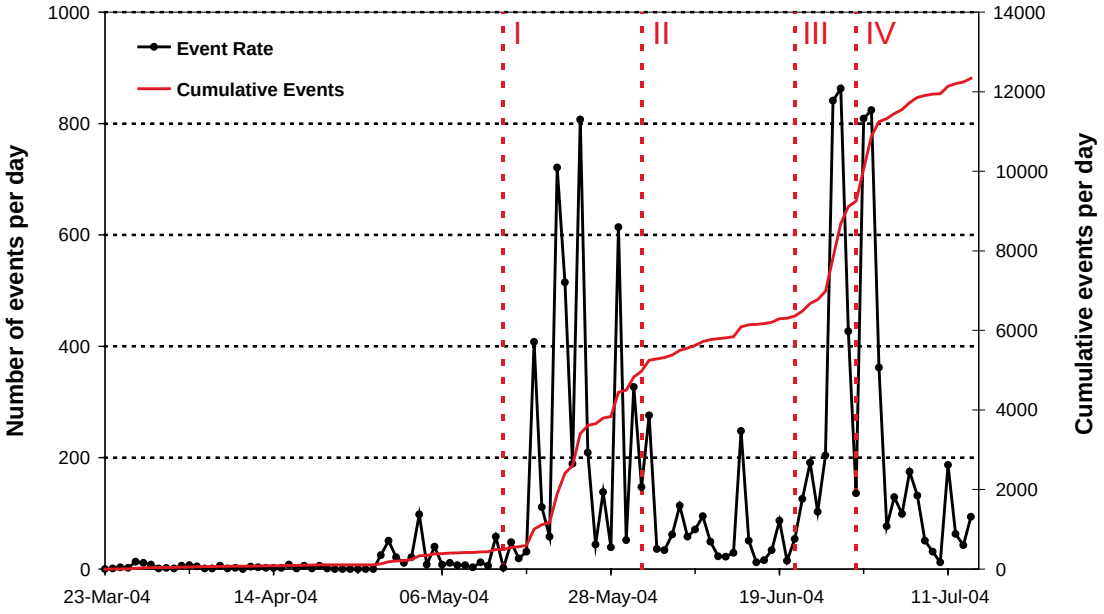

Figure 5-20. *AE located event rate during the heating phase of the experiment. Black line shows the event rate per day and the red line chows the cumulative event rate per day. Lines I to IV are related to changes in heater power from Table 5-1.*

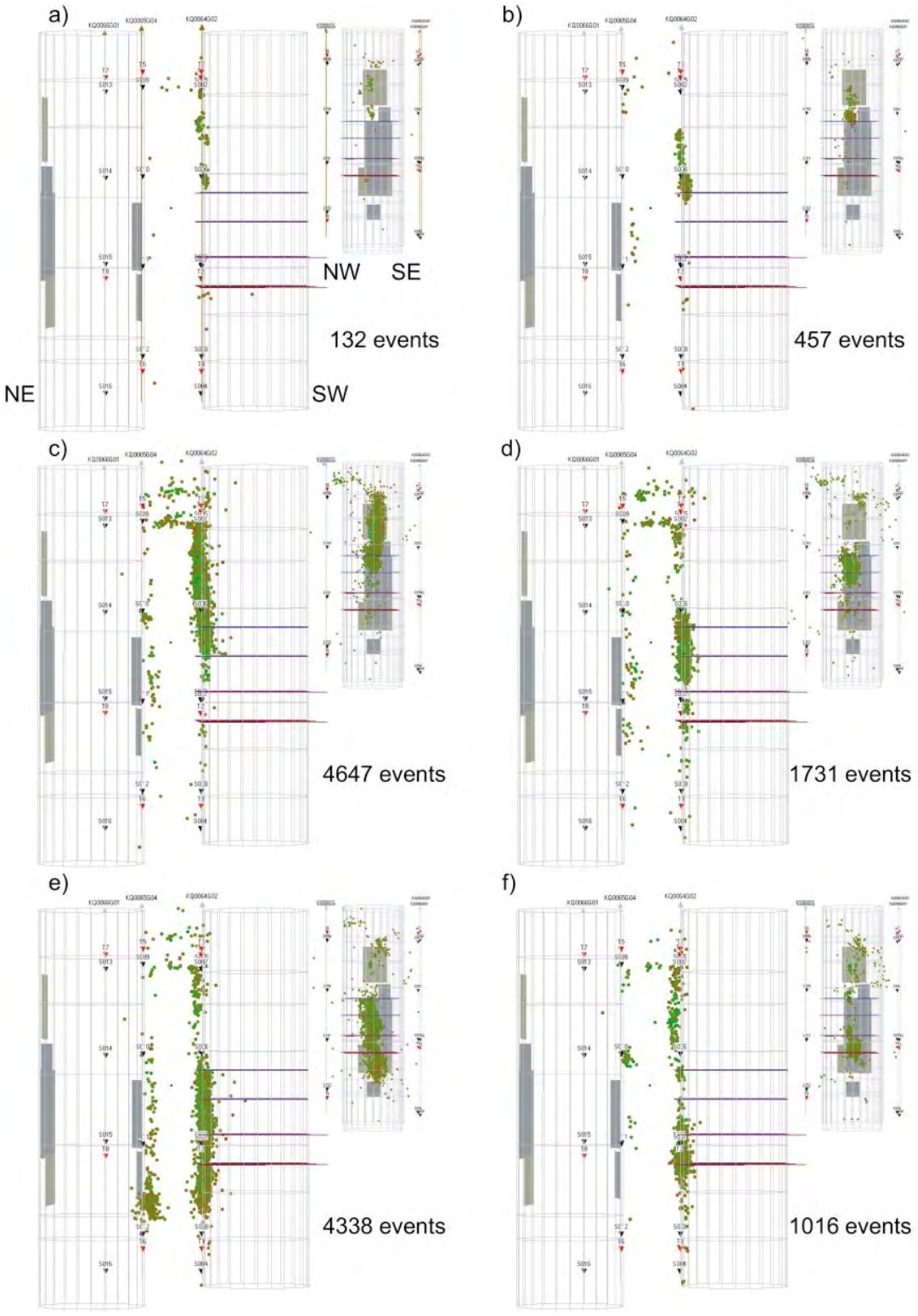

Figure 5-21. *AE events during the heating phase of the experiment. Dates are a) 23/03/2004 to 28/04/04; b) 28/04/04 to 17/05/2004; c) 17/05/2004 to 02/06/2004; d) 02/06/2004 to 25/06/2004; e) 25/06/2004 to 03/07/2004; f) 03/07/2004 to 14/07/2004. Main view is looking south-east. Inset is looking north-east. Grey shaded areas are steel plates used to cover the spalled zones created during the drilling of the first hole.*

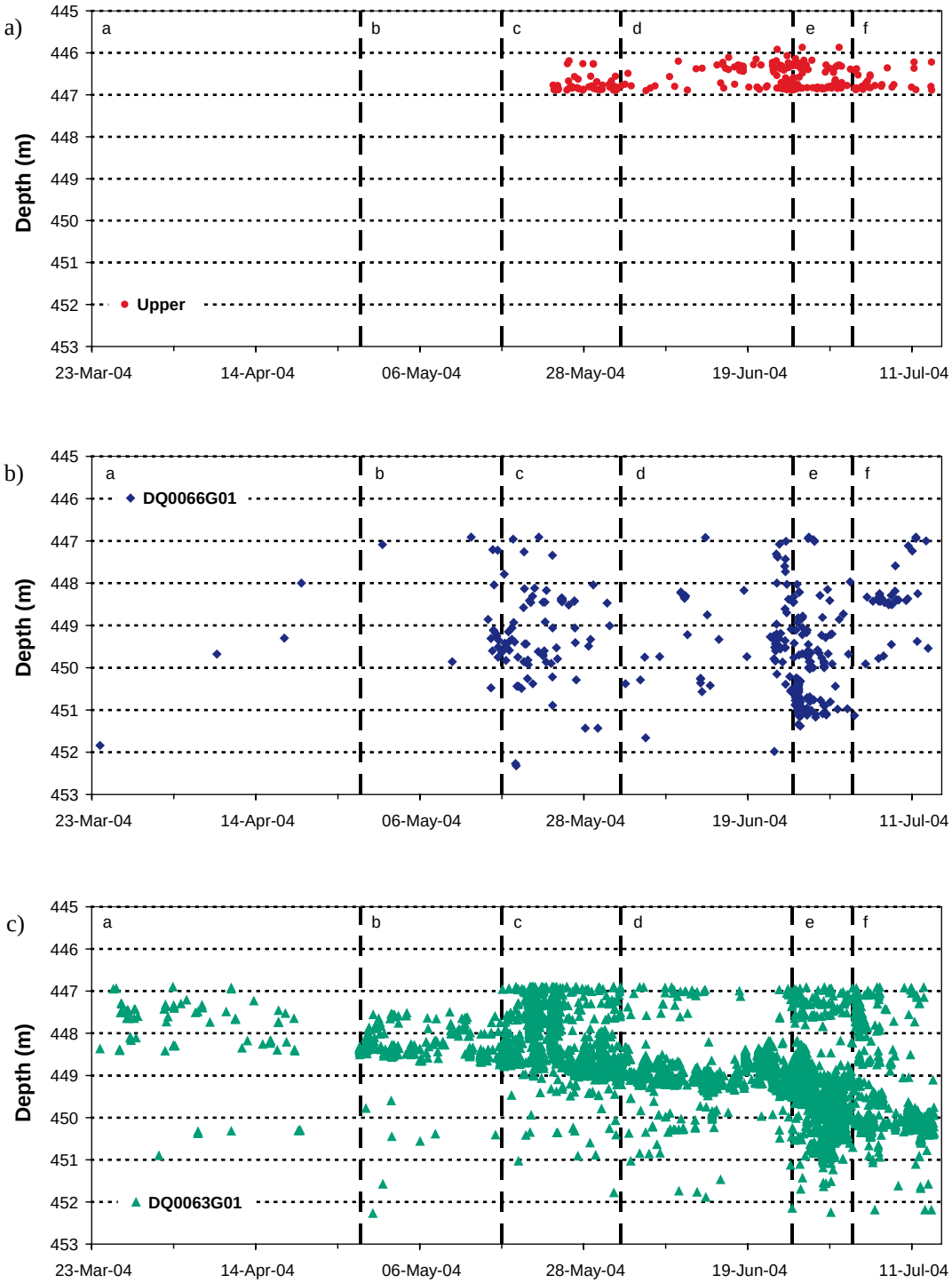

Figure 5-22. *Chainage plot of selected events during heating. (a) 250 events in upper region near tunnel (above 446.9 m); (b) 564 events in lower region (deeper than 446.9 m) in damaged zone adjacent to deposition hole DQ0066G01; (c) 11,198 events in lower region (deeper than 446.9 m) in damaged zone adjacent to deposition hole DQ0063G01. Time periods a–f are those used in Figure 5-21.*

6 Results from ultrasonic surveys

Ultrasonic velocity surveys were undertaken regularly during the whole of the APSE. The times of the surveys are described in Section 3.3. The survey on 10 December 2003 was chosen as the reference survey for the cross-correlation procedure described in Section 3.4. Velocity and amplitude results for every raypath that could be processed are plotted in Appendix 5 and 6. Velocities on some ray paths cannot be processed due to small P or S-wave signals. A list of the raypaths for which P- and S-wave velocity has been measured is displayed in Table 6-1 and includes 54 P-wave measurements and 23 S-wave measurements on 350 separate surveys. A graph is given for each raypath, and grouped for pairs of instrumentation boreholes shown in Figure 6-1.

A: Skimming deposition hole DQ0063G01
B: Centre of pillar
C: North west of pillar
D: South east of pillar
E: Skimming deposition hole DQ0066G01

Observed velocity and amplitude changes can be attributed to various factors and are caused by a change in the material's bulk properties. Table 6-2 gives the changes that would be expected during the Pillar Stability Experiment. It should also be noted that the raypaths used here travel through different volumes of the rock mass with the resulting signal depending on an accumulated effect along the entire raypath. In order to make a detailed interpretation of the measurements the velocity and amplitude variations need to be integrated with mechanical and thermal stress modelling. This integrated analysis has not been performed here, instead the results are summarised for each of the instrumentation-borehole pairs given above.

Table 6-1. Raypaths for which P- and S-waves could be computed for at least part of the period between 13th October 2003 and 14th July 2004.

Receiver	Pulser # 1	2	3	4	5	6	7	8
1			V_P	V_p, V_s	V_p	V_p, V_s	V_p	
2								
3			V_p	V_p	V_p	V_p		V_p
4			V_p, V_s	V_p	V_p, V_s	V_p		V_p
5	V_p	V_p			V_p, V_s	V_p	V_p	V_p
6	V_p	V_p, V_s			V_p, V_s	V_p, V_s	V_p	V_p
7	V_p, V_s	V_p			V_p	V_p, V_s		V_p
8	V_p, V_s	V_p, V_s			V_s	V_p		V_p
9	V_p	V_p, V_s	V_p	V_p, V_s				
10	V_p, V_s	V_p	V_p, V_s	V_p, V_s				
11	V_p, V_s	V_p	V_p, V_s	V_p, V_s				
12	V_p	V_p	V_s	V_p, V_s				
13	V_p		V_p					
14			V_p					
15								
16								

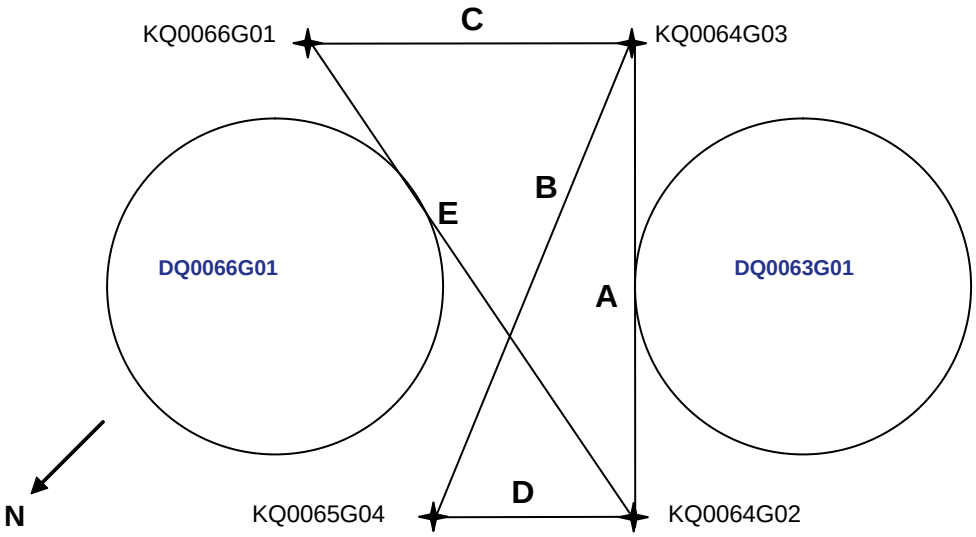

Figure 6-1. *Schematic diagram of the APSE in plan view showing raypath labelling between pairs of boreholes.*

Table 6-2. Summary of the observed signal changes expected during the Pillar Stability Experiment.

Description	Observed signal changes
Decreasing compressional stresses (or increasing tensional stresses) acting to open microfractures.	Reduction of P and S-wave velocities and signal amplitudes.
Increasing compressional stresses (or decreasing tensional stresses) acting to close microfractures.	Increase of P and S-wave velocities and signal amplitudes.
Accumulation of new microfractures due to rock degradation.	Reduction of P and S-wave velocities and signal amplitudes.
Increase of fluid content (saturation) of microfractures.	Increase of P-wave velocity. No effect on S-wave velocity.
Decrease of fluid content (de-saturation) of microfractures.	Decrease of P-wave velocity. No effect on S-wave velocity.

6.1 Anomalous measurements

Two of the receivers show anomalous behaviour that cannot be attributed to known phases of the experiment.

- An inspection of the graphs shows a short term variation to velocity on raypaths involving receiver 8 between 11 May and 27 May 2004. There is an initial increase of about 20 $m.s^{-1}$ then a decrease that is often greater than the increase. Amplitudes for this receiver show a similar response of an increase to a peak on 20 May 2004. Receiver 8 is located at a depth of 451.32 m, close to the bottom of borehole KQ0064G02. Transmitter 4 is situated only 25 cm beneath receiver 8 in the same borehole. No change is observed to either the velocities or the amplitudes for the raypaths involving transmitter 4.
- All raypaths involving receiver 15 display a short term change in amplitude in the first month of recording. The change involves an initial increase of about 8 dB followed by a decrease of between 18 and 28 dB. Figure 6-2 shows examples of S-wave amplitude change plots which exhibit this variation. A very similar pattern is observed for P-wave amplitude change. Excavation of deposition hole DQ0066G01 does not commence until 2 December 2003, so the observed variation is probably due to a change in coupling of receiver 15.

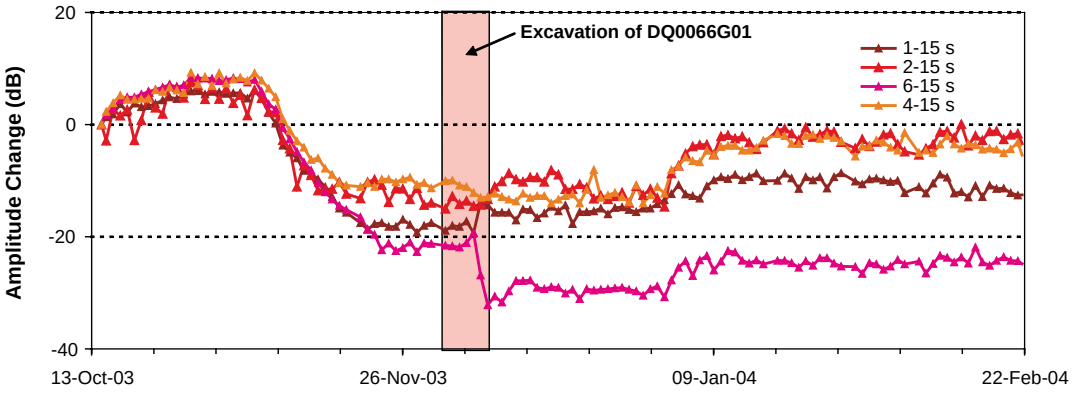

Figure 6-2. *S-wave amplitude change plots for a selection of raypaths involving receiver 15 until 22 February 2004.*

6.2 Raypaths skimming DQ0063G01

The raypaths between instrument boreholes KQ0064G03 and KQ0064G02 travel within centimetres of deposition hole DQ0063G01, passing through any excavation damaged zone, and are termed skimming. They also pass through the region of high compressive stresses generated around the void. The receivers involved are 1, 2, 3, 4, 5, 6, 7, 8 and transmitters 1, 2, 3, 4.

Until the 3 March 2004, the raypaths in this direction travel through undisturbed rock. Between 4 and 11 March 2004, the deposition hole DQ0063G01 is excavated to a depth of 5.6 m below the level of the tunnel floor. On some raypaths there is a significant decrease in velocity during this time of between 5 to 30 $m.s^{-1}$. In particular this is displayed by raypaths t1 to r5, t1 to r9, and t3 to r1. A decrease in velocity would be expected during this time because induced stresses causes microfractures to form around the excavation in the damaged zone through which the raypaths travel. Amplitudes show a similar decrease for most of the raypaths.

Many of the raypaths (e.g. t2 to r6, t2 to r7 and t4 to r4) exhibit an increase in velocity in the days following excavation (Figure 6-3) of approximately 10 $m.s^{-1}$. An increase could be the result of changes to the stress field caused by excavation of the deposition hole. Consequently, although there is a region directly around the deposition hole where micro-cracks will form, further out stresses could be acting to close microfractures and pore spaces leading to an increase in velocity. These velocity increases counteract any decreases in velocity caused by new fracturing and result in a net increase.

During the heating stage of the experiment many of the raypaths show a decrease in velocity in two stages. This agrees with the event rate in Section 5.2, in which the cumulative number of events increases in two phases between May and June 2004. Figure 6-4 shows example velocity plots during heating. The heaters are switched on at point I and a decrease in velocity of approximately 20 $m.s^{-1}$ occurs afterwards. At time II the thermal output is lowered in one heater and the velocity remains constant. It is not until the final increase in heater power at time III that velocity continues to decrease again, this time by approximately 15 $m.s^{-1}$.

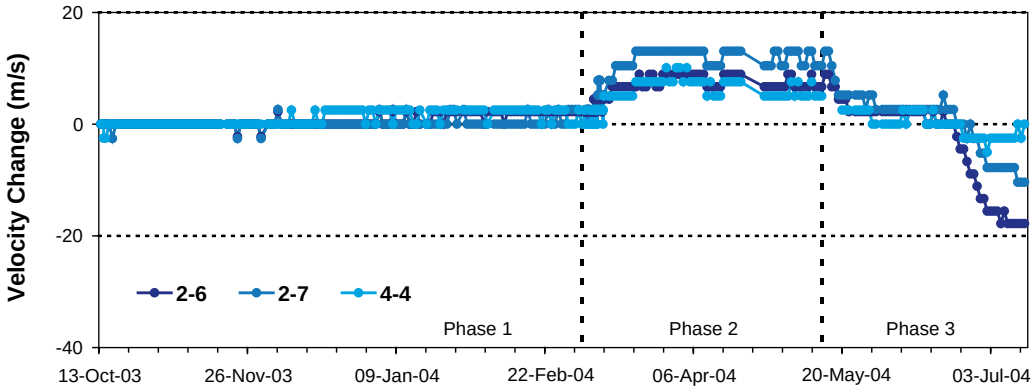

Figure 6-3. *P-wave velocity change graphs for raypaths skimming DQ0063G01. Phases of the experiment from Table 1-1 are also shown.*

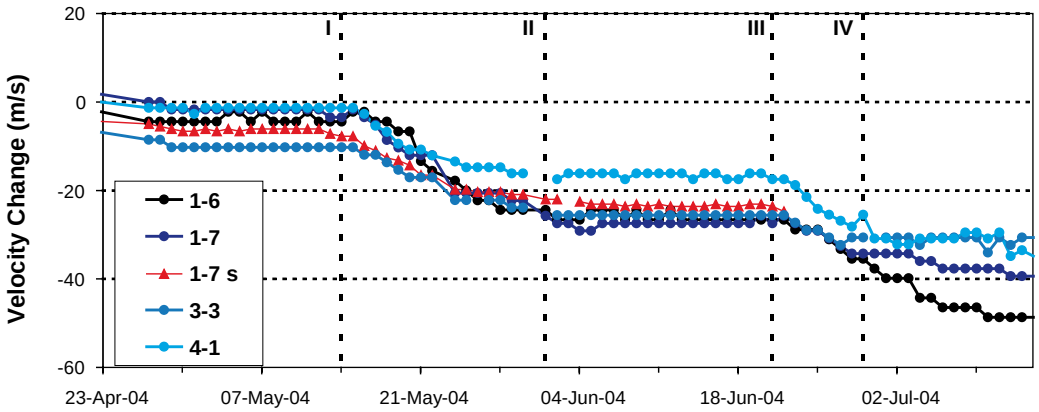

Figure 6-4. *P- and S-wave velocity change graphs during heating for raypaths skimming DQ0063G01. Times represented by I to IV are associated with heating changes in Table 5-1.*

6.3 Raypaths through the centre of the pillar

The raypaths between instrument boreholes KQ0064G03 and KQ0065G04 travel through the centre of the pillar. The receivers involved are 1, 2, 3, 4, 9, 10, 11, 12 and transmitters 1, 2, 5, 6.

Small changes are observed in P- and S-wave velocity (of the order 5 $m.s^{-1}$) during the excavation phases of the experiment. These are not believed to be significant. The amplitudes, similarly, do not show significant changes. The raypaths do not travel through the region of AE activity associated with spalling (Figure 5-3), and therefore are unlikely to pass through the region of greatest microfracture damage. The small velocity changes observed may relate to changes in the stress regime induced by the excavation.

Two stages of decrease in velocity are observed during the heating phase of the experiment. This is similar to the effect observed in the raypaths which skim DQ0063G01. Selections of the raypaths are displayed in Figure 6-5.

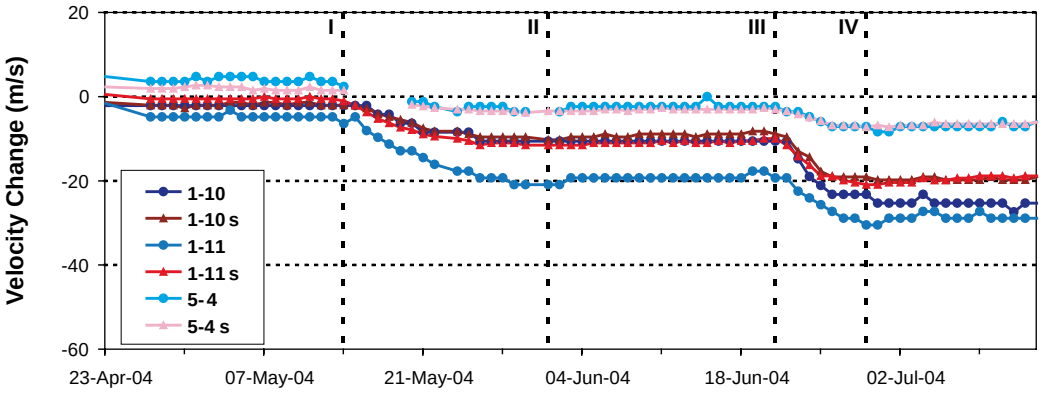

Figure 6-5. *P- and S-wave velocity change graphs during heating for raypaths through the centre of the pillar. Times represented by I to IV are associated with heating changes in Table 5-1.*

6.4 Raypaths skimming DQ0066G01

The raypaths between instrument boreholes KQ0064G02 and KQ0066G01 travel within centimetres of deposition hole DQ0066G01, passing through any excavation damaged zone, and are termed skimming. They also pass through the region of high compressive stresses generated around the void. The receivers involved are 5, 6, 7, 8, 13, 14, 15, 16 and transmitters 3, 4. 7, 8. Relatively, few of these ray paths could be processed due to the effect of the sub-vertical feature described in Section 5.1. This feature is believed to interfere with signals between instrumentation borehole KQ0066G01 and the other boreholes causing signal amplitudes to be reduced.

Figure 6-6 shows P-wave velocity change for two raypaths which display large decreases during excavation of deposition hole DQ0066G01. Raypath t3 to r14 exhibits a decrease of 28 $m.s^{-1}$ over a single day and raypath t8 to r6 exhibits a 36 $m.s^{-1}$ decrease over 2 days. These changes are believed to be caused by an accumulation of microfracture damage close to the deposition hole wall during excavation. Some reduction in velocity is observed on these ray paths during the heating phase (Phase 3).

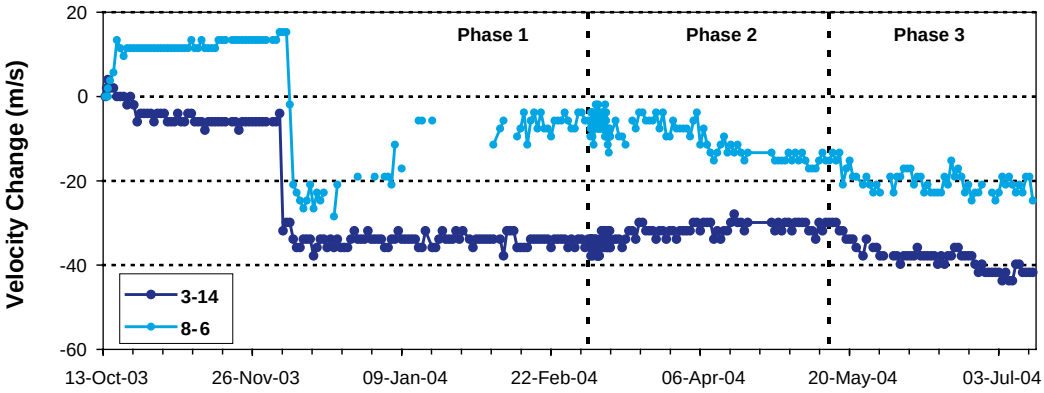

Figure 6-6. *P- and S-wave velocity change graphs over the whole experiment for two raypaths skimming DQ0066G01. Phases of the experiment from Table 1-1 are also shown.*

6.5 Raypaths parallel with tunnel

There are two sets of results which do not include raypaths that pass through the pillar. Instead, these run parallel to the tunnel, to the north west and south east of the deposition holes. These raypaths are far enough away from the deposition holes to not be effected by microcraking caused during excavation, but are close to the heater boreholes.

In general, the velocities show no significant change until heating commences on 14 May 2004, when many of the raypaths display a very large decrease in velocity over time. Example plots are shown in Figure 6-7. This effect is likely to be the result of the close proximity of the ray paths to the heater boreholes.

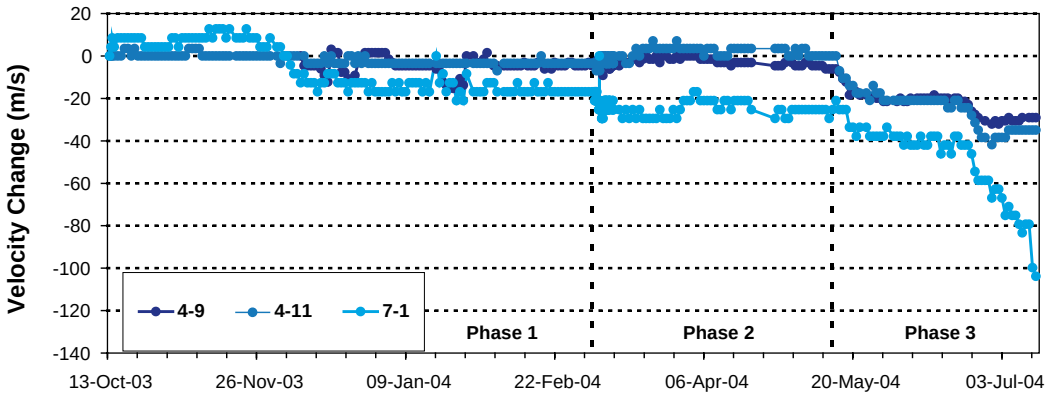

Figure 6-7. *Example P- wave velocity change graphs over the whole experiment for raypaths parallel to the tunnel. Phases of the experiment from Table 1-1 are also shown.*

7 Results summary and conclusions

- This report describes the results from acoustic emission (AE) and ultrasonic monitoring of the Äspö Pillar Stability Experiment (APSE) at SKB's Hard Rock Laboratory (HRL), Sweden. The APSE is being undertaken to demonstrate the current capability to predict spalling in a fractured rock mass using numerical modelling techniques. It is also designed to demonstrate the effect of backfill and confining pressure on the propagation of micro-cracks in rock adjacent to deposition holes within a repository /Anderson 2002/. A summary of the AE and ultrasonic survey results is given in the following sections.

- In order to realise the objectives of the experiment a pillar of rock between two deposition holes has been monitored using an array of ultrasonic transducers. The array geometry has been designed to be sensitive to Acoustic Emissions (AEs) occurring within the pillar volume and to provide ultrasonic surveys with ray paths passing through critical regions of the rock mass. By monitoring for AE activity and undertaking regular, repeated velocity surveys the response of the rock pillar to excavation, heating and variations in confinement pressure can be assessed. The entire data set has been collated by ASC and processed for final AE locations and ultrasonic velocity measurements. These results are provided with this document so that they can be effectively compared to results obtained from several numerical modelling studies, and to mechanical and thermal measurements conducted around the pillar volume, in an 'integrated analysis' performed by SKB staff. This document has provided an in-depth summary of the AE and ultrasonic survey results for future reference.

- The pillar has been produced by excavating two 1.8 m diameter deposition holes 1 m apart. These were bored in 0.8 m steps using a Tunnel Boring Machine (TBM) specially adapted for vertical drilling. Each step took approximately 3 to 5 hours to complete. The first deposition hole, DQ0066G01, was drilled between 2nd and 8th December 2003. This was then confined to 0.7 MPa internal pressure using a specially designed water-filled bladder in early February 2004 /Andersson et al. 2004/. The second deposition hole, DQ0063G01, was excavated between 4th and 11th March 2004.

- Ultrasonic velocities have been measured prior to the excavation of the deposition holes. A mean P-wave velocity of 6,051 m.s^{-1}, and mean S-wave velocity of 3,394 m.s^{-1}, have been obtained in a weakly (1.5%) transversely isotropic rock mass. This has a fast direction orthogonal to the tunnel direction (north west to south east and around to the vertical). The slow velocity direction is thus parallel to the tunnel, orthogonal to the major fracture set and maximum principal stress direction. When considering the uncertainties in absolute velocity the anisotropy is not believed to be significant. The measured velocities are consistent with those obtained at the Prototype Repository and are slightly higher than at the Canister Retrieval Tunnel. Small variations in the observed velocities between the experiments (< 100 m.s^{-1}) are likely to be the result of small variations in rock type between the different regions of the HRL. Litholigical differences in the Äspö Diorite are recognised to be the result of different mixtures of dioritic compositions, varying in chemistry and grain sizes.

- It has been observed that low amplitude signals are systematically received on instrumentation borehole KQ0066G01 during the ultrasonic surveys. Sensor coupling with the borehole wall can cause small variations in signal amplitude between individual sensors,

however, in this experiment all four boreholes have the same instrumentation configuration and are installed in exactly the same manner. Variations in sensor coupling should therefore be similar across the array. Hence, the reduction of signals on KQ0066G01 must be a result of the rock mass. The observed response has been interpreted as due to the water-bearing fracture (fract_1) observed by /Staub et al. 2003/. Assuming that this fracture is reasonably linear over a few metres then borehole KQ0066G01 is positioned on the opposite side of the fracture to the other boreholes, and thus raypaths travelling to this borehole will have to pass through it. Waves at the high frequencies used here will lose energy as they cross the interface between the fracture faces and hence the amplitude of the recorded signal will decrease. Velocity measurements are not observed to be effected by the fracture. This is consistent with full-waveform modelling of synthetic fractures by /Hildyard and Young 2002/ where velocity measurements are observed to be sensitive to a bulk change in rock properties (i.e. a large population of smaller fractures) rather than travelling through a single large fracture.

7.1 Acoustic emission results

- A total of 36,676 AE triggers were recorded over the monitoring period, between 13th December 2003 and 14th July 2004. Of these 15,198 have produced AE locations. Calibration tests performed in deposition hole DQ0063G01 yield an estimated uncertainty of 4 cm. Pencil lead breaks provide a means of illustrating the sensitivity of the array, which is capable of picking up cracking on the millimetre scale. The entire AE data set shows an intense clustering of events located along the length of the deposition holes to approximately 1 m from their floors. Figure 7-1 shows AE locations during the excavation and heating phases of the experiment. Clustering of events is primarily contained in a damage zone orthogonal to the maximum principal stress, represented by a semi-circle of tightly packed AEs extending from the edge of each hole approximately 20 cm into the pillar. Very few events are situated in the centre of the pillar, although clusters of events occur in the top metre of the pillar volume in two sub-horizontal features that cross the pillar. The uppermost feature is believed to be associated with the floor of the tunnel, beneath the concrete roadbed, and the lowermost feature is associated with a mapped shear zone.

- Instrument Magnitudes have been calculated for all located events. A very similar distribution of AE locations is observed for all magnitude ranges. This result indicates that the AE locations presented here are unbiased by array sensitivity, as sensitivity variations would result in larger numbers of smaller magnitude AEs being recorded in different parts of the rock mass. The plots also highlight that there is no preferred spatial distribution to the largest events, but instead these are distributed throughout the regions of high activity. This suggests that there is no intense focus of high stresses in the volume. The magnitudes provide a ‘b-value’ of 4.4. This is much higher than earthquake seismology where b-values are usually around 1.0. However, it is a similar magnitude to b-values recorded in other high-frequency AE experiments and in dynamic numerical models of rock fracture.

- Acquisition system triggers, channel hit counts and processed locations all show a consistent temporal distribution for the AE activity. During background monitoring, preceding excavation of the first deposition hole, no activity was recorded. Excavation of the two deposition holes produces increased activity. This is much larger for the second deposition hole when the pillar is formed. The activity decays away after excavation over approximately two weeks. An increase in the number of hit counts is also observed

between 24 January and 4 February 2004, during what is believed to be the pressurisation phase of DQ0066G01 prior to excavation of DQ0063G01. Heating of the pillar causes increased activity occurring in two sets between May and July 2004. The sets of activity correspond to two heating periods; the second period being caused by an increase in thermal output by the heaters used.

- During excavation of the first deposition hole, DQ0066G01, in December 2003, AEs locate in clusters down the pillar side of the deposition hole. A maximum of 120 events per day occur. A single relatively tight cluster of events at approximately 1 m depth corresponds to the intersection of a near horizontal feature. The largest activity occurs at 3.6 m depth. The cluster occurs 1.2 m behind the advancing deposition-hole face and is probably a result of increasing stresses in a weaker part of the rock mass during deeper excavation. Activity qualitatively correlates with spalling observed in the deposition hole.

- In early February a water-filled bladder was installed in deposition hole DQ0066G01 and on 4th February the pressure inside the bladder was increased to 0.7 MPa applying confinement to the deposition-hole walls. A drop in event rate is observed following confinement, although the event rate was already quite low in the month prior to this.

- The event rate is greater during drilling of DQ0063G01, in March 2004, than in the previous deposition hole with a maximum of 820 events located on a single day. Events are observed to locate on the completed, and also confined, first deposition hole during excavation of the second one. This result indicates that a disturbance of the stress field around deposition hole DQ0066G01 is occurring, caused by excavation of the second hole. The development of two features in the pillar, close to the tunnel floor, has been observed creating a ‘bridge’ of activity crossing between the two deposition holes. The AEs are either located on two sub-horizontal features or on a single plane with a dip of approximately 20° in a NE direction. The uppermost events correlate with the rock floor of the tunnel, beneath the concrete roadbed. The lowermost events correlate with a ‘shearzone’ mapped in the sidewalls of the deposition holes. As excavation progresses, a zone of intense AE activity occurs, extending from close to the top of the deposition hole. and migrating down the hole to a depth of approximately 2.5 m. The highest event rates are observed after excavation is completed. The AE activity correlates well with a zone of breakout damage observed in the open hole after excavation. Similarly large amounts of activity is not observed in the confined deposition hole, suggesting the confinement pressure applied here is sufficient to inhibit breakout occurring.

- Heating of the pillar in May 2004 causes the event rate to increase rapidly. Three days after the heaters are turned on a peak of 807 events occurs, reducing to less than 250 events per day a week later. When the power of the heaters is increased a month afterwards, a second set of activity is observed with 800 events being located in a single day, four days after the thermal output was increased. A consistent lag of a few days (3–4) is thus observed between when the heaters are adjusted and when the rock responds to the adjustment. The events initially cluster in previously active regions down the open deposition hole, DQ0063G01. As the temperature increases this cluster grows larger, extending upward to the rock floor of the tunnel and then migrating downward reaching a depth of approximately 5 m below the tunnel floor. A large number of events also locate on the features crossing the pillar in the first 1 m beneath the tunnel floor and also in the wall of DQ0066G01; these are approximately positioned in the original clusters developed during excavation of this hole.

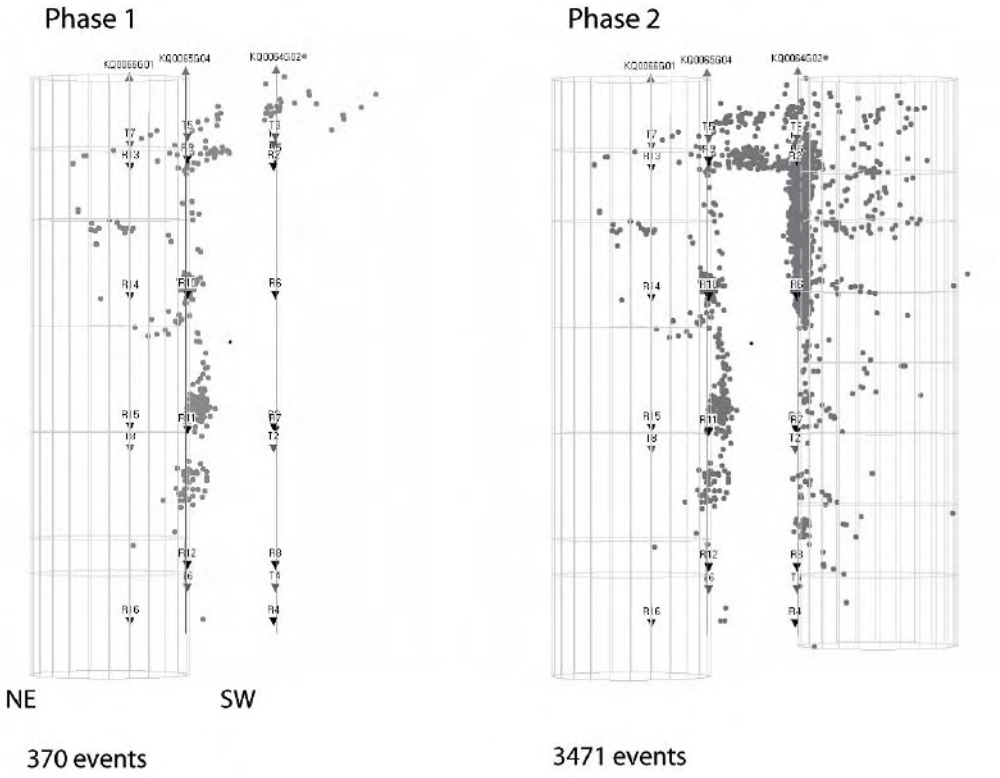

Figure 7-1. *Summary plot of all events located during three phases of the experiment. The AEs are grouped according to which phase they occur in (see Table 1-1).*

7.2 Ultrasonic velocity results

- Ultrasonic velocity surveys were undertaken regularly during the whole of the APSE. Velocity and amplitude results, for every raypath that could be processed, are provided with this document. These include 54 separate P-wave velocity measurements and 23 S-wave velocity measurements on 350 surveys conducted over the monitoring period. The observed velocity and amplitude changes can be attributed to various factors and are caused by a change in the material's bulk properties. The raypaths on which the measurements have been taken are grouped into pairs of instrumentation boreholes that travel through different volumes of the rock mass. In order to make a detailed interpretation of the measurements the velocity and amplitude variations need to be integrated with mechanical and thermal stress modelling. This integrated analysis has not been performed here, instead the results are summarised for each of the instrumentation-borehole pairs.

- The raypaths between instrument boreholes KQ0064G03 and KQ0064G02 travel within centimetres of deposition hole DQ0063G01, passing through the excavation damaged zone imaged by the AEs, and are termed skimming. They also pass through the region of high compressive stresses generated around the void. Some ray paths show a significant decrease in velocity during excavation of this deposition hole of between 5 to 30 $m.s^{-1}$. A similar effect has been observed in previous experiments at the HRL and is probably caused by microfractures forming in the excavation damaged zone through which the raypaths travel. Amplitudes show a similar decrease. Some ray paths exhibit an increase in velocity of approximately 10 $m.s^{-1}$ over the days following excavation. An increase could be the result of increasing stresses in some volumes of the rock mass, caused by excavation of the deposition hole, acting to close microfractures and pore spaces. These velocity increases may counteract any decreases in velocity caused by new fracturing and result in a net increase.

- During the heating stage of the experiment many of the skimming raypaths show a decrease in velocity in two stages that correlates very well with the AE results and known changes in the thermal output of the heaters. These velocity decreases (of the order 50 $m.s^{-1}$) could be related to a desaturation of the rock mass, new fracture growth or expansive stresses causing an opening of pre-existing fractures. The latter is unlikely as modelled increasing compressive stresses /Andersson 2002/ will act to close preferentially-orientated fractures.

- During the excavation phases of the experiment, small changes are observed in P- and S-wave velocity (of the order ± 5 $m.s^{-1}$) on raypaths that travel through the centre of the pillar. These are not believed to be significant but may relate to small changes in the stress regime induced by the excavation. Decreases in velocity (of the order 20 $m.s^{-1}$) are observed during the heating phase of the experiment. These are similar in nature to those recorded for the skimming raypaths, but are lower in magnitude. Again, the velocities do not return to their original state indicating a permanent change in the rock mass during this period.

8 Recommendations

The following are suggested recommendations for future studies.

- An integrated analysis of the results should be performed by correlating the acoustic emission and ultrasonic survey data provided here with data from temperature and displacement sensors installed around the pillar and with geological mapping of fracture and breakout locations. The data should also be related to the available results from both static and dynamic numerical modelling packages. This study is believed to be scheduled for SKB staff to perform. The experiment should be split up into excavation, heating and depressurisation phases, as each of these provide different effects on the induced stress regime. The experiment's results suggest that the pillar walls are in a critical stress state where small variations in environmental factors (such as temperature or confining stress) result in measurable changes in induced damage. The experiment data therefore represents a unique opportunity to map how mechanical and thermal effects (and the coupling between these) map through to induced damage in the rock mass.

- The acoustic emission data is of sufficiently good quality (in spatial resolution and waveform signals) that advanced amplitude studies (source mechanism inversion) can be performed. This would allow an analysis of the failure mode and orientation for a subset of the data containing the most suitable events – believed to number in their 100 s to 1,000 s. This analysis would follow the method successfully applied to a selection of AEs recorded during the Prototype Experiment /Pettitt et al. 2000/. Figure 8-1 shows some preliminary mechanism results for randomly selected events recorded in the Pillar Stability Experiment. The principal aim of the analysis would be to provide fracturing modes and orientations for AE data from different regions of the pillar volume through each of the experiment phases. The data can then be fed into the integrated analysis described above for correlation with the other measurements and modelling results and would ultimately provide greater understanding of the processes involved in damaging the rock mass.

- The OMNIBUS project, in which ASC is a partner and the scientific coordinator, is a project funded by the European Commission (EC) as part of the fifth framework EURATOM programme. The project has focused on developing the hardware, software and techniques used for ultrasonic surveys. In particular, a spectral analysis method of processing ultrasonic surveys is being developed and implemented into ASC's InSite Seismic Processing software /Pettitt et al. 2004b/. The process uses a full-waveform modelling of experimental scenarios (using the WAVE^{3D} package /Hildyard and Young 2002/) containing different crack densities, sizes, geometries and fluid content and then performing a direct correlation with recorded signals in the amplitude and phase frequency domains. The velocity results can be inverted into dynamic elastic moduli, crack density and saturation values. The pillar volume would be split into different regions and processed through the different experimental phases. Through this approach it would be possible to provide an interpretation of the factors most affecting the ultrasonic results in the rock mass around the pillar, and thus construct a quantitative model of the damage conditions through the experiment.

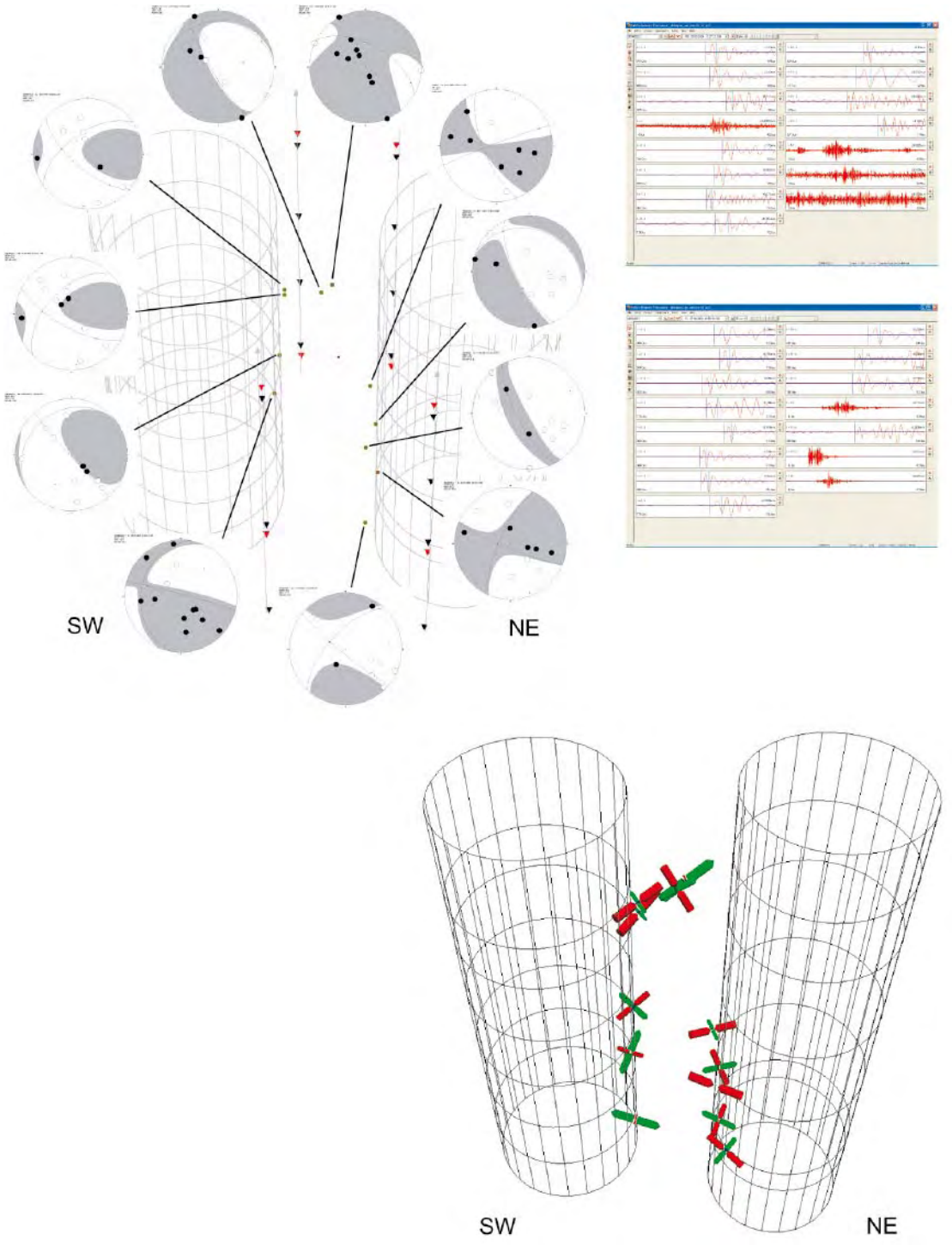

Figure 8-1. *Preliminary results from analysis of source mechanisms on selected AEs at the APSE (from Instrument Magnitude range –0.16 to 0.311). a) Lower hemisphere plots AEs at a variety of locations around the pillar; b) Waveforms of two events showing clear arrivals; c) Source mechanisms from moment tensor inversion displaying the tensile axis (green), pressure axis (red) and null axis (blue).*

9 References

Andersson J C, 2002. Äspö Pillar Stability Experiment: Feasibility Study, International Progress Report IPR-03-01, Svensk Kärnbränslehantering AB.

Andersson J C, Martin C D, Christiansson R, 2004. SKB's Äspö Pillar Stability Experiment, Sweden, in 6th North America Rock Mechanics Symposium (Narms), Houston, Texas.

Andersson J C, 2004. Pers. comm.

Breckenridge F R, Proctor T M, Hsu N N, Fich S E, Eitzen D G, 1990. Transient sources for acoustic emission work, in Proc. 10th Int. Acoust. Emission Symp, NDI Japan, pp 20–37.

Falls S D, Young R P, 1996. Examination of the excavation disturbed zone in the Swedish ZEDEX tunnel using acoustic emission and ultrasonic velocity measurements, in Proceedings of Eurock '96, Turin, Italy, 1996, Balkema, Rotterdam, pp 1337–1344.

Hazzard J F, 1998. Numerical modelling of acoustic emissions and dynamic rock behaviour, Ph.D. thesis, Keele University, Keele, Staffordshire, UK.

Hildyard M W, Young R P, 2002. Modelling seismic waves around underground openings, Pure and Applied Geophysics, 159, 247–276.

Pettitt W S, 1998. Acoustic emission source studies of microcracking in rock, Ph.D. thesis, Keele University, Keele, Staffordshire, UK.

Pettitt W S, Baker C, Young R P, 1999a. Acoustic Emission and Ultrasonic Monitoring During the Excavation of Deposition Holes in the Canister Retrieval Test, International Progress Report IPR-01-02, Svensk Kärnbränslehantering AB.

Pettitt W S, Baker C, Young R P, 1999b. Acoustic emission and ultrasonic monitoring during the excavation of deposition holes in the Prototype Repository, International Progress Report IPR-01-01, Svensk Kärnbränslehantering AB.

Pettitt W S, Baker C, Young R P, 2000. Analysis of the in-situ principle stress field at the HRL using acoustic emission data, International Progress Report IPR-01-09, Svensk Kärnbränslehantering AB.

Pettitt W S, Baker C, Young R P, Dahlström L O, Ramqvist G, 2002. The assessment of damage around critical engineering structures using induced seismicity and ultrasonic techniques, Pure and Applied Geophysics, 159, 179–195.

Pettitt W S, Haycox J R, 2003. Acoustic emission and monitoring of deposition hole DA3545G01 March–September 2003, in SAFETI Year 2 Progress Report, University of Liverpool, UK.

Pettitt W S, Baker C, Collins D, Young R P, 2004a. InSite Seismic Processor User Operations Manual Version 2.12, Applied Seismology Consultants Ltd, UK.

Pettitt W S, Collins D S, Hildyard M W, Young R P, Balland C, Bigarré P, 2004b. An Ultrasonic Tool for Examining the Excavation Damaged Zone around Radioactive Waste Repositories – The OMNIBUS project, in EC Euradwaste04 Conference, Luxembourg.

Staub I, Janson T, Fredriksson A, 2003. Äspö Pillar Stability Experiment: Geology and properties of the rock mass around the experiment volume, International Progress Report IPR-03-02, Svensk Kärnbränslehantering AB.

Staub I, Andersson J C, Magnor B, 2004. Äspö Pillar Stability Experiment: Geology and mechanical properties of the rock at TASQ, SKB R-04-01, Svensk Kärnbränslehantering AB.

Young R P, Collins D S, Hazzard J, Heath A, Baker C, Pettitt W S, Billaux D, Cundall P, Potyondy D, Decker F, 2004. An innovative 3-D numerical modelling procedure for simulating repository-scale excavations in rock – The SAFETI project, in EC Euradwaste04 Conference, Luxembourg.

Appendix 1

Example waveforms

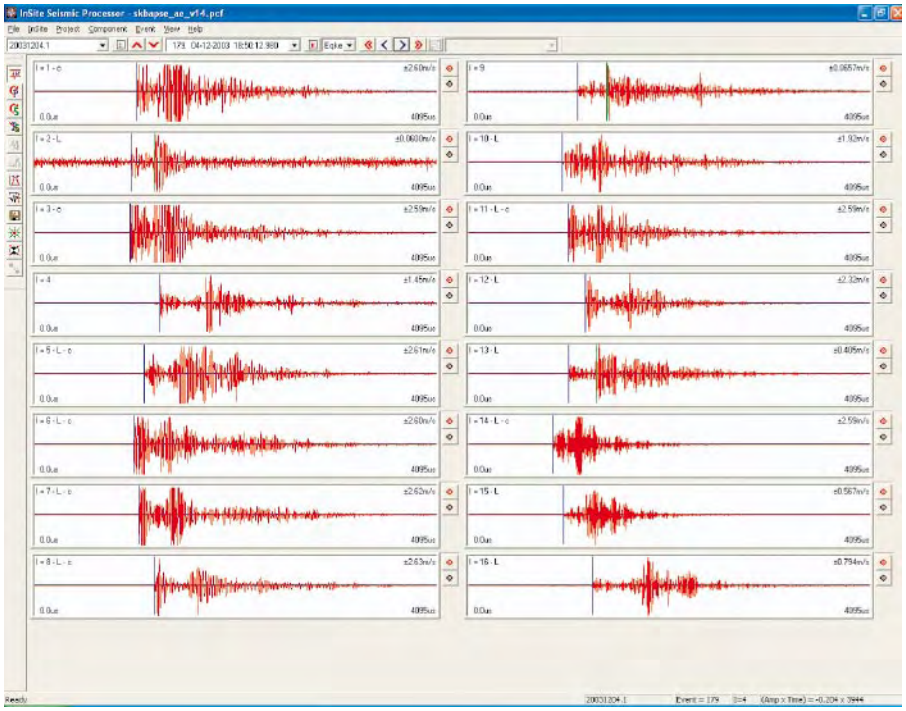

Figure A1-1. *Waveform from an AE recorded after the cessation of drilling of deposition hole DQ0066G01 (Round #2).*

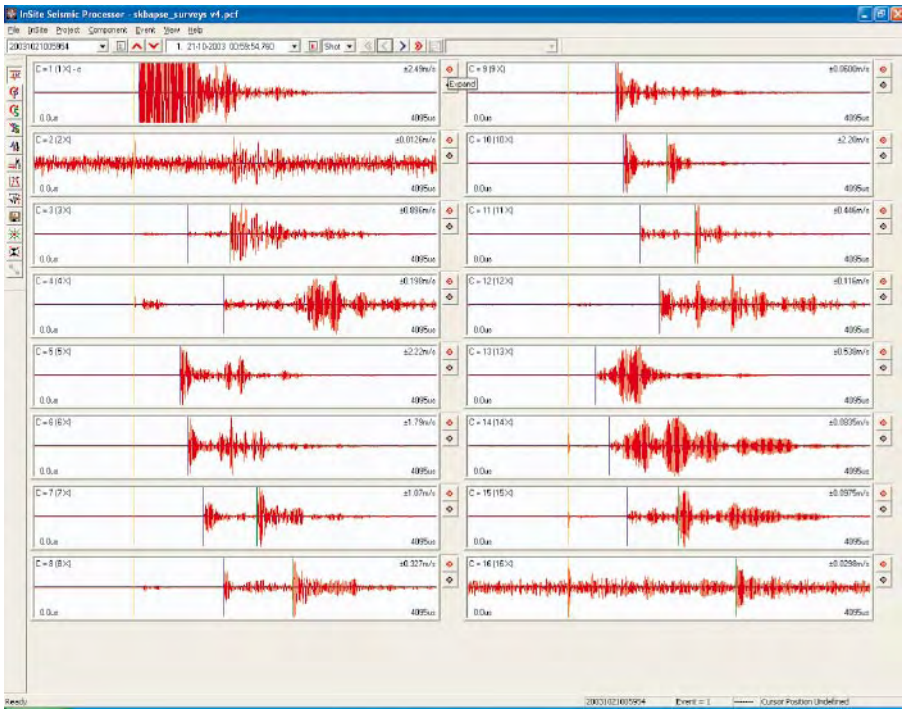

Figure A1-2. *Example waveforms from an ultrasonic survey 20031021005954 conducted prior to the start of excavation of deposition hole DQ0066G01.*

Appendix 2A

Velocity processing parameters

Event initialisation	
View/process waveforms by	Channel
Channel-view width-to-height ratio	6
Waveform response type	Set from sensor
Sampling time	1
Time units	Microseconds
Pre-signal points	200
Spline sampling time	0.2
Waveform to point	1,023
P-time correction	0
S-time correction	0
Automatically update channel settings	SET
Project files	NULL

Auto picking	
Allow P-wave-autopicking	YES, use max peak in the auto-pick function
Back-window length	100
Front-window length	25
Picking threshold	5
Min peak-to-peak amplitude	0
Allow S-wave autopicking	YES, use first peak in the auto-pick function
Back-window length	100
Front-window length	35
Picking threshold	5
Min peak-to-peak amplitude	0
Allow automatic amplitude picking	NO
Use velocity window picking	YES
P-wave min velocity/max velocity	4,500, 6,500
S-wave min velocity/max velocity	2,500, 3,500

Cross-correlation	
CCR events	Referenced to a survey
Reference component	“20031210010008”
Reference event	NULL
Window construction method	Front to back
Window comparison method	Joint
Window parameters	Back-window length = 15
	Front-window length = 30
	Rise-time multiplier = NULL
	Power to raise waveform = 1
	Split to a spline function = YES
	Obtain absolute waveform = NOT SET

Appendix 2B

AE processing parameters

Event initialisation	
View/process waveforms by	Instrument
Channel-view width-to-height ratio	6
Waveform response type	Set from sensor
Sampling time	1
Time units	Microseconds
Pre-signal points	200
Spline sampling time	0.2
Waveform to point	1,023
P-time correction	0
S-time correction	0
Automatically update channel settings	SET
Project files	NULL

Auto picking	
Allow P-wave-autopicking	YES, use max peak in the auto-pick function
Back-window length	100
Front-window length	25
Picking threshold	5
Min peak-to-peak amplitude	0
Allow S-wave autopicking	YES, use first peak in the auto-pick function
Back-window length	100
Front-window length	35
Picking threshold	5
Min peak-to-peak amplitude	0
Allow automatic amplitude picking	NOT SET
Use velocity window picking	YES
P-wave min velocity/max velocity	4,500, 6,500
S-wave min velocity/max velocity	2,500, 3,500

Waveform filter	
Filter events automatically on reading	NOT SET
Band-pass filter using sensor settings	SET
Default filter parameters	Not used

Event filter	
Date and time	NOT SET
Location volume	Minimum (N,E,D) = (306.3, 114.3, 442.6) Maximum (N,E,D) = (330, 135, 455.9)
L magnitude	NOT SET
Location error	0.1
Independent instruments	Minimum = 10

Locater	
Method	SIMPLEX INTO GEIGER
Method settings	Tolerence = 0.01
Simplex settings	LPNorm = 1
	P-wave weighting = 1
	S-wave weighting = 0.25
	Use outlier identification = NOT SET
	Arrival error factor = ×2
Geiger settings	Tolerence (Loc. units) = 0.01
	Step size (Loc.units) = 0.01
	Max iterations = 100
	Conditional no. limit = 10000000000
Velocity structure	Homogeneous isotropic
Velocity structure settings	P-wave velocity = 6,051m/s
	S-wave velocity = 3,394 m/s
	Attenuation = 200
	Q(S) value = 100
Data to use	P-wave and S-wave arrivals
Distance units	Metres
Wotrking time units	Microseconds
Min P-wave arrivals	7
Min S-wave arrivals	0
Min independent arrivals	7
Max residual	25
Start point	Start at the centroid of the array
Write report to RPT	NOT SET
Source parameters	Set to calculate automatically

Source parameters	
P-wave back/front window	10/50
S-wave back/front window	10/50
Minimum no. of instruments to use	3
Apply attenuation corrections (Q)	NOT SET
Source density	2640
Source shear modulus	39131400000
Average radiation coeff.	$F_P = 0.52$; $F_S = 0.63$
Source coefficients, K_p	$K_P = 2.01$; $K_S = 1.32$
Magnitude calculations	Instrument mag: 1, 0
	Moment mag: Not used

Appendix 3

AE hit count rate

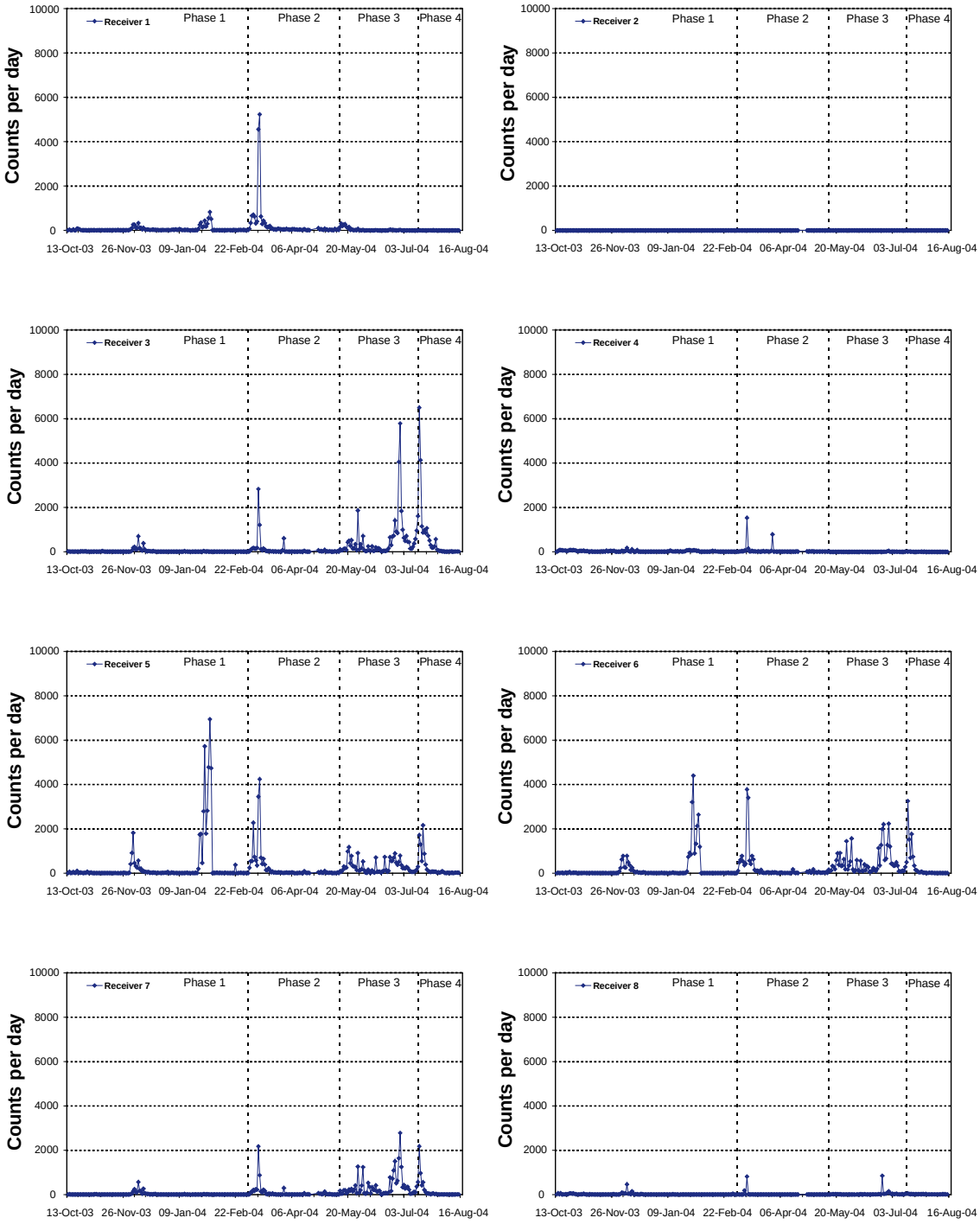

Figure A3-1. *Count rate per day for each receiver (Constant Y-Max). Day is set to between 21:00 and 06:00 in order to avoid noise. Values were manually checked for large numbers signifying some form of noise.*

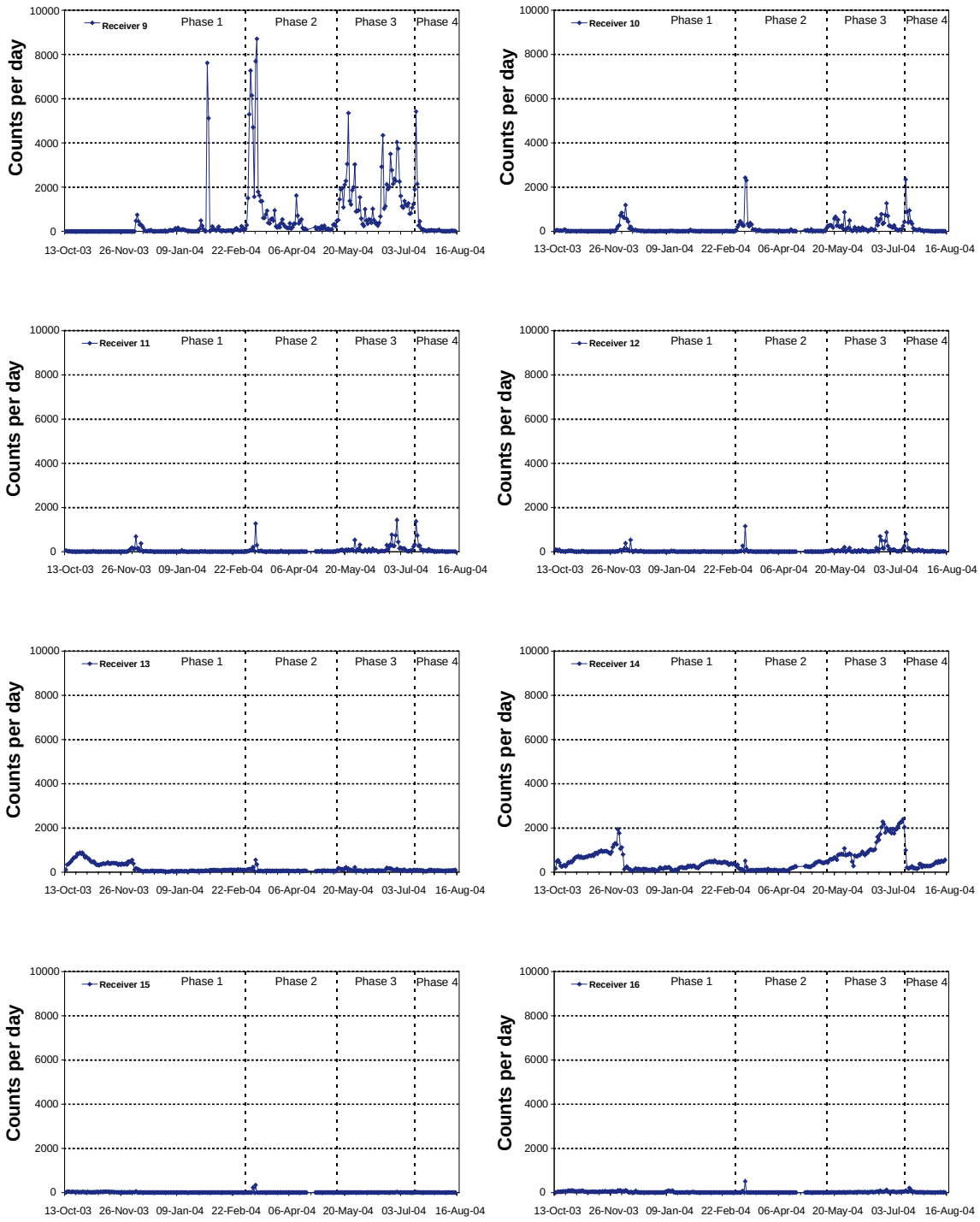

Figure A3-1 (cont). *Count rate per day for each receiver (Constant Y-Max). Day is set to between 21:00 and 06:00 in order to avoid noise. Values were manually checked for large numbers signifying some form of noise.*

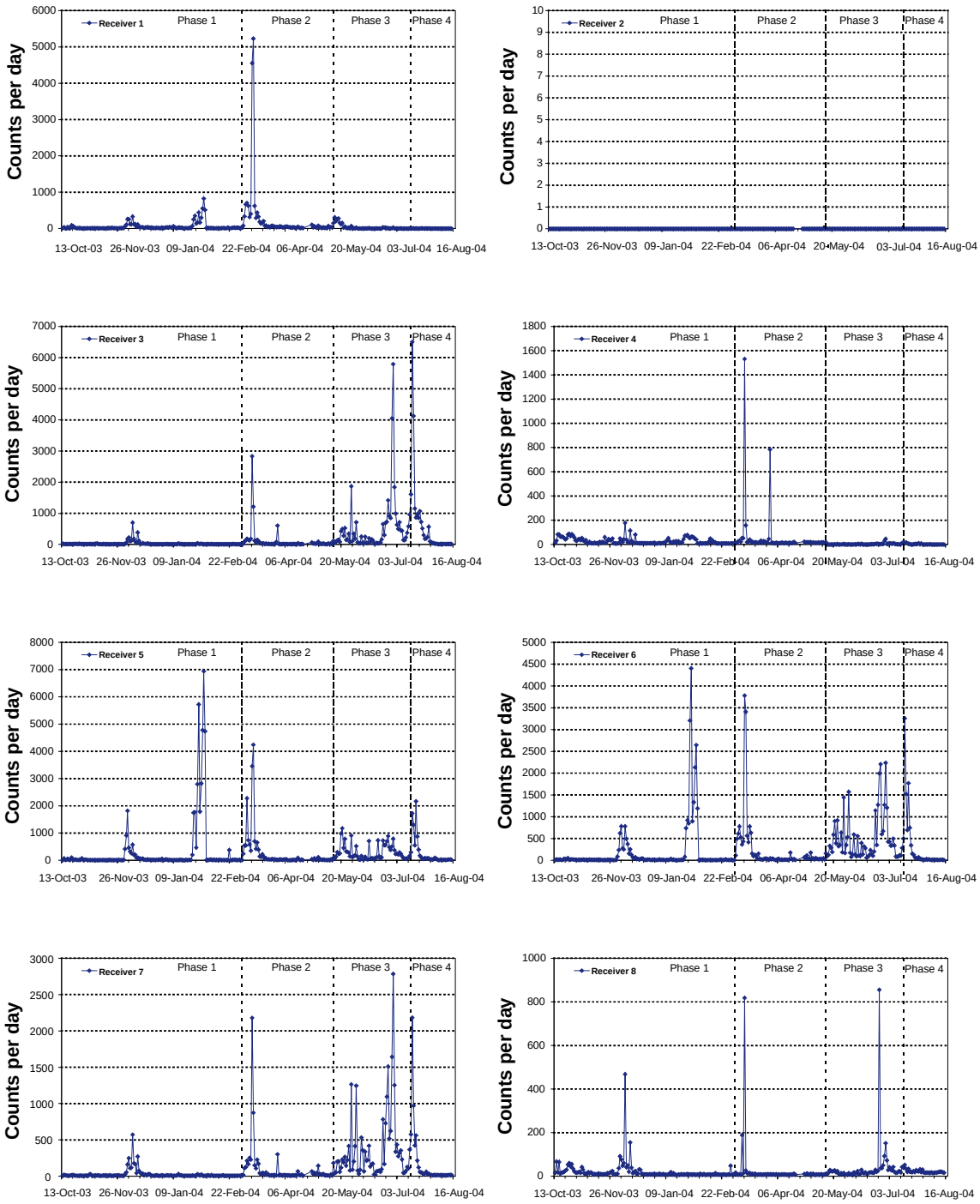

Figure A3-2. *Count rate per day for each receiver (Variable Y-Max). Day is set to between 21:00 and 06:00 in order to avoid noise. Values were manually checked for large numbers signifying some form of noise.*

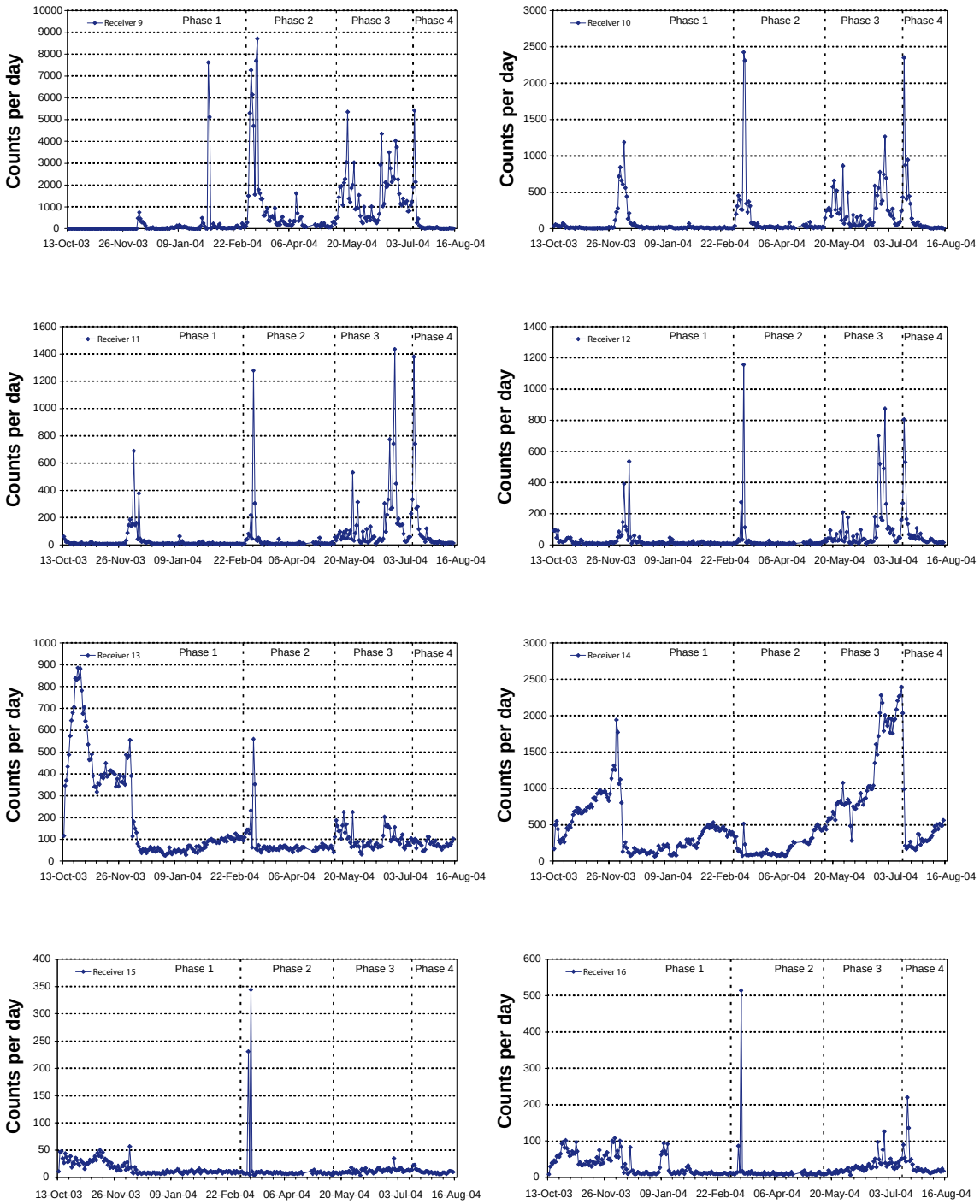

Figure A3-2 (cont). *Count rate per day for each receiver (Variable Y-Max). Day is set to between 21:00 and 06:00 in order to avoid noise. Values were manually checked for large numbers signifying some form of noise.*

Appendix 4

Location of calibration hits

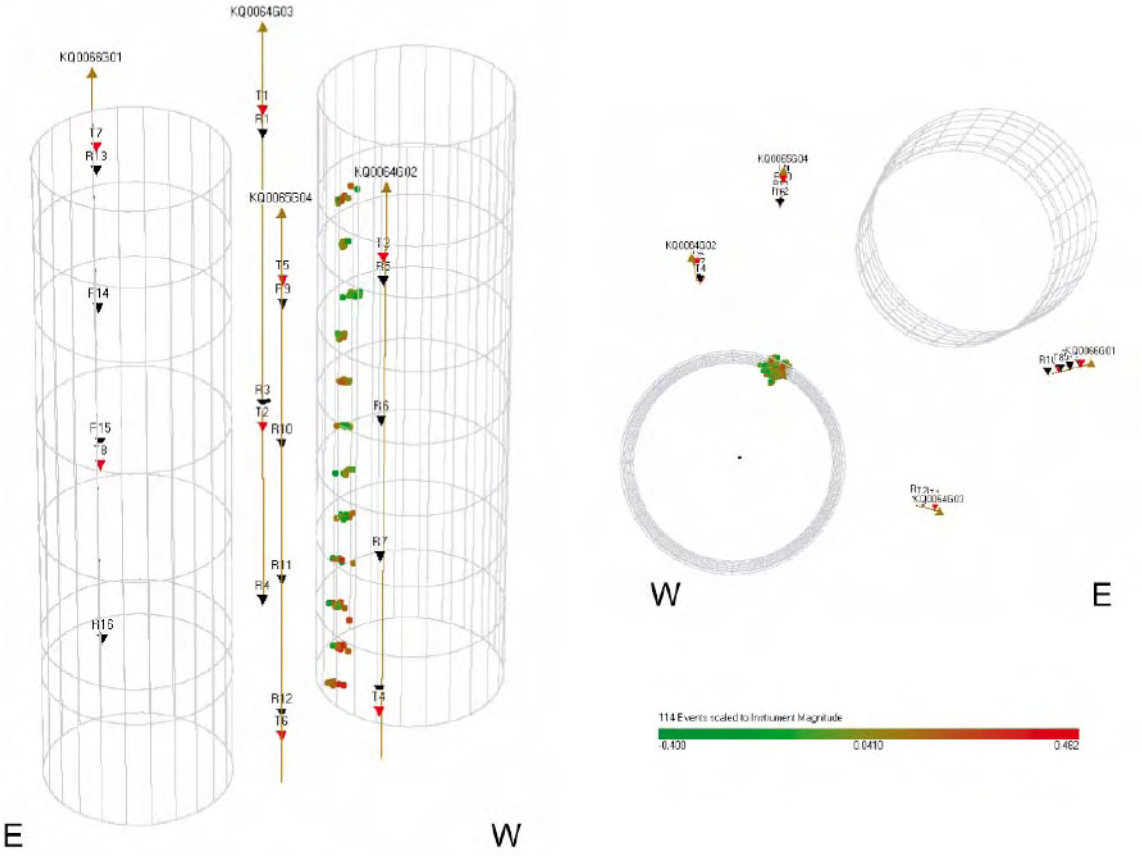

Figure A4-1. *Computed locations for Screwdriver shots conducted in DQ0063G01.*

Table A4-1. Average and standard deviation of the difference in distance between each calibration hit and the mean location of the cluster, undertaken on the screwdriver hits.

Calibration Cluster #	Depth from concrete roadway (m)	Average of distances to mean location (m)	Standard deviation of distances to mean location (m)
1	0.5	0.076	0.050
2	1.0	0.026	0.010
3	1.5	0.050	0.027
4	2.0	0.036	0.022
5	2.5	0.031	0.018
6	3.0	0.037	0.021
7	3.5	0.044	0.032
8	4.0	0.052	0.037
9	4.5	0.046	0.032
10	5.0	0.063	0.043
11	5.5	0.061	0.036
12	6.0	0.046	0.026

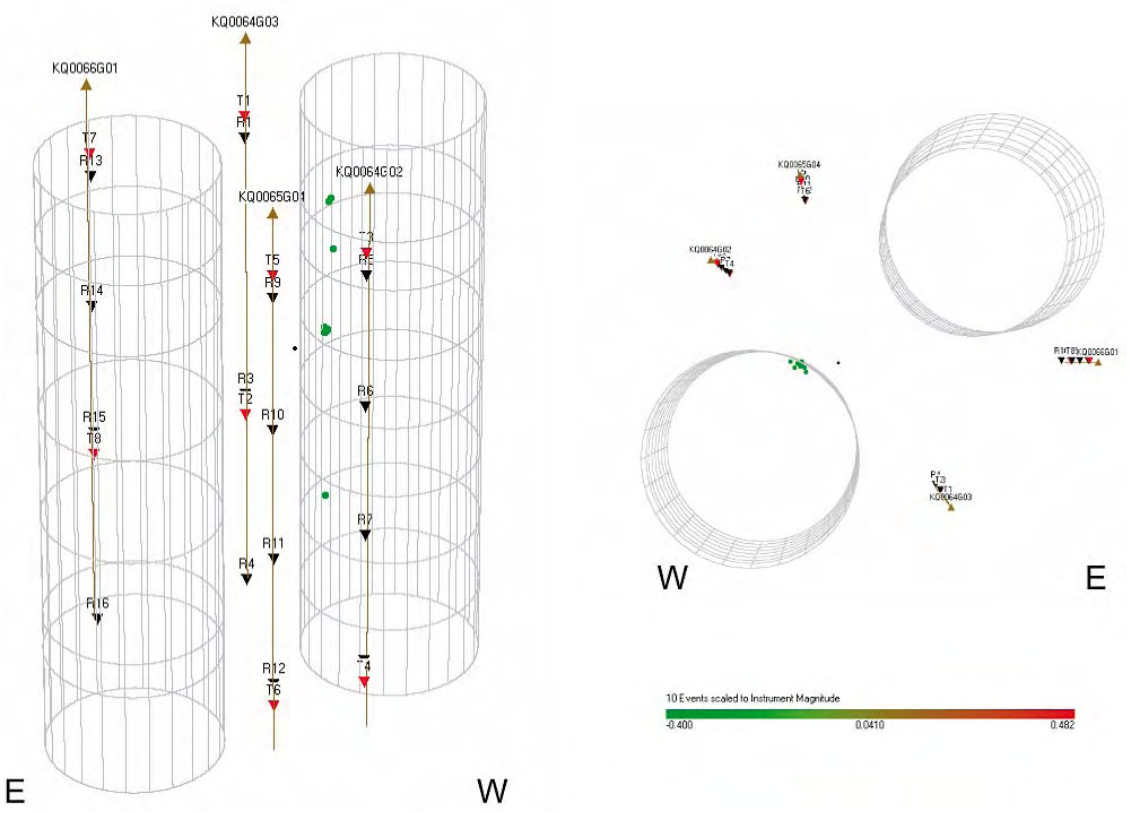

Figure A4-2. *Computed locations of pencil break tests (green markers) conducted in DQ0063G01.*

Appendix 5

Velocity survey results

P- and S-wave velocity change graphs from 13 October 2003 are displayed in the following appendices. Raypaths shown are for a transmitter, t_n, to receivers, r_n, with increasing depth. The schematic diagram in the right margin indicates the relative locations of the transmitter (red) and receivers (gold). The graphs are split up into raypaths on pairs of boreholes. The sections are split accordingly:

A: Skimming deposition hole DQ0063G01

B: Centre of pillar

C: North west of pillar

D: South east of pillar

E: Skimming deposition hole DQ0066G01

A: Skimming deposition hole DQ0063G01

P- and S-wave velocity change graphs from 13 October 2003 are displayed in the following appendices. Raypaths shown are for a transmitter, t_n, to receivers, r_n, with increasing depth. The schematic diagram in the right margin indicates the relative locations of the transmitter (red) and receivers (gold). The graphs are split up into raypaths on pairs of boreholes.

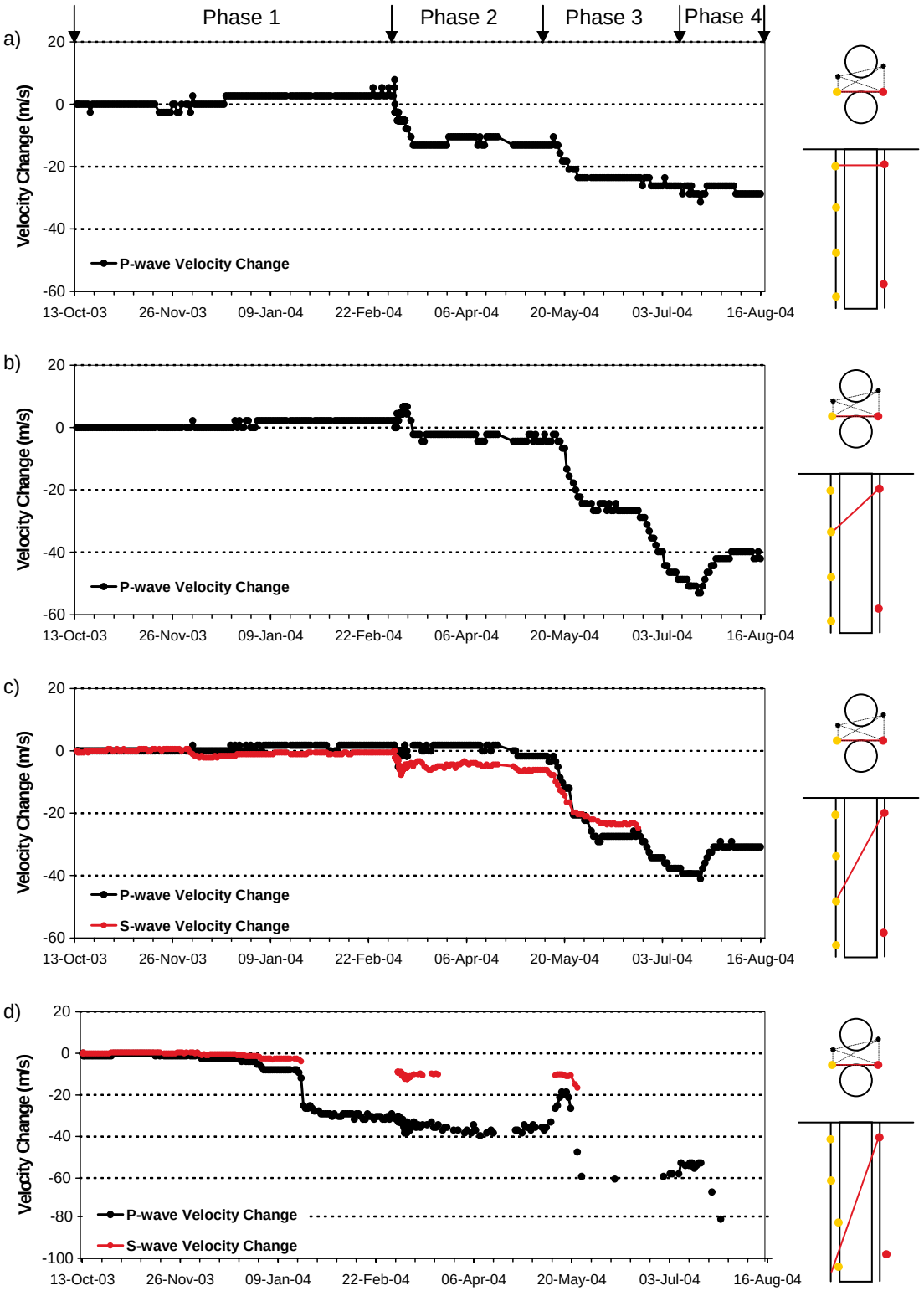

Boreholes KQ0064G03 and KQ0064G02 **a)** t_n=1, r_n=5; **b)** t_n=1, r_n=6; **c)** t_n=1, r_n=7; **d)** t_n=1, r_n=8

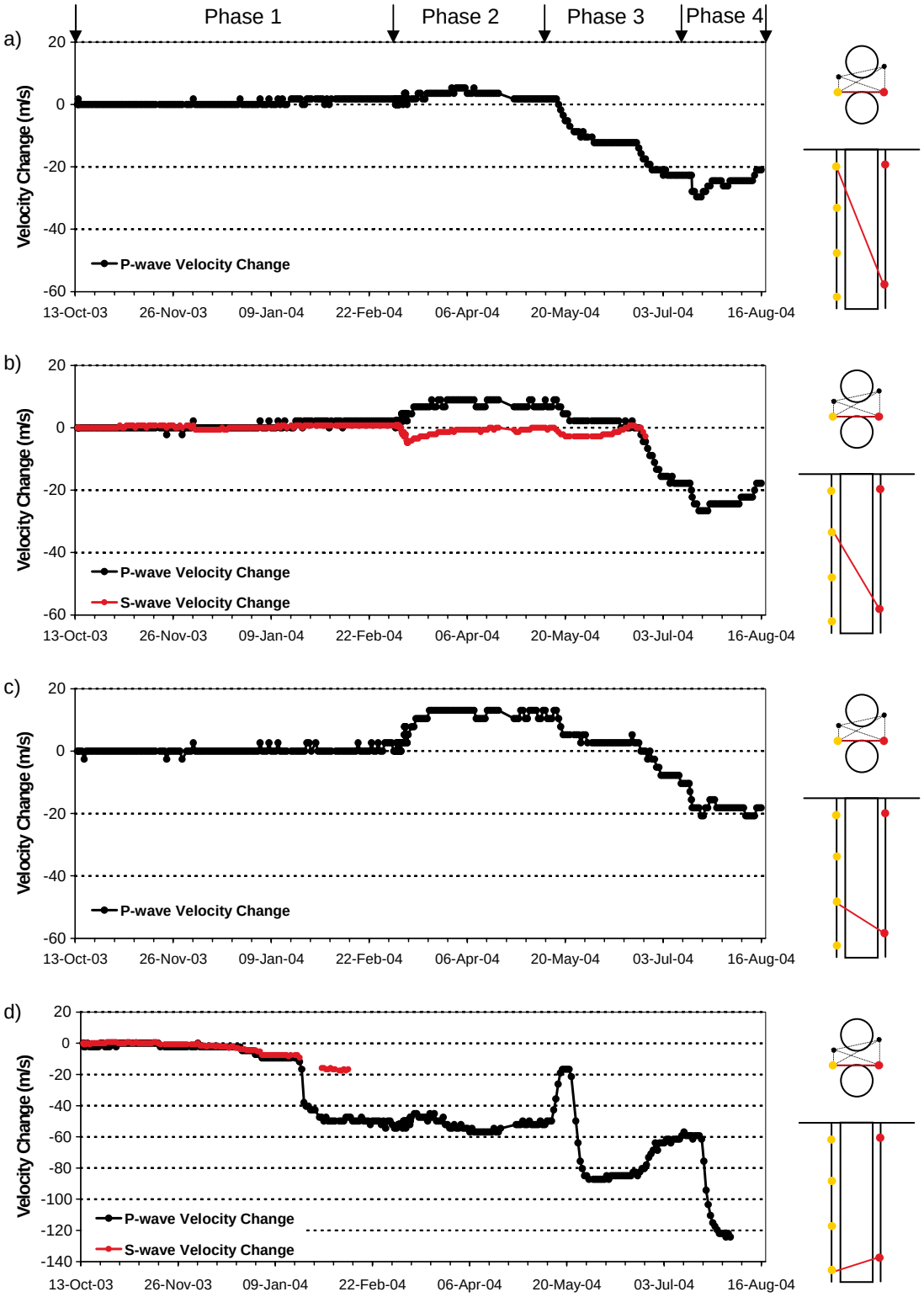

Boreholes KQ0064G03 and KQ0064G02 **a)** t_n=2, r_n=5; **b)** t_n=2, r_n=6; **c)** t_n=2, r_n=7; **d)** t_n=2, r_n=8

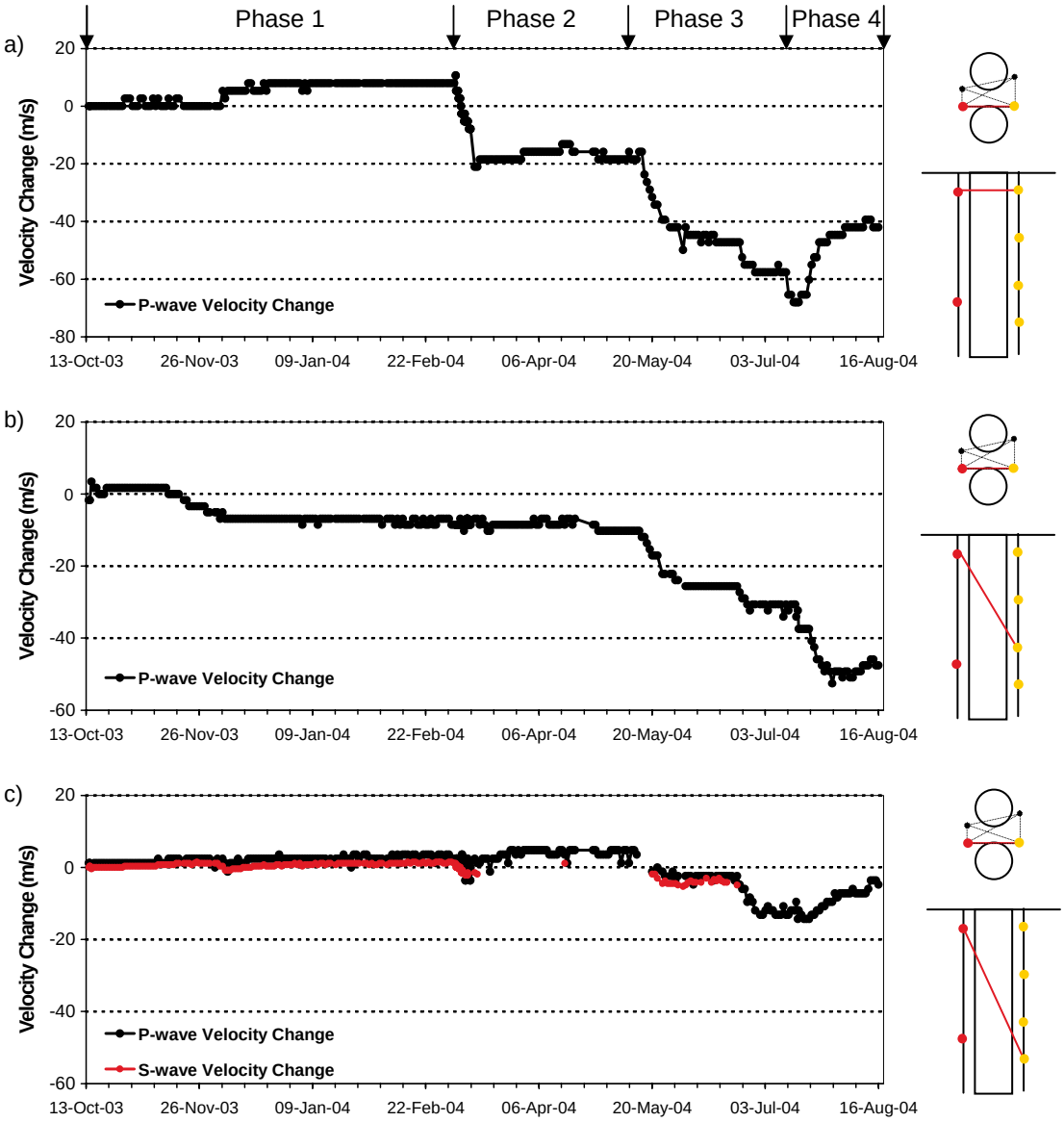

Boreholes KQ0064G03 and KQ0064G02 **a)** t_n=3, r_n=1; **b)** t_n=3, r_n=3; **c)** t_n=3, r_n=4

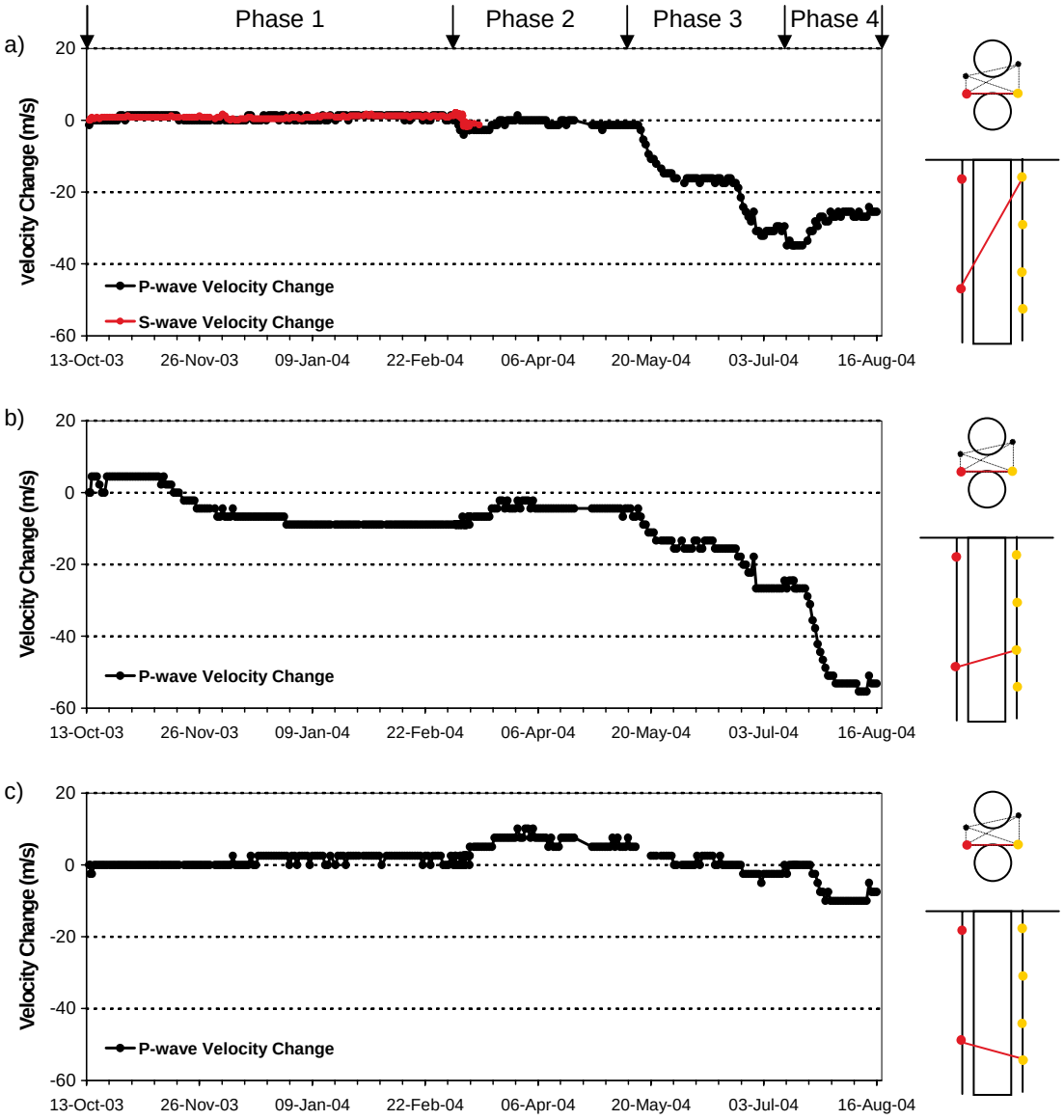

Boreholes KQ0064G03 and KQ0064G02 **a)** t_n=4, r_n=1; **b)** t_n=4, r_n=3; **c)** t_n=4, r_n=4

B: Centre of pillar

P- and S-wave velocity change graphs from 13 October 2003 are displayed in the following appendices. Raypaths shown are for a transmitter, t_n, to receivers, r_n, with increasing depth. The schematic diagram in the right margin indicates the relative locations of the transmitter (red) and receivers (gold). The graphs are split up into raypaths on pairs of boreholes.

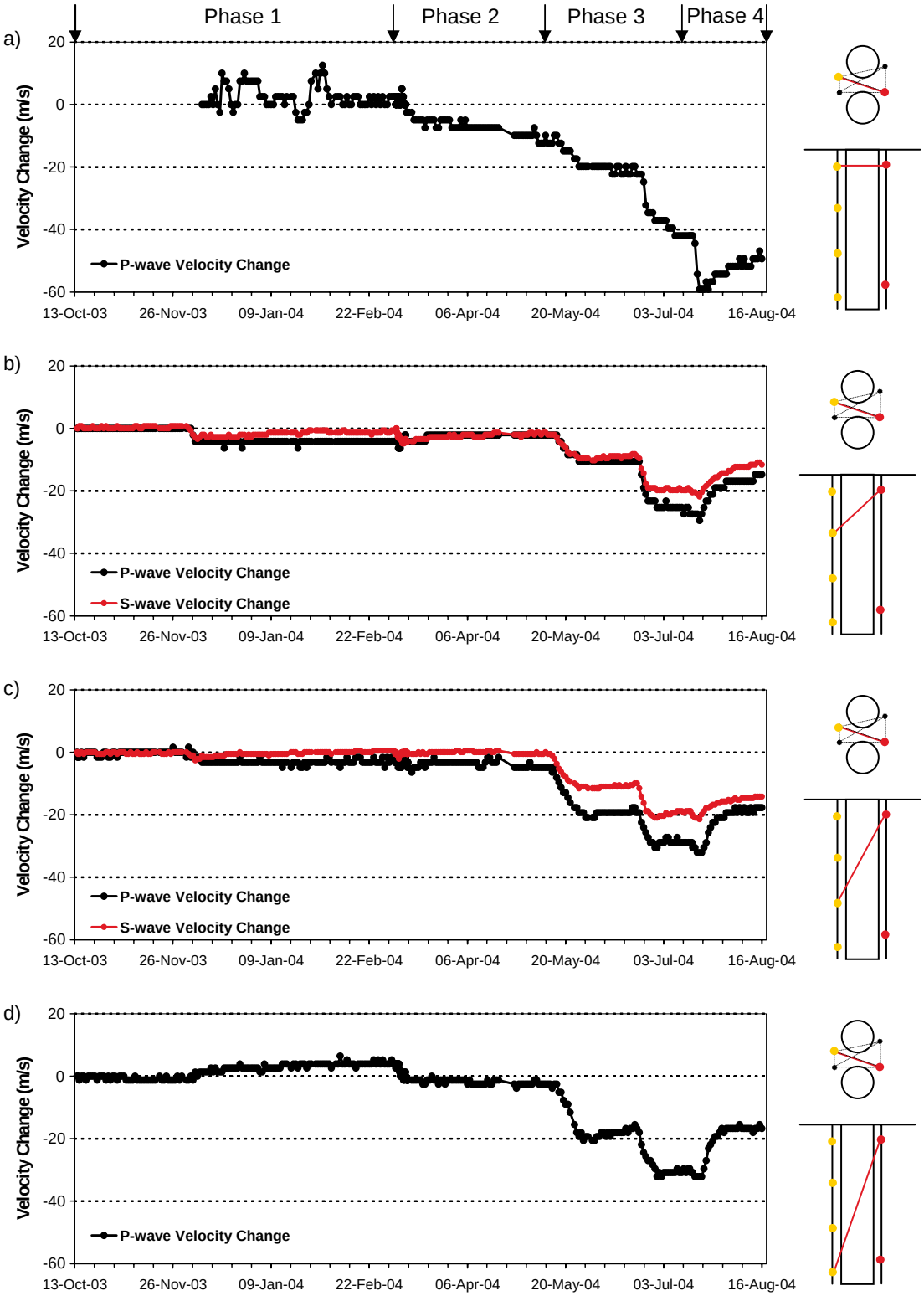

Boreholes KQ0064G03 and KQ0065G04 **a)** t_n=1, r_n=9; **b)** t_n=1, r_n=10; **c)** t_n=1, r_n=11; **d)** t_n=1, r_n=12

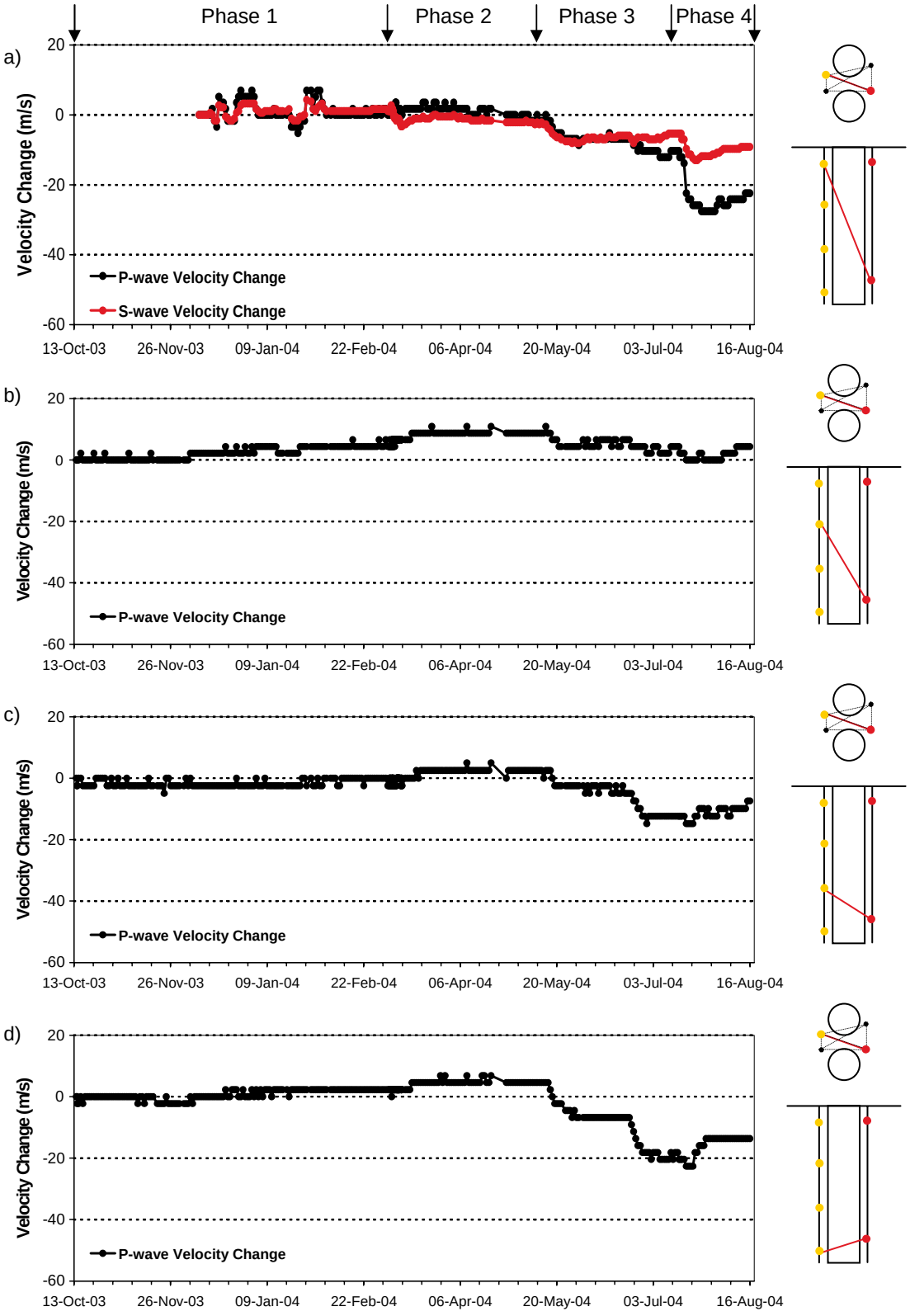

Boreholes KQ0064G03 and KQ0065G04 **a)** t_n=2, r_n=9; **b)** t_n=2, r_n=10; **c)** t_n=2, r_n=11; **d)** t_n=2, r_n=12

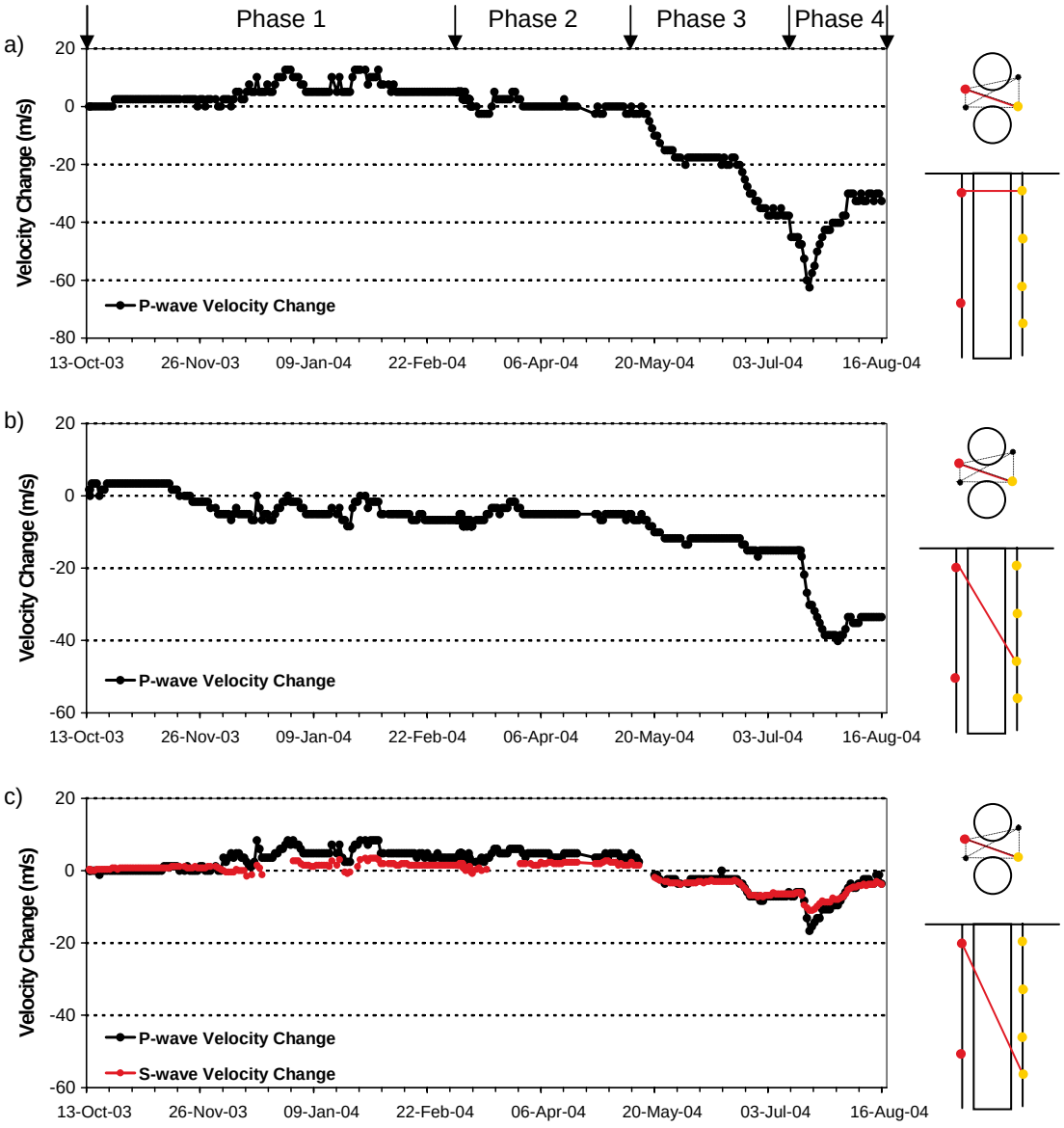

Boreholes KQ0064G03 and KQ0065G04 **a)** t_n=5, r_n=1; **b)** t_n=5, r_n=3; **c)** t_n=5, r_n=4

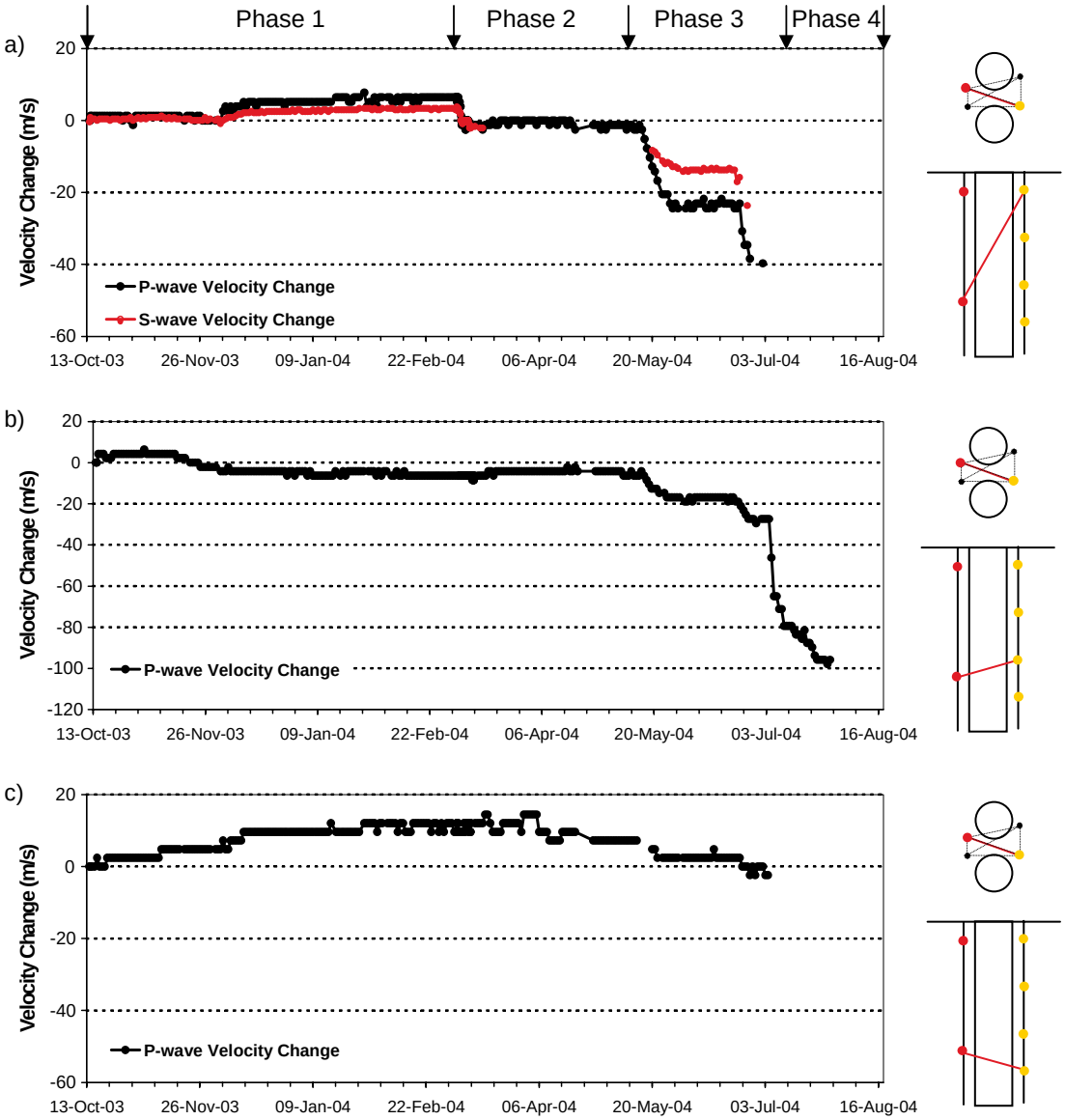

Boreholes KQ0064G03 and KQ0065G04 **a)** t_n=6, r_n=1; **b)** t_n=6, r_n=3; **c)** t_n=6, r_n=4

C: North west of pillar

P- and S-wave velocity change graphs from 13 October 2003 are displayed in the following appendices. Raypaths shown are for a transmitter, t_n, to receivers, r_n, with increasing depth. The schematic diagram in the right margin indicates the relative locations of the transmitter (red) and receivers (gold). The graphs are split up into raypaths on pairs of boreholes.

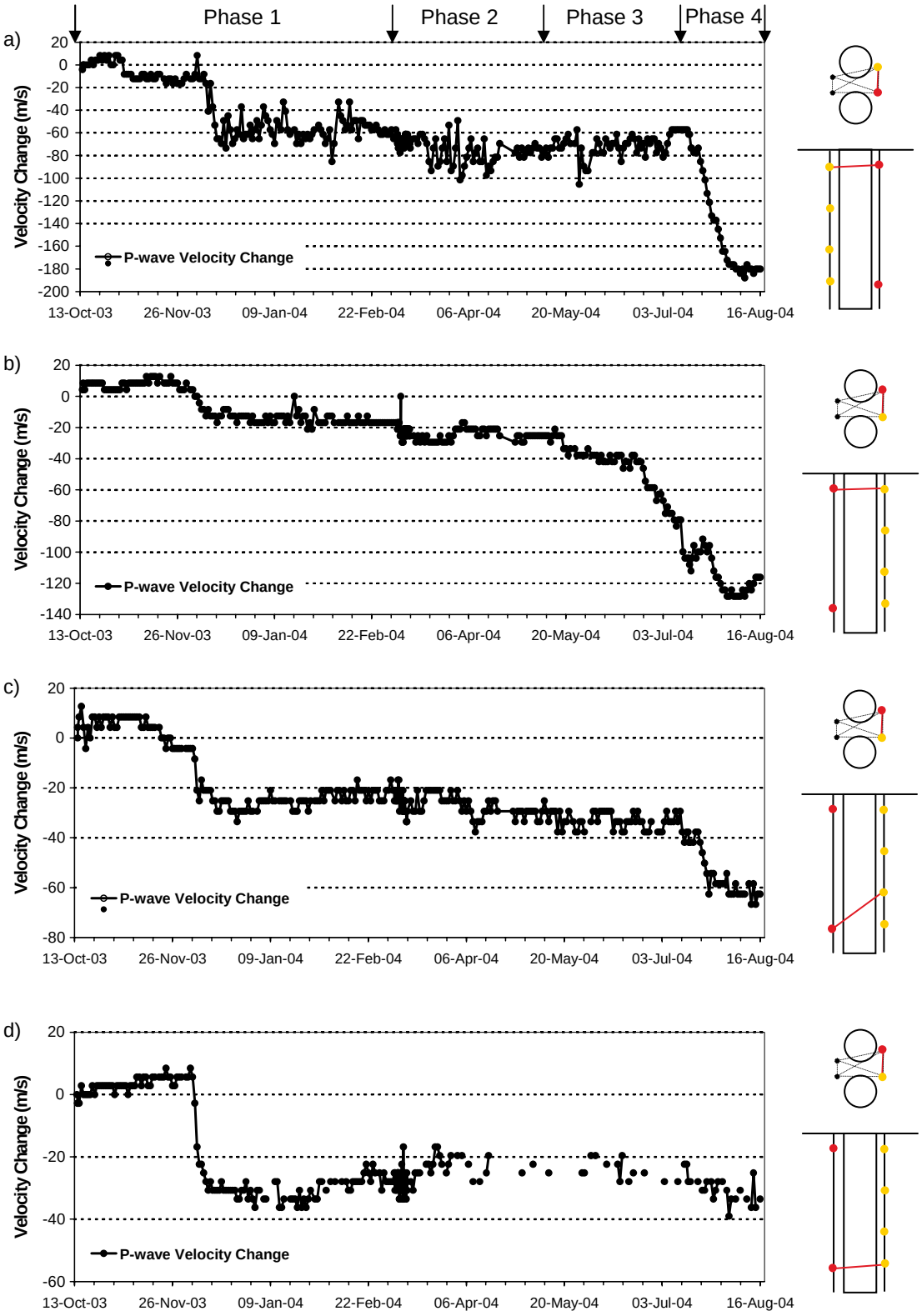

Boreholes KQ0064G03 and KQ0066G01 **a)** t_n=1, r_n=13; **b)** t_n=7, r_n=1; **c)** t_n=8, r_n=3; **d)** t_n=8, r_n=4

D: South east of pillar

P- and S-wave velocity change graphs from 13 October 2003 are displayed in the following appendices. Raypaths shown are for a transmitter, t_n, to receivers, r_n, with increasing depth. The schematic diagram in the right margin indicates the relative locations of the transmitter (red) and receivers (gold). The graphs are split up into raypaths on pairs of boreholes.

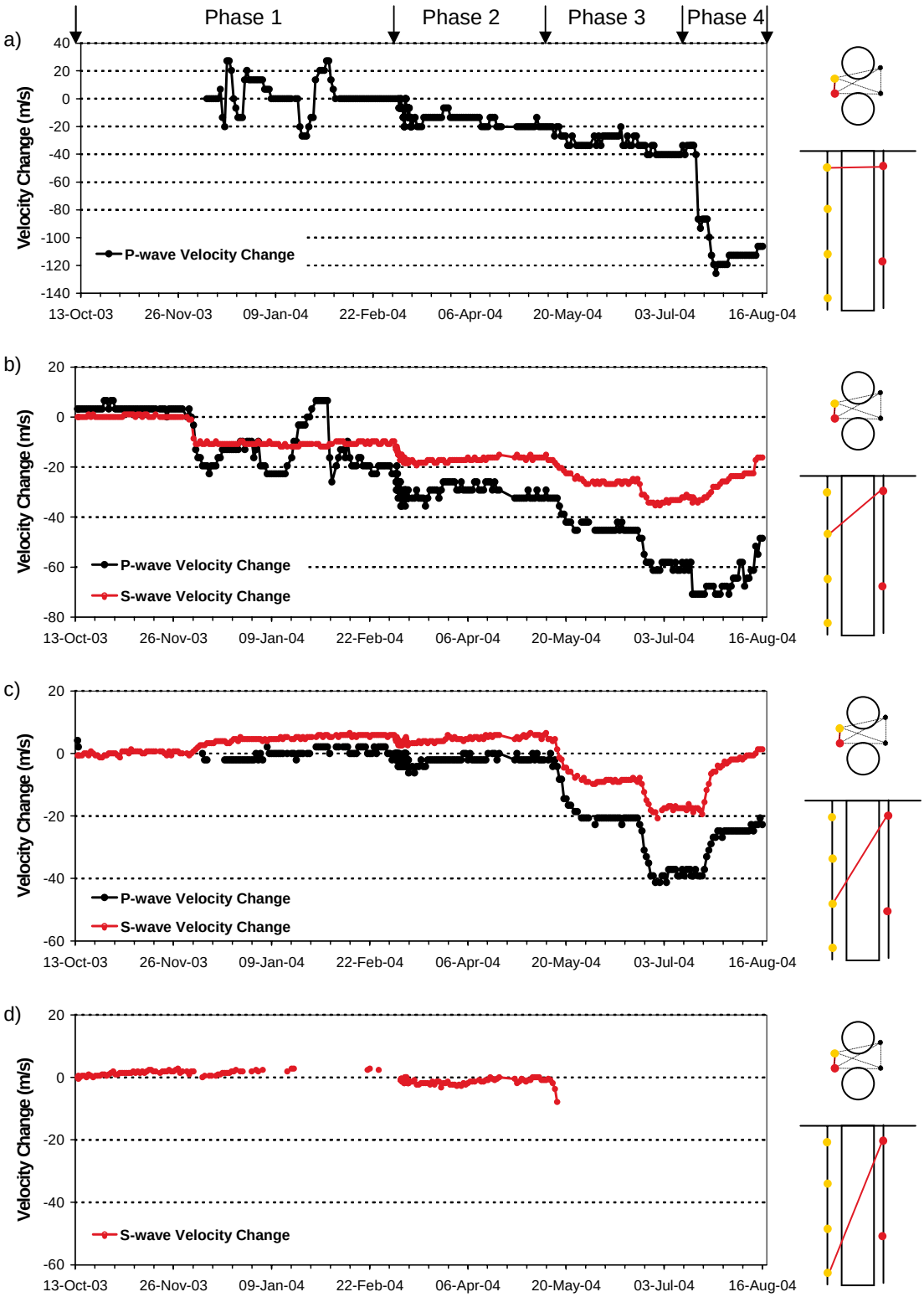

Boreholes KQ0064G02 and KQ0065G04 **a)** t_n=3, r_n=9; **b)** t_n=3, r_n=10; **c)** t_n=3, r_n=11; **d)** t_n=3, r_n=12

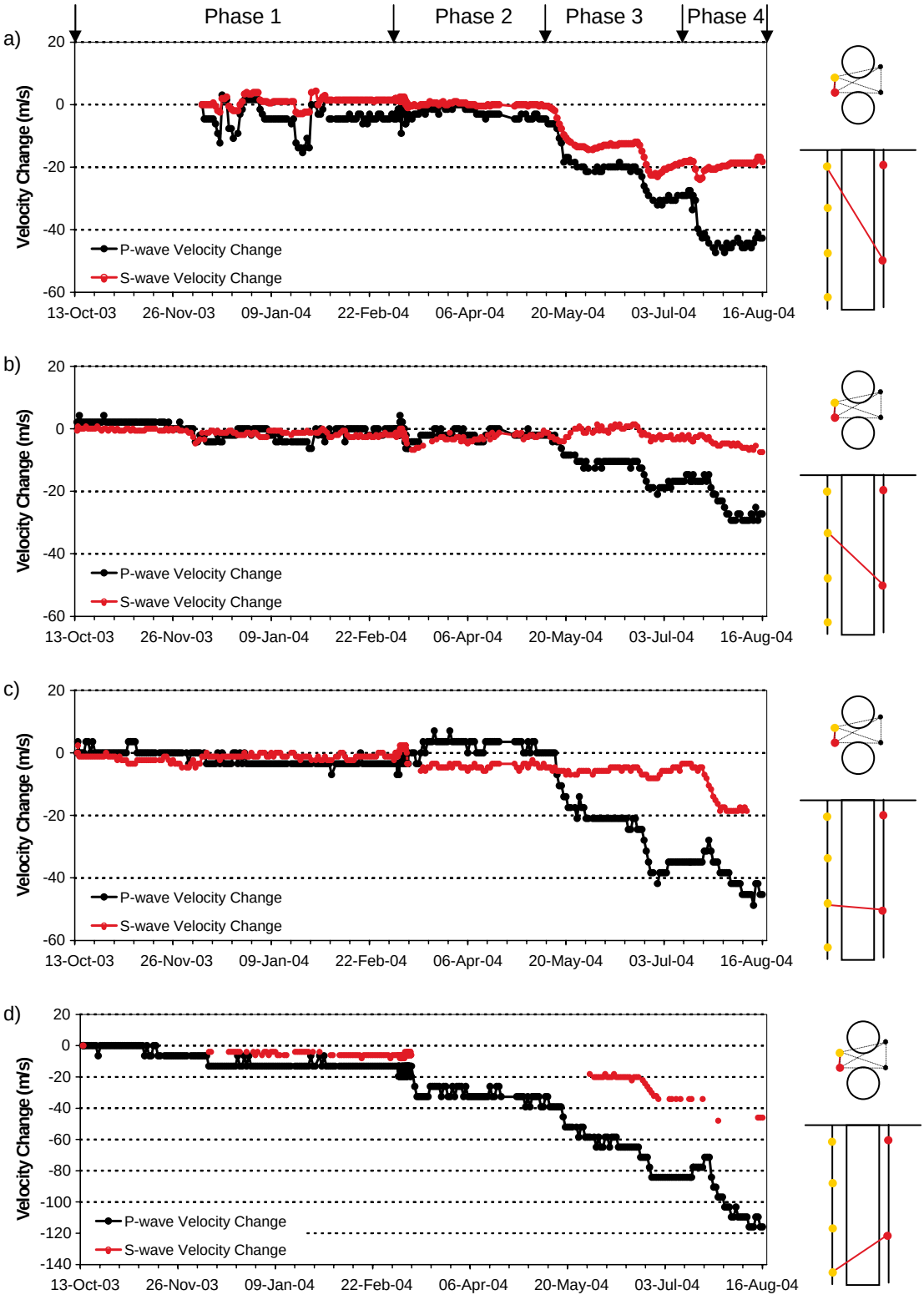

Boreholes KQ0064G02 and KQ0065G04 **a)** t_n=4, r_n=9; **b)** t_n=4, r_n=10; **c)** t_n=4, r_n=11; **d)** t_n=4, r_n=12

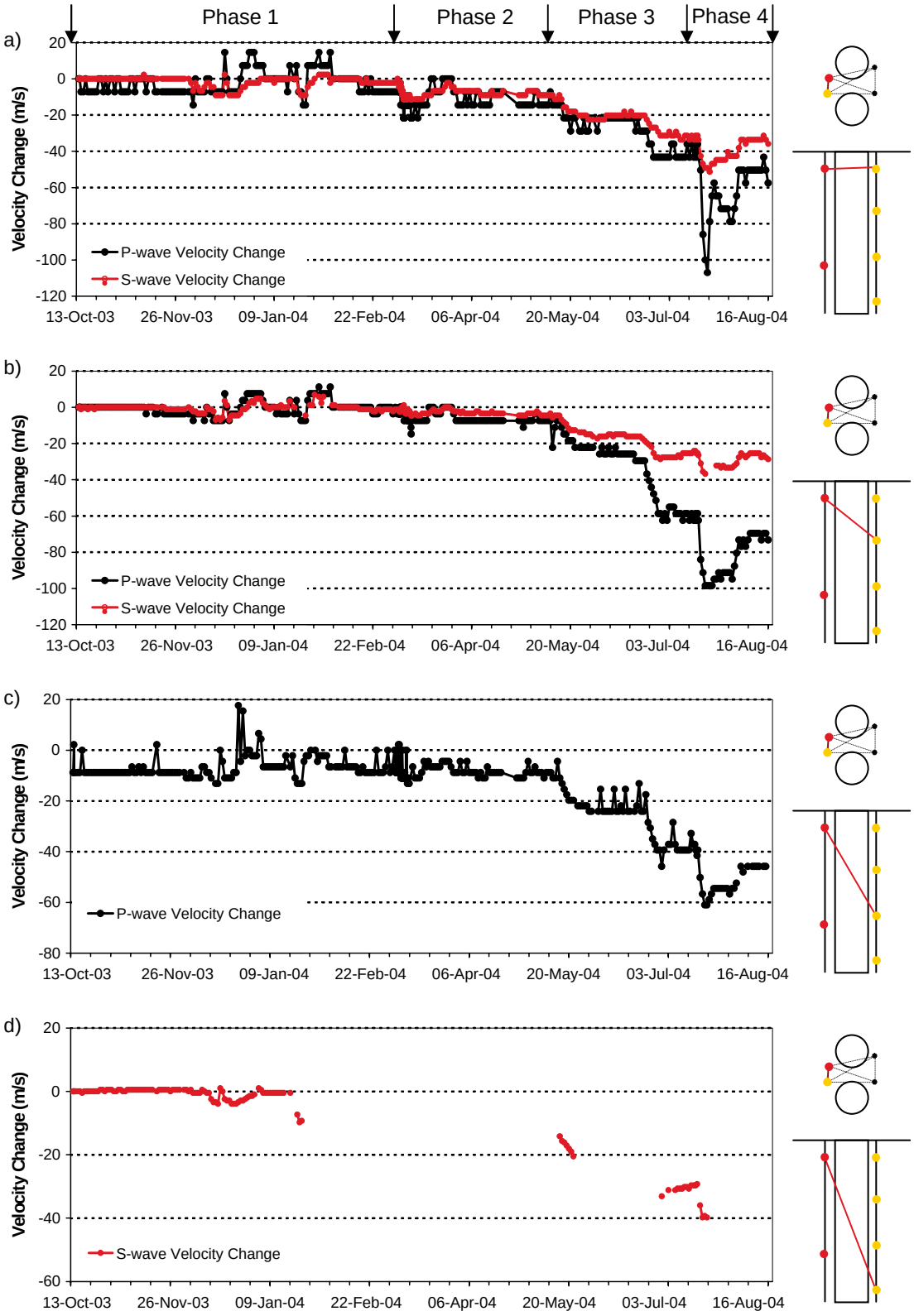

Boreholes KQ0064G02 and KQ0065G04 **a)** t_n=5, r_n=5; **b)** t_n=5, r_n=6; **c)** t_n=5, r_n=7; **d)** t_n=5, r_n=8

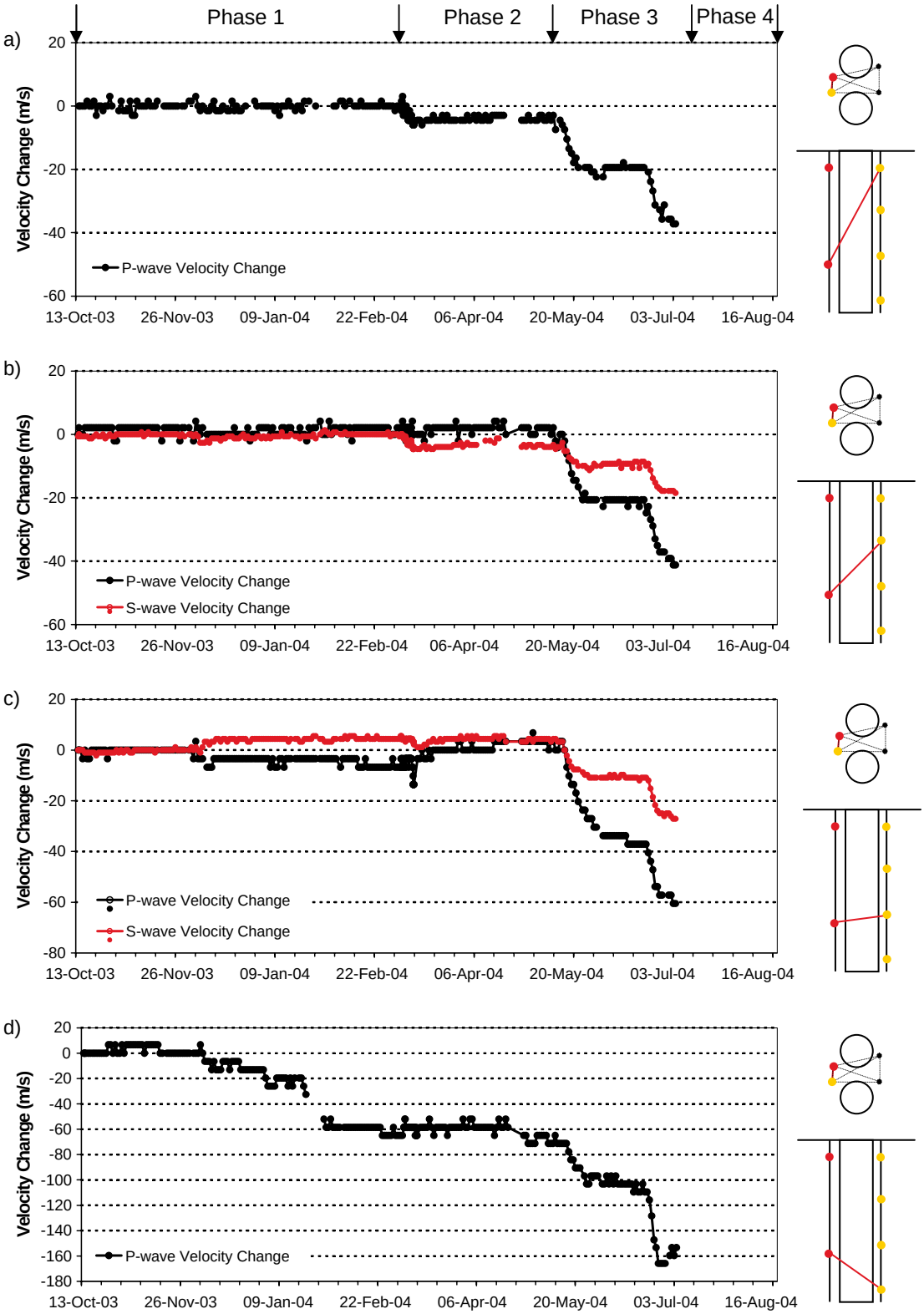

Boreholes KQ0064G02 and KQ0065G04 **a)** t_n=6, r_n=5; **b)** t_n=6, r_n=6; **c)** t_n=6, r_n=7; **d)** t_n=6, r_n=8

E: Skimming deposition hole DQ0066G01

P- and S-wave velocity change graphs from 13 October 2003 are displayed in the following appendices. Raypaths shown are for a transmitter, t_n, to receivers, r_n, with increasing depth. The schematic diagram in the right margin indicates the relative locations of the transmitter (red) and receivers (gold). The graphs are split up into raypaths on pairs of boreholes.

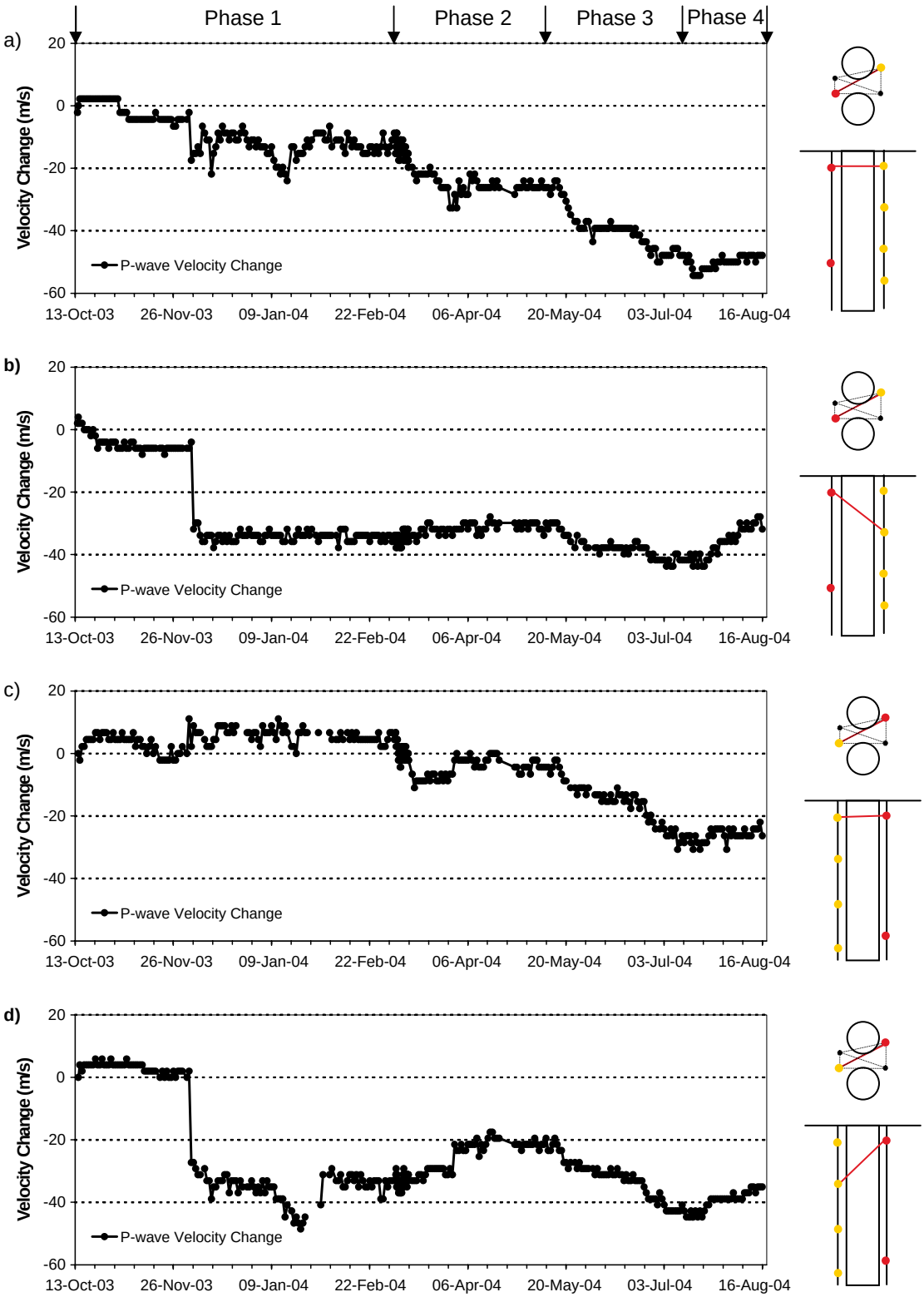

Boreholes KQ0064G02 and KQ0066G01 **a)** t_n=3, r_n=13; **b)** t_n=3, r_n=14; **c)** t_n=7, r_n=5; **d)** t_n=7, r_n=6

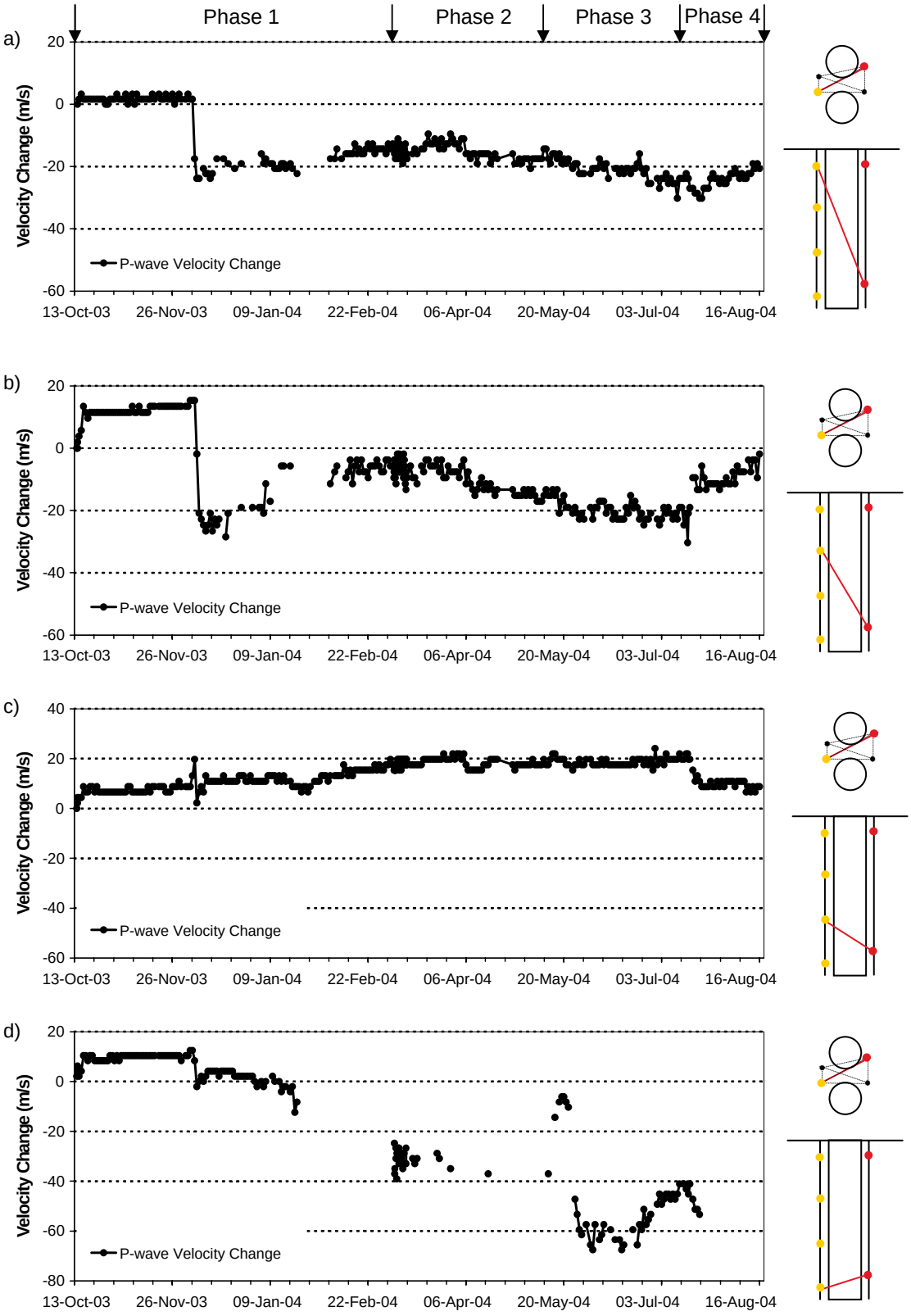

Boreholes KQ0064G02 and KQ0066G01 **a)** t_n=8, r_n=5; **b)** t_n=8, r_n=6; **c**) t_n=8, r_n=7; **d)** t_n=8, r_n=8

Appendix 6

Amplitude survey results

P- and S-wave amplitude change graphs from 13 October 2003 are displayed in the following appendices. Amplitude change is measured in decibels (dB), which is not effected by raypath length, orientation or coupling of sensors. This allows amplitude variation of different raypaths to be compared on the same plot. Raypaths shown are for a transmitter, t_n, to receivers, r_n, with increasing depth. The schematic diagram in the right margin indicates the relative locations of the transmitter (red) and receivers (gold). The graphs are split up into raypaths on pairs of boreholes. The sections are split accordingly:

A: Skimming deposition hole DQ0063G01

B: Centre of pillar

C: North west of pillar

D: South east of pillar

E: Skimming deposition hole DQ0066G01

A: Skimming deposition hole DQ0063G01

P- and S-wave amplitude change graphs from 13 October 2003 are displayed in the following appendices. Amplitude change is measured in decibels (dB), which is not effected by raypath length, orientation or coupling of sensors. This allows amplitude variation of different raypaths to be compared on the same plot. Raypaths shown are for a transmitter, t_n, to receivers, r_n, with increasing depth. The schematic diagram in the right margin indicates the relative locations of the transmitter (red) and receivers (gold). The graphs are split up into raypaths on pairs of boreholes.

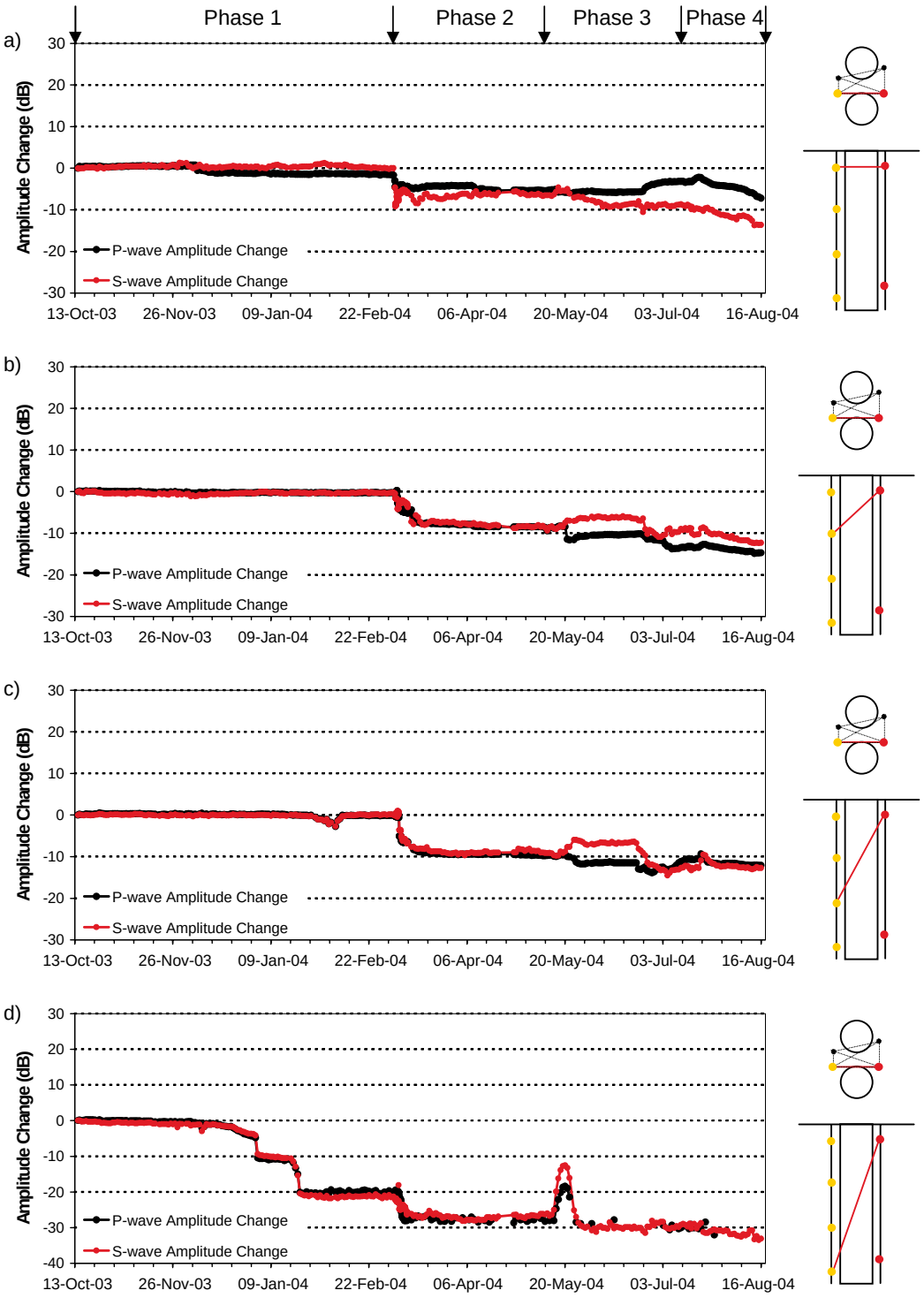

Boreholes KQ0064G03 and KQ0064G02 **a)** t_n=1, r_n=5; **b)** t_n=1, r_n=6; **c)** t_n=1, r_n=7; **d)** t_n=1, r_n=8

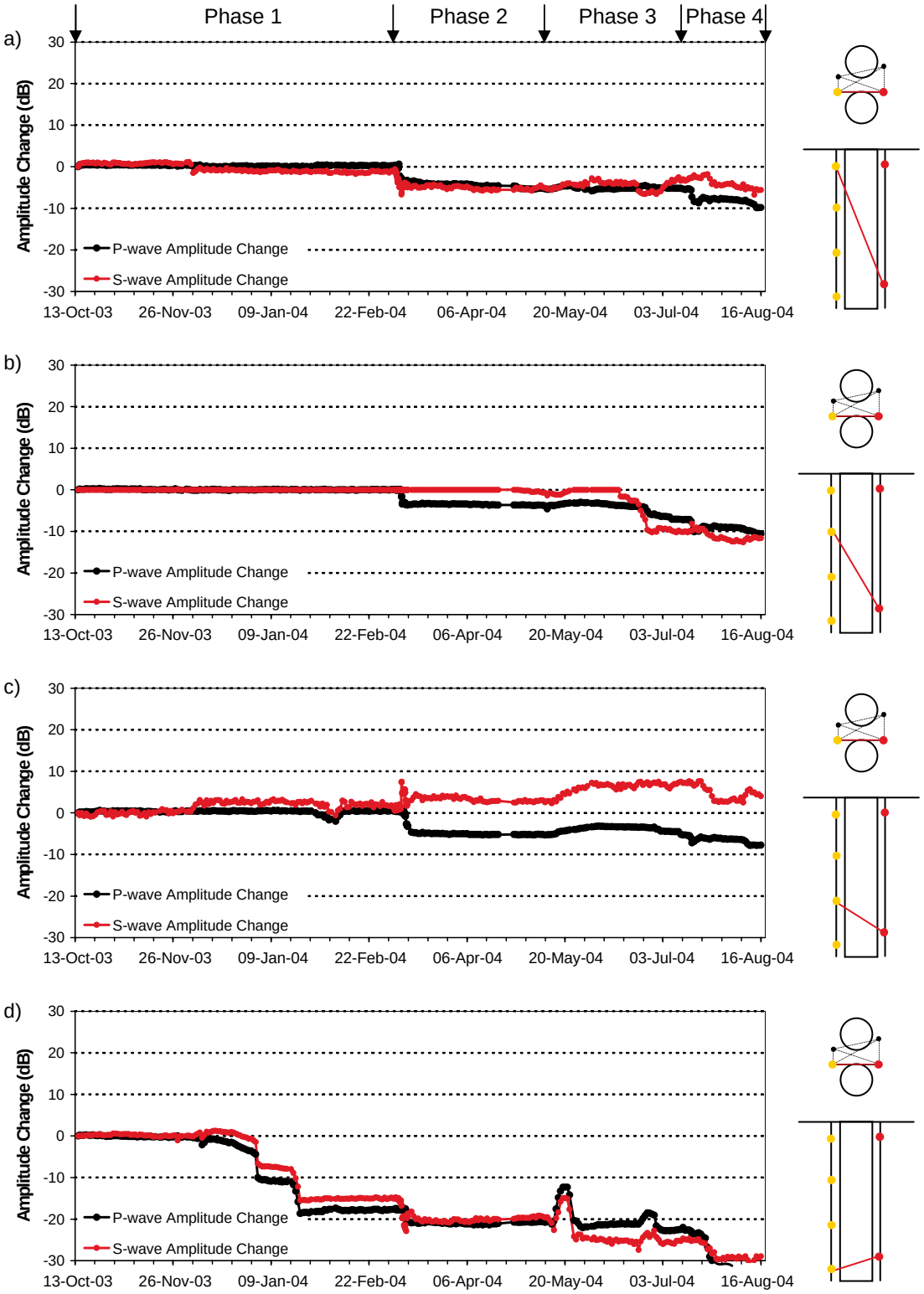

Boreholes KQ0064G03 and KQ0064G02 **a)** t_n=2, r_n=5; **b)** t_n=2, r_n=6; **c)** t_n=2, r_n=7; **d)** t_n=2, r_n=8

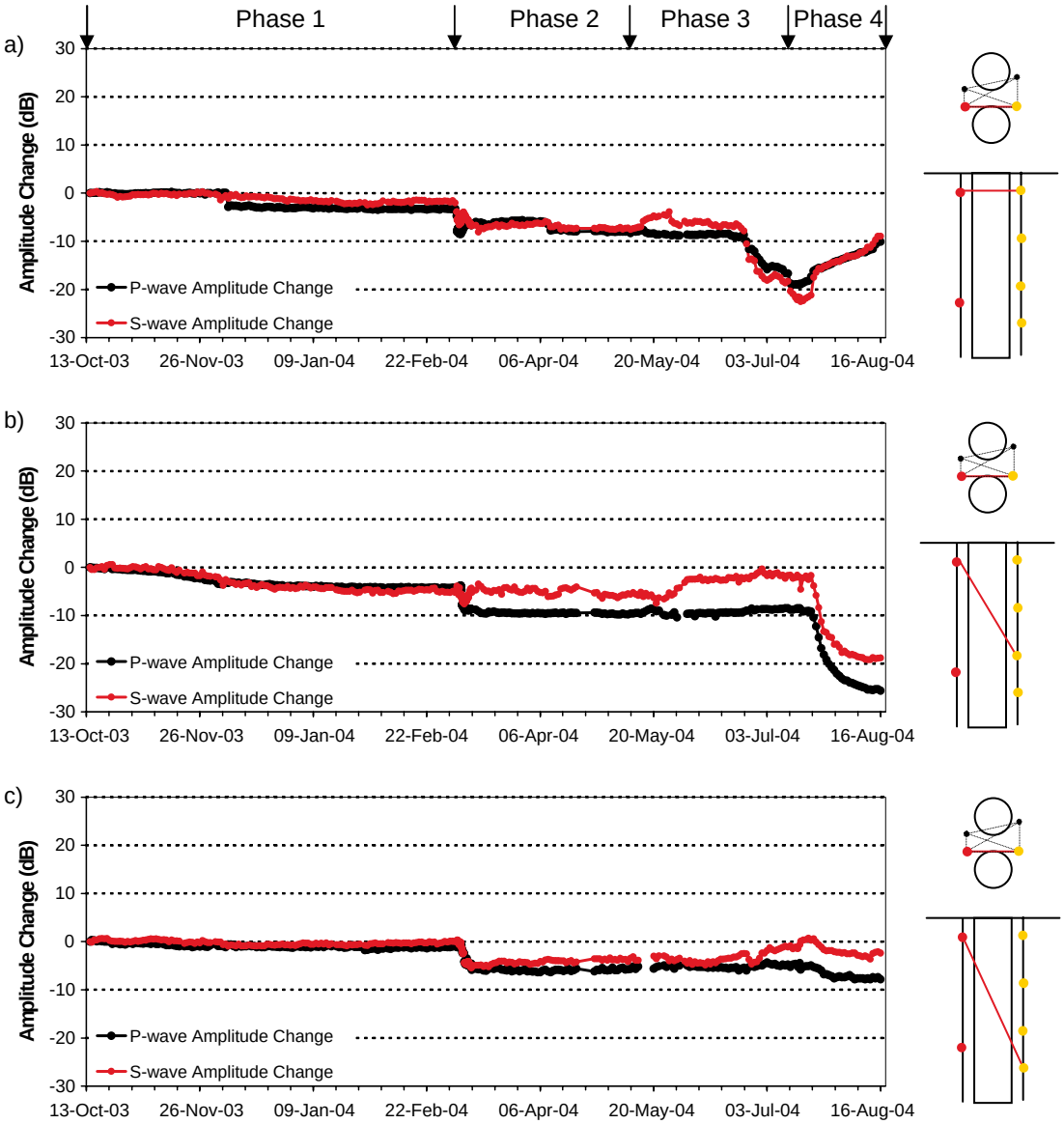

Boreholes KQ0064G03 and KQ0064G02 **a)** t_n=3, r_n=1; **b)** t_n=3, r_n=3; **c)** t_n=3, r_n=4

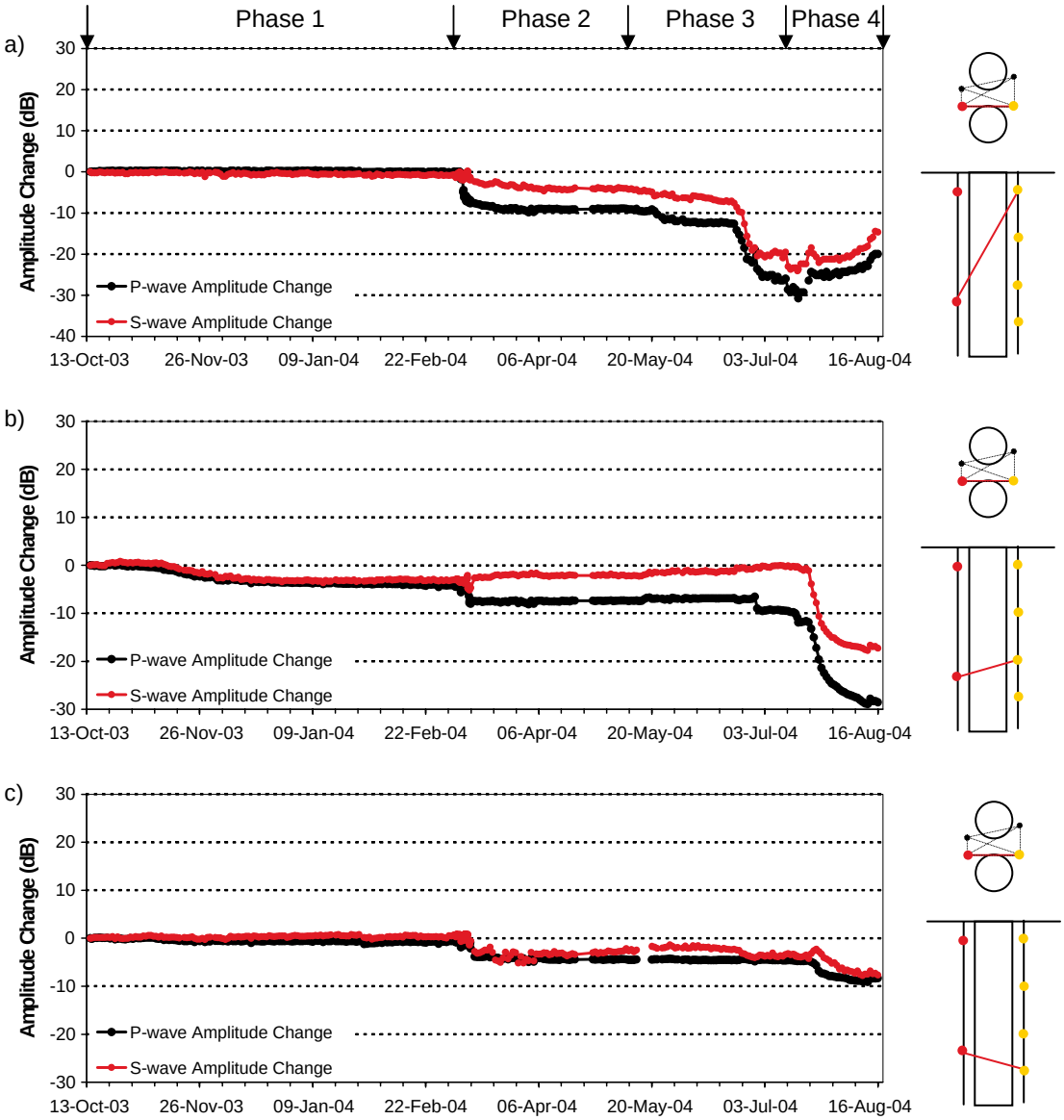

Boreholes KQ0064G03 and KQ0064G02 **a)** t_n=4, r_n=1; **b)** t_n=4, r_n=3; **c)** t_n=4, r_n=4

B: Centre of pillar

P- and S-wave amplitude change graphs from 13 October 2003 are displayed in the following appendices. Amplitude change is measured in decibels (dB), which is not effected by raypath length, orientation or coupling of sensors. This allows amplitude variation of different raypaths to be compared on the same plot. Raypaths shown are for a transmitter, t_n, to receivers, r_n, with increasing depth. The schematic diagram in the right margin indicates the relative locations of the transmitter (red) and receivers (gold). The graphs are split up into raypaths on pairs of boreholes.

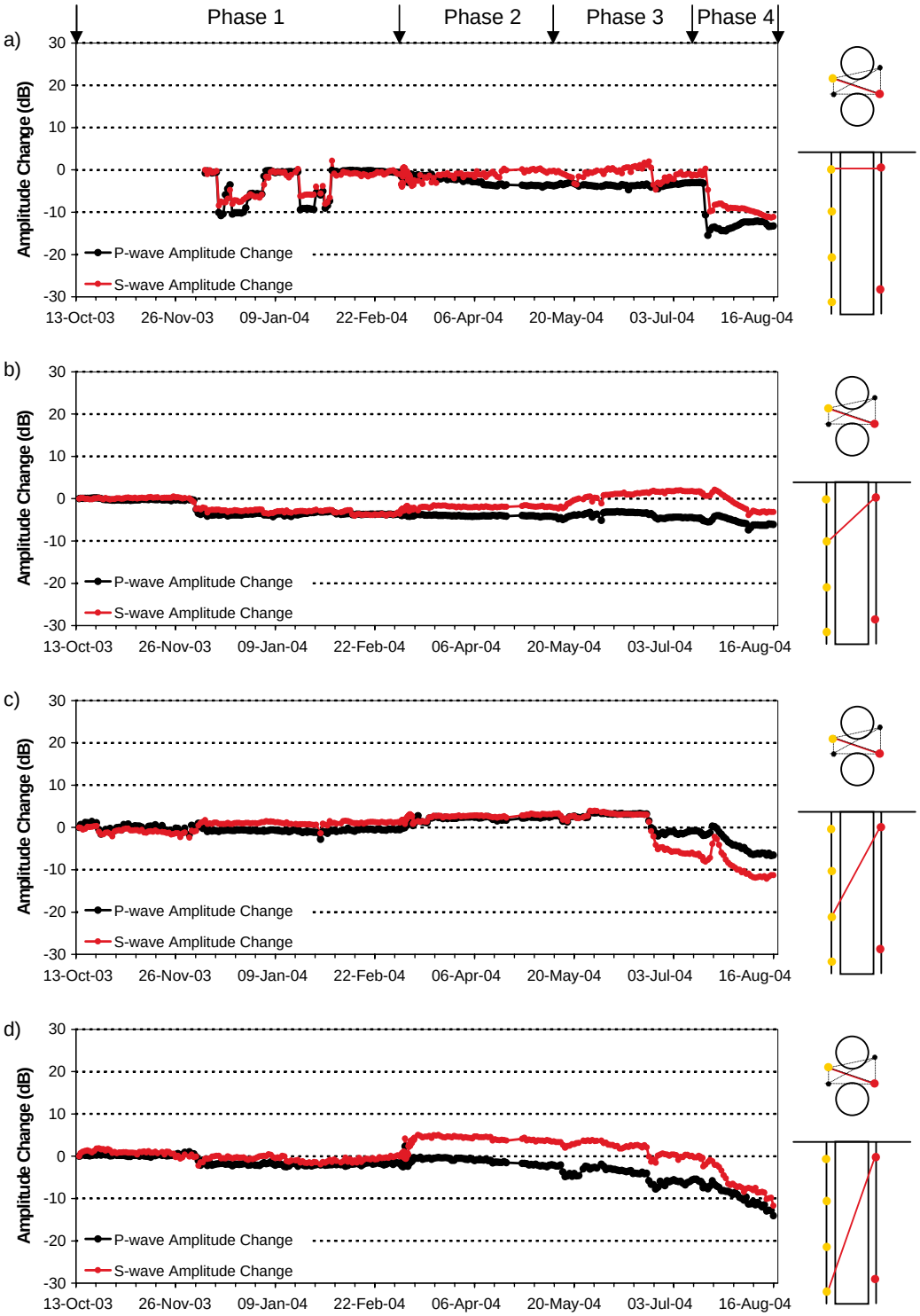

Boreholes KQ0064G03 and KQ0065G04 **a)** t_n=1, r_n=9; **b)** t_n=1, r_n=10; **c)** t_n=1, r_n=11; **d)** t_n=1, r_n=12

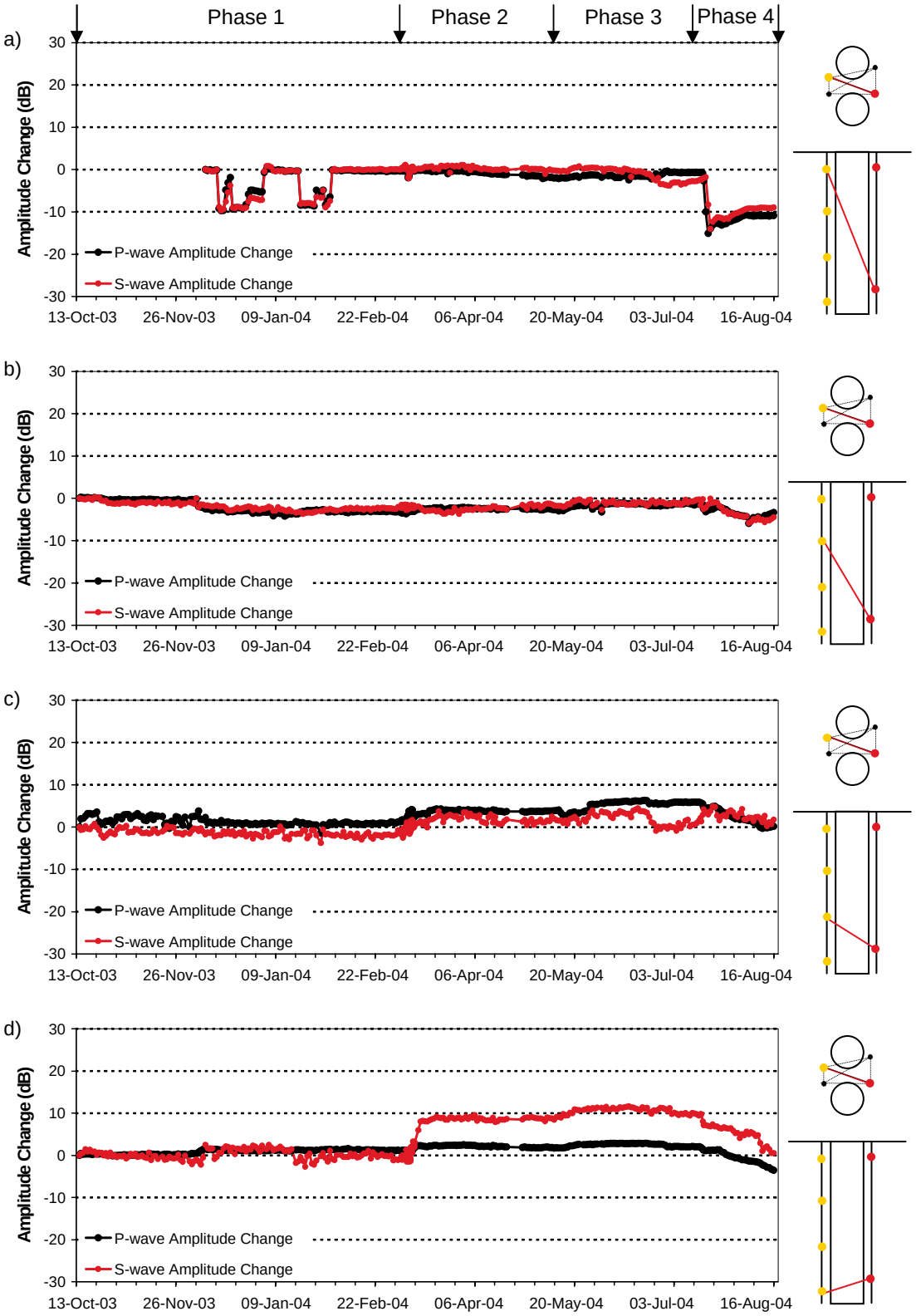

Boreholes KQ0064G03 and KQ0065G04 **a)** t_n=2, r_n=9; **b)** t_n=2, r_n=10; **c)** t_n=2, r_n=11; **d)** t_n=2, r_n=12

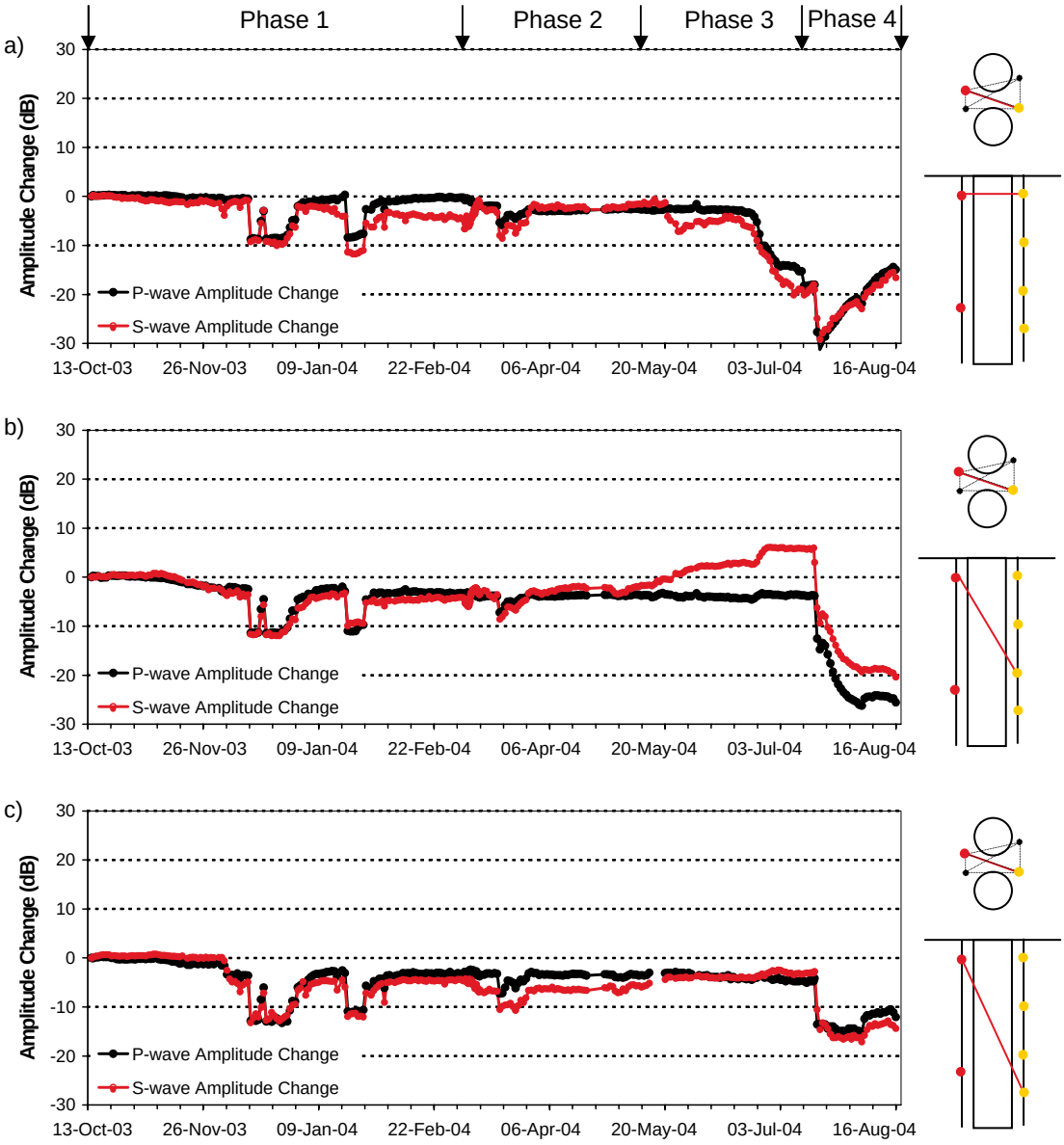

Boreholes KQ0064G03 and KQ0065G04 **a)** t_n=5, r_n=1; **b)** t_n=5, r_n=3; **c)** t_n=5, r_n=4

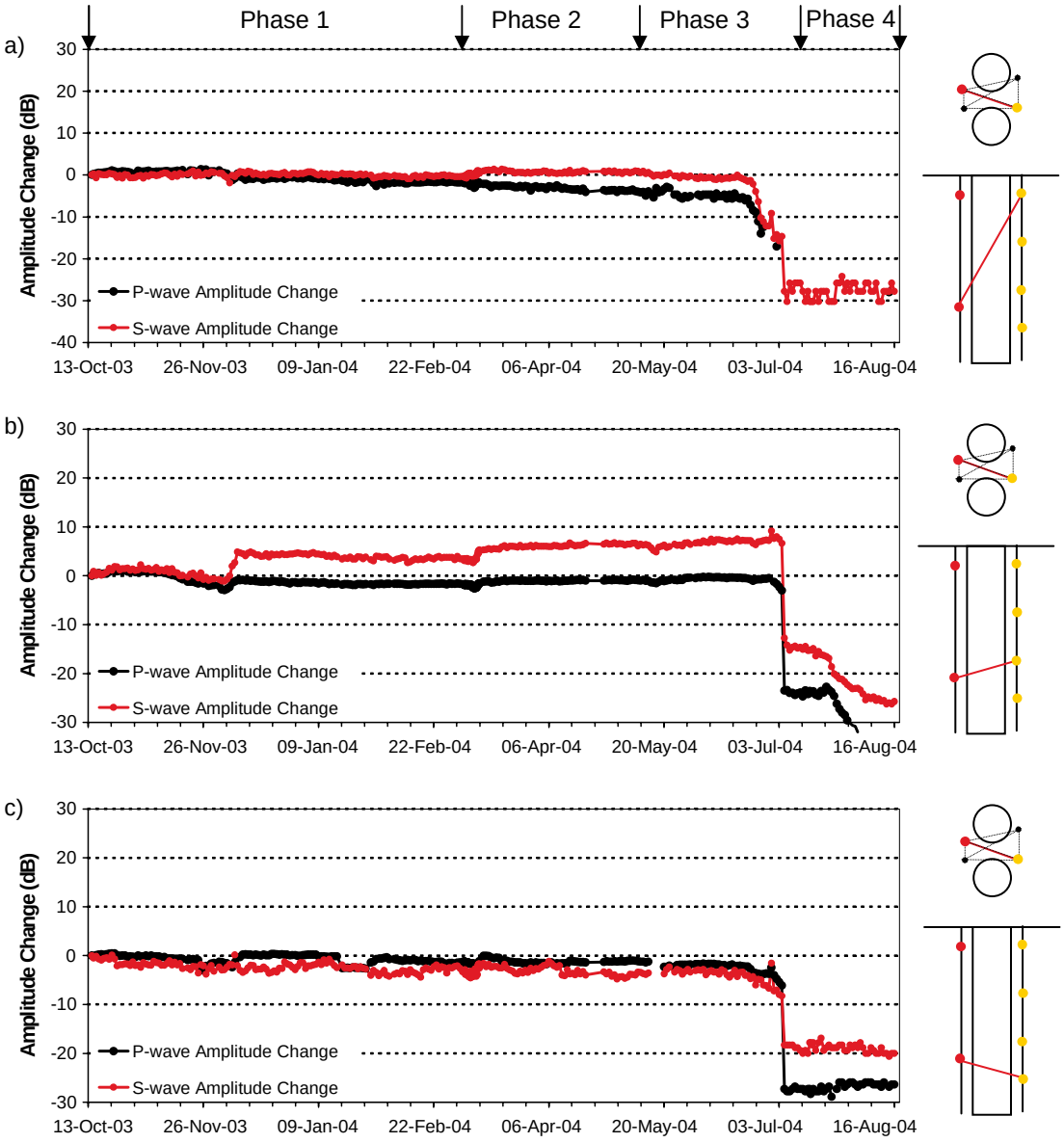

Boreholes KQ0064G03 and KQ0065G04 **a)** t_n=6, r_n=1; **b)** t_n=6, r_n=3; **c)** t_n=6, r_n=4

C: North west of pillar

P- and S-wave amplitude change graphs from 13 October 2003 are displayed in the following appendices. Amplitude change is measured in decibels (dB), which is not effected by raypath length, orientation or coupling of sensors. This allows amplitude variation of different raypaths to be compared on the same plot. Raypaths shown are for a transmitter, t_n, to receivers, r_n, with increasing depth. The schematic diagram in the right margin indicates the relative locations of the transmitter (red) and receivers (gold). The graphs are split up into raypaths on pairs of boreholes.

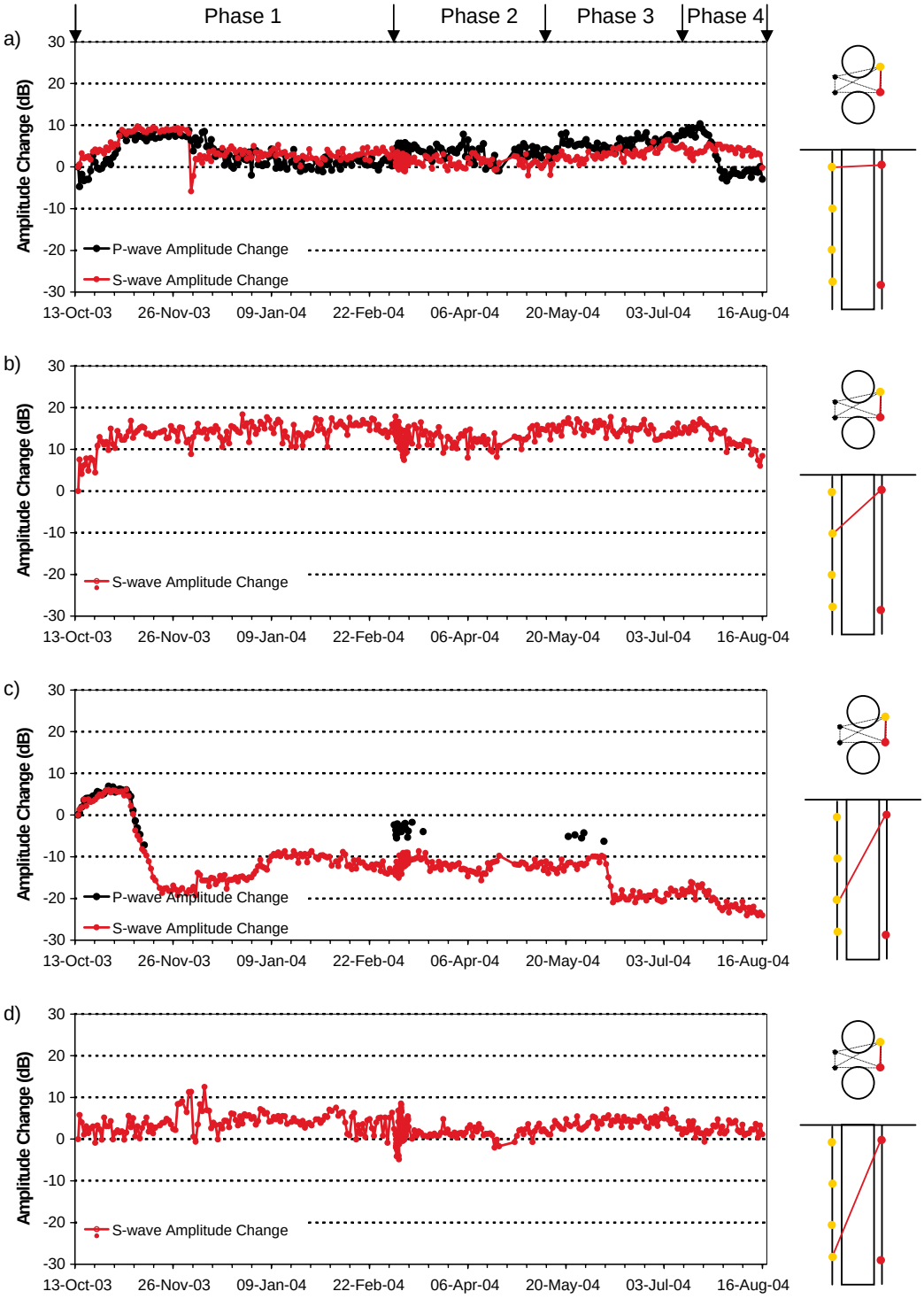

Boreholes KQ0064G03 and KQ0066G01 **a)** t_n=1, r_n=13; **b)** t_n=1, r_n=14; **c)** t_n=1, r_n=15; **d)** t_n=1, r_n=16

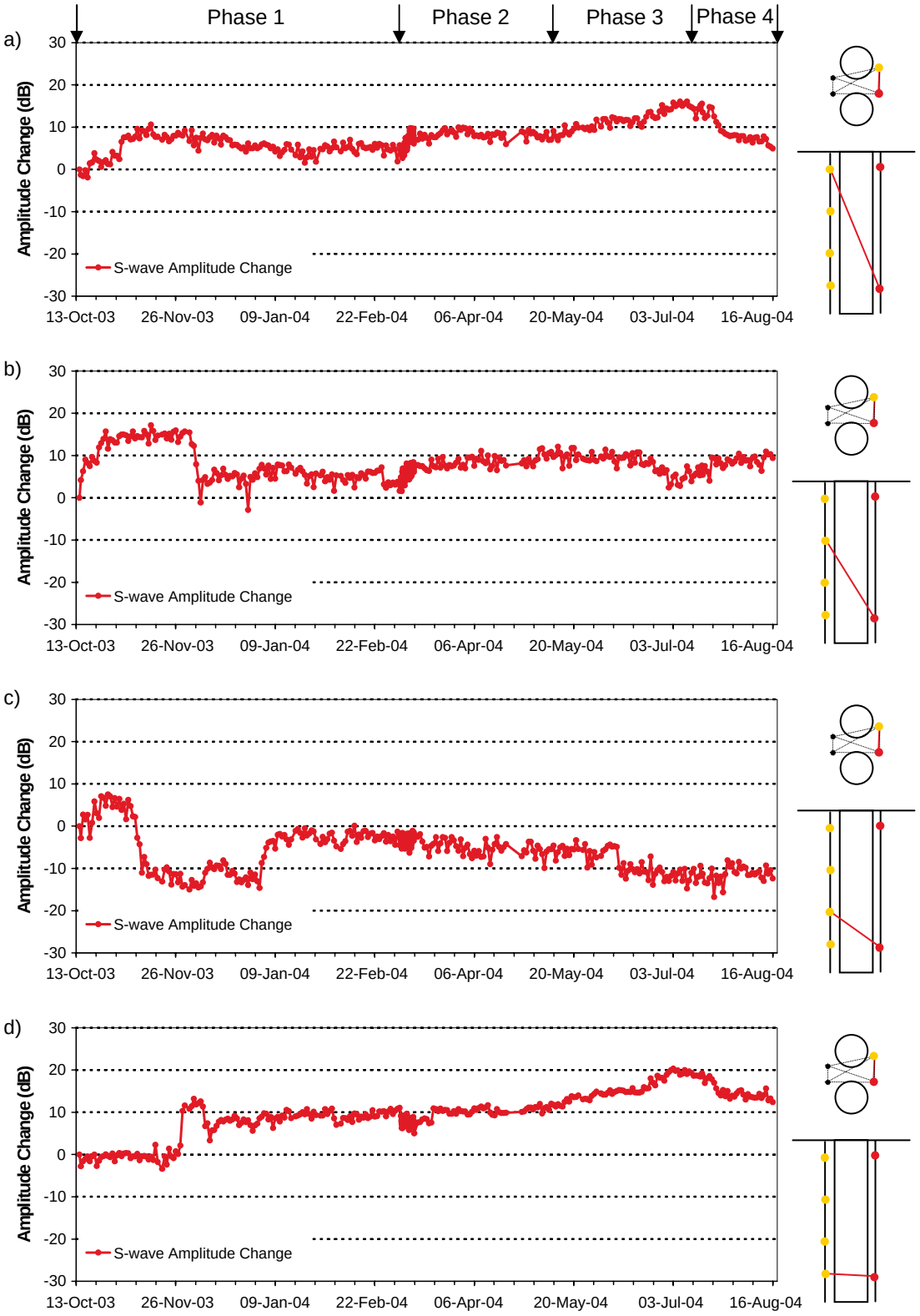

Boreholes KQ0064G03 and KQ0066G01 **a)** t_n=2, r_n=13; **b)** t_n=2, r_n=14; **c)** t_n=2, r_n=15; **d)** t_n=2, r_n=16

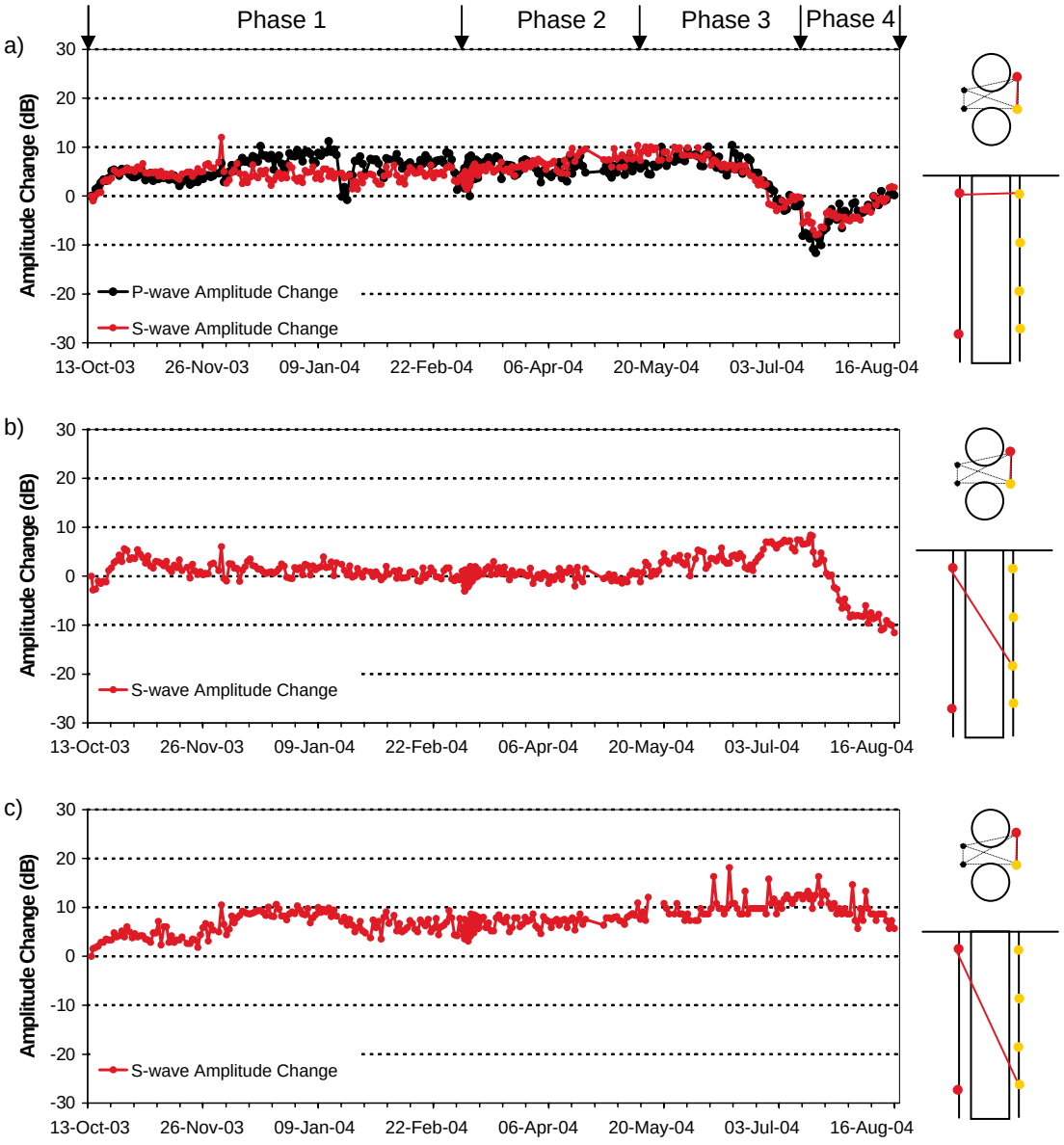

Boreholes KQ0064G03 and KQ0066G01 **a)** t_n=7, r_n=1; **b)** t_n=7, r_n=3; **c)** t_n=7, r_n=4

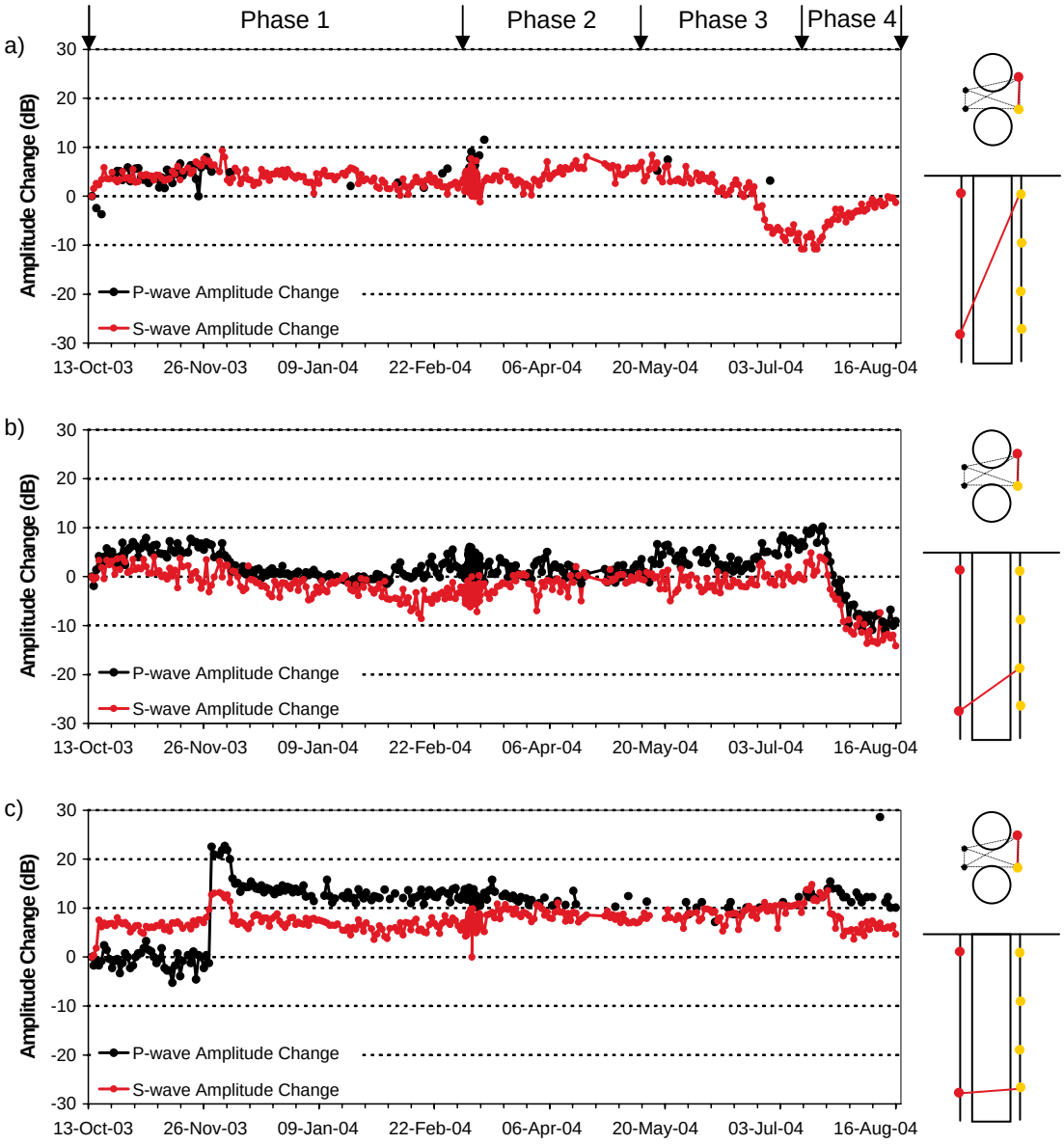

Boreholes KQ0064G03 and KQ0066G01 **a)** t_n=8, r_n=1; **b)** t_n=8, r_n=3; **c)** t_n=8, r_n=4

D: South east of pillar

P- and S-wave amplitude change graphs from 13 October 2003 are displayed in the following appendices. Amplitude change is measured in decibels (dB), which is not effected by raypath length, orientation or coupling of sensors. This allows amplitude variation of different raypaths to be compared on the same plot. Raypaths shown are for a transmitter, t_n, to receivers, r_n, with increasing depth. The schematic diagram in the right margin indicates the relative locations of the transmitter (red) and receivers (gold). The graphs are split up into raypaths on pairs of boreholes.

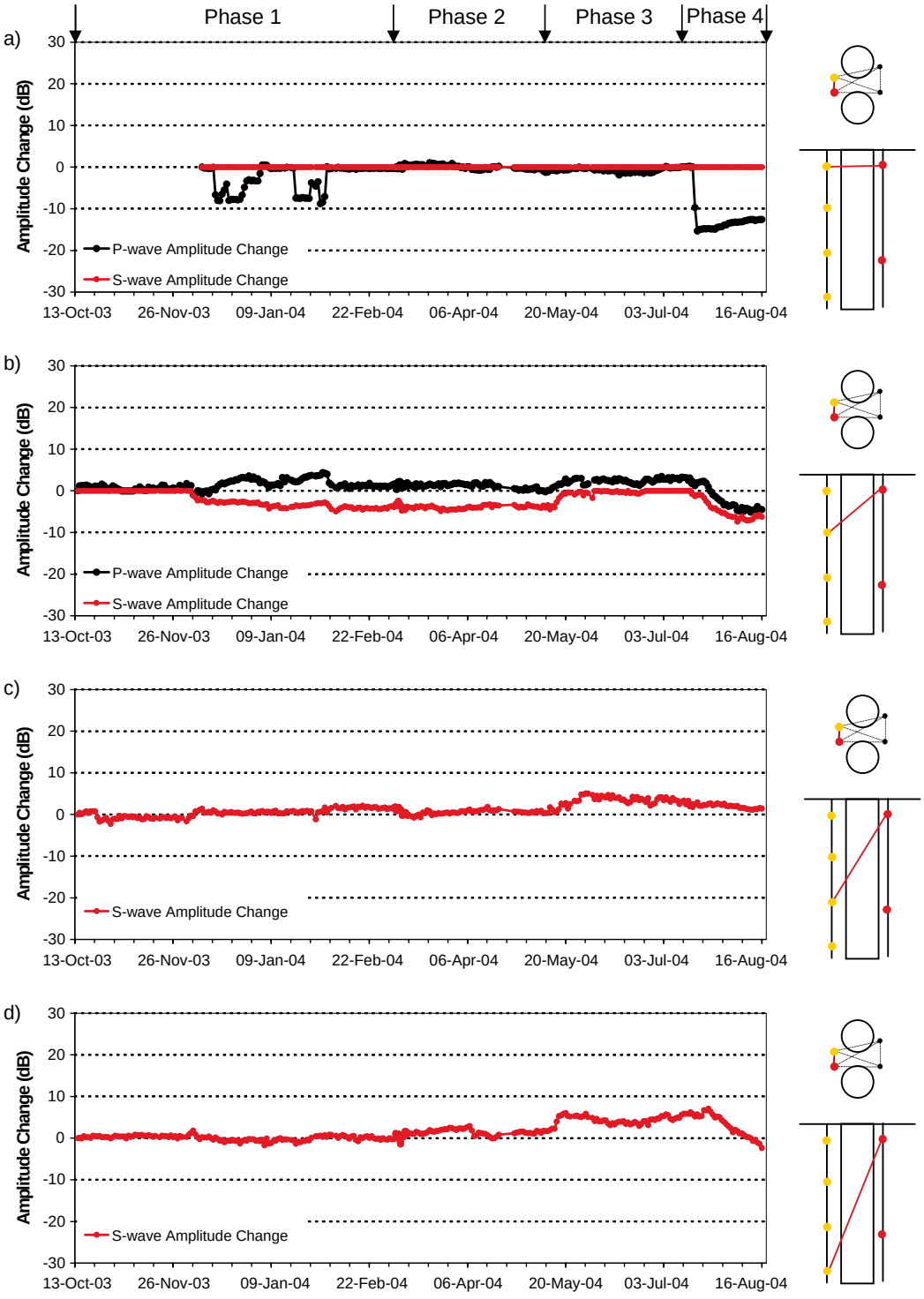

Boreholes KQ0064G02 and KQ0065G04 **a)** t_n=3, r_n=9; **b)** t_n=3, r_n=10; **c)** t_n=3, r_n=11; **d)** t_n=3, r_n=12

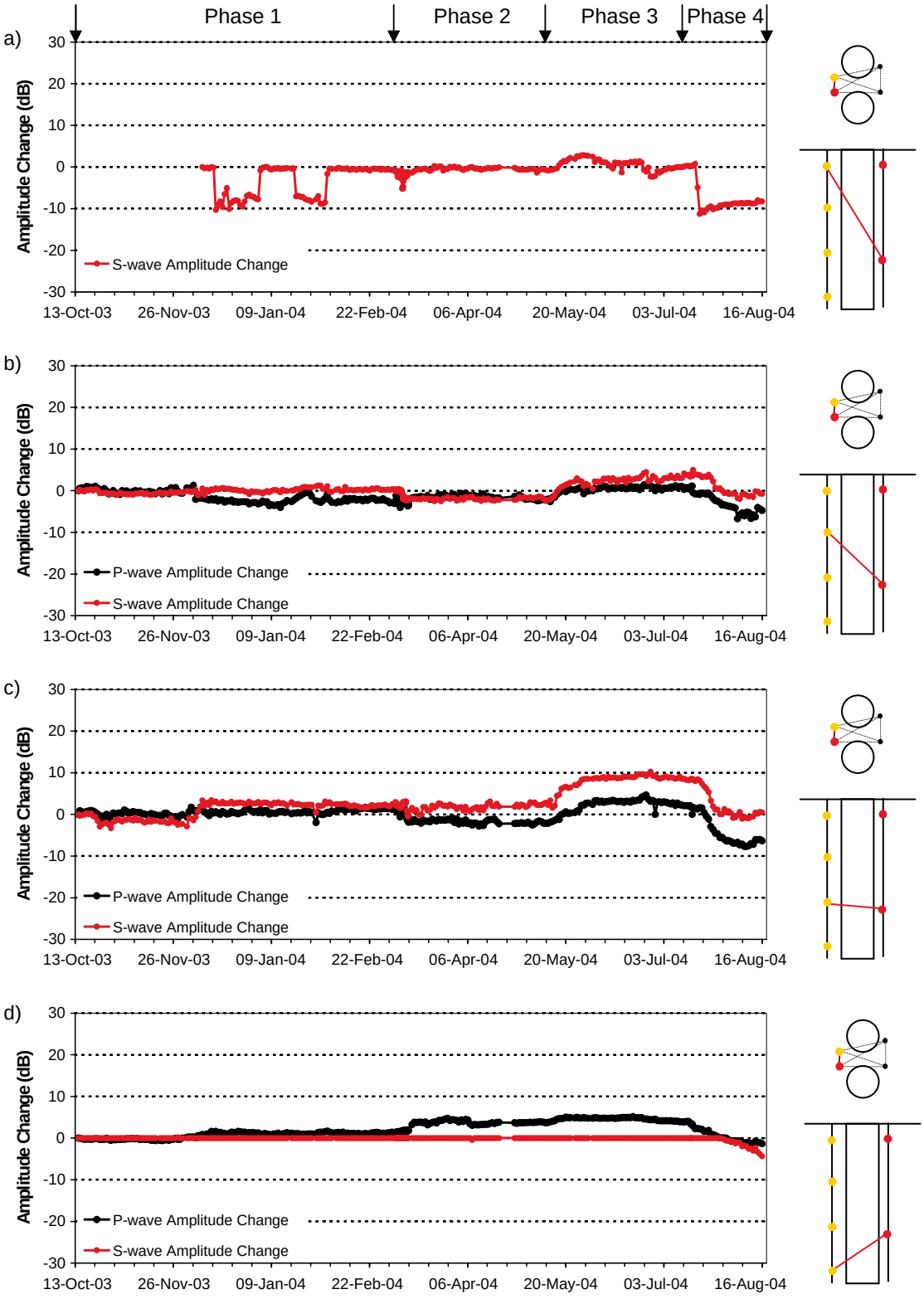

Boreholes KQ0064G02 and KQ0065G04 **a)** t_n=4, r_n=9; **b)** t_n=4, r_n=10; **c)** t_n=4, r_n=11; **d)** t_n=4, r_n=12

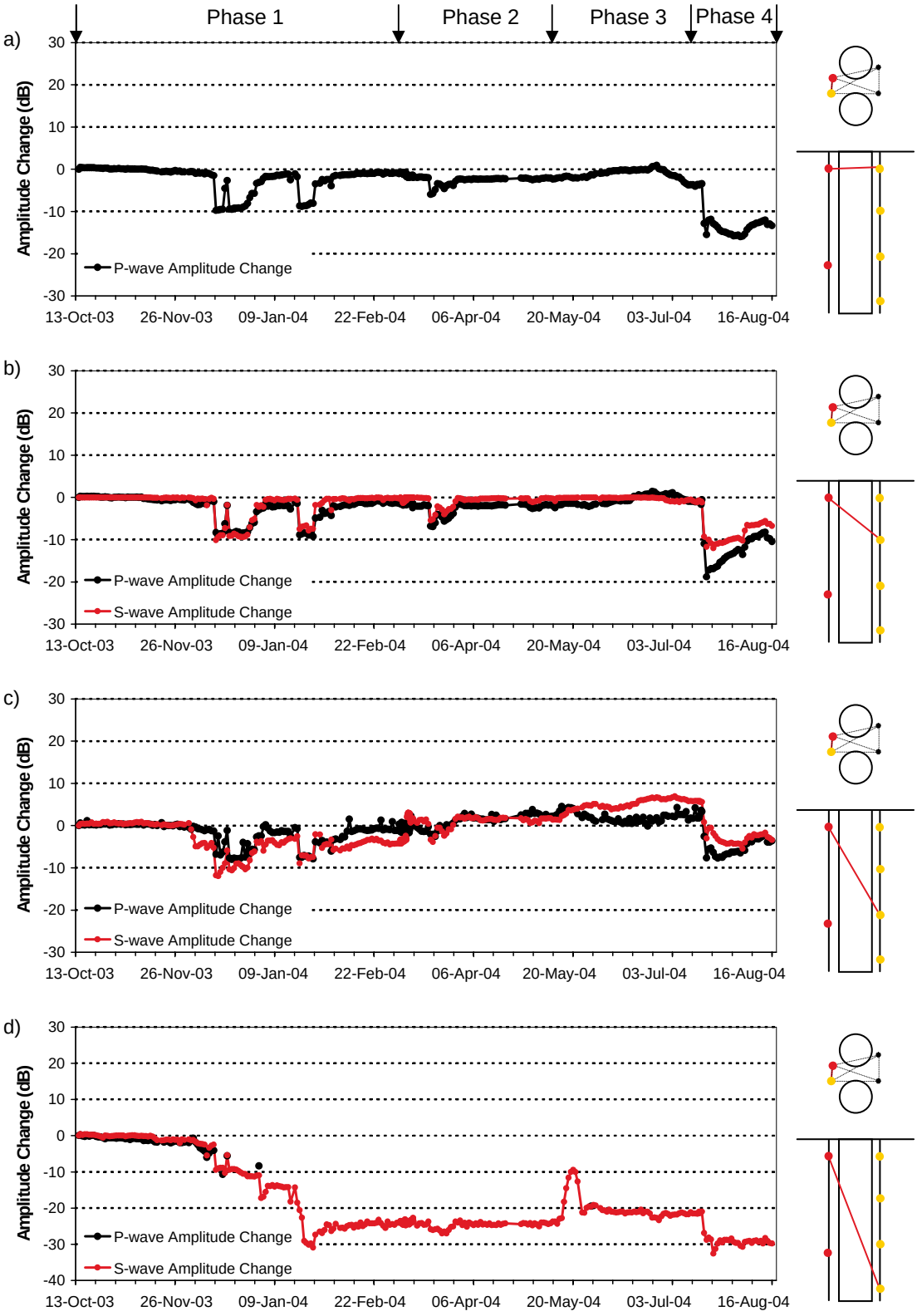

Boreholes KQ0064G02 and KQ0065G04 **a)** t_n=5, r_n=5; **b)** t_n=5, r_n=6; **c)** t_n=5, r_n=7; **d)** t_n=5, r_n=8

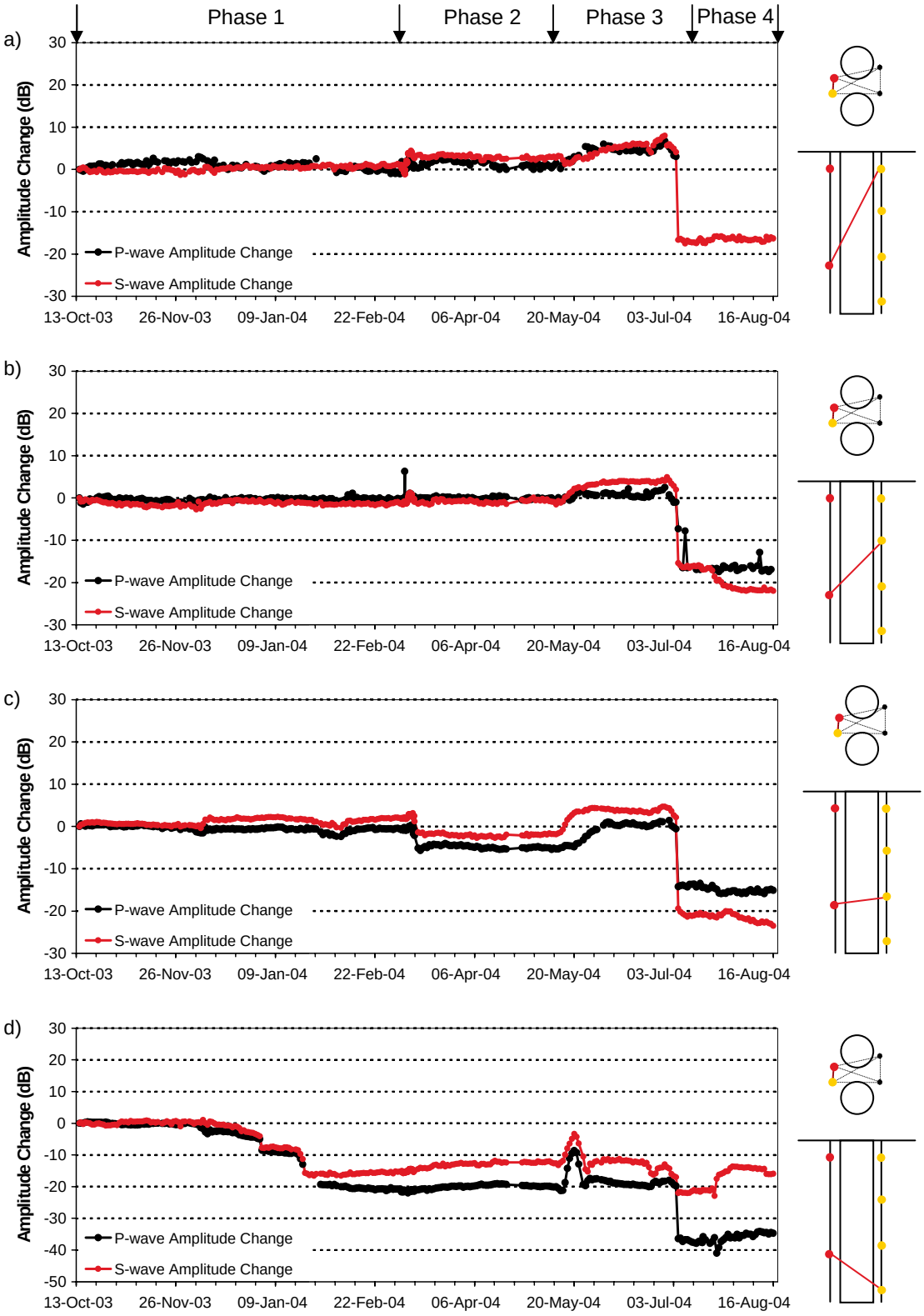

Boreholes KQ0064G02 and KQ0065G04 **a)** t_n=6, r_n=5; **b)** t_n=6, r_n=6; **c)** t_n=6, r_n=7; **d)** t_n=6, r_n=8

E: Skimming deposition hole DQ0066G01

P- and S-wave amplitude change graphs from 13 October 2003 are displayed in the following appendices. Amplitude change is measured in decibels (dB), which is not effected by raypath length, orientation or coupling of sensors. This allows amplitude variation of different raypaths to be compared on the same plot. Raypaths shown are for a transmitter, t_n, to receivers, r_n, with increasing depth. The schematic diagram in the right margin indicates the relative locations of the transmitter (red) and receivers (gold). The graphs are split up into raypaths on pairs of boreholes.

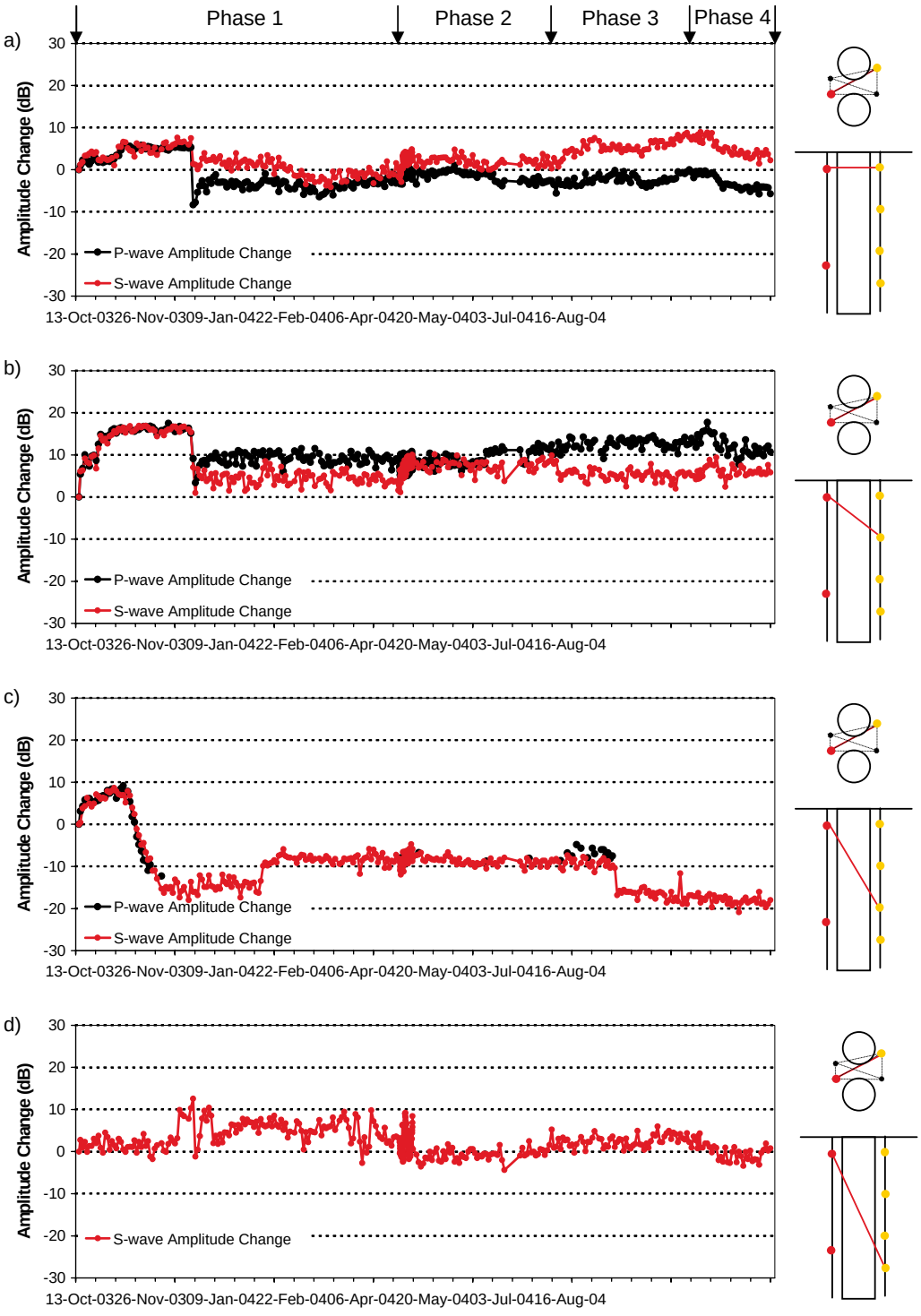

Boreholes KQ0064G02 and KQ0066G01 **a)** t_n=3, r_n=13; **b)** t_n=3, r_n=14; **c)** t_n=3, r_n=15; **d)** t_n=3, r_n=16

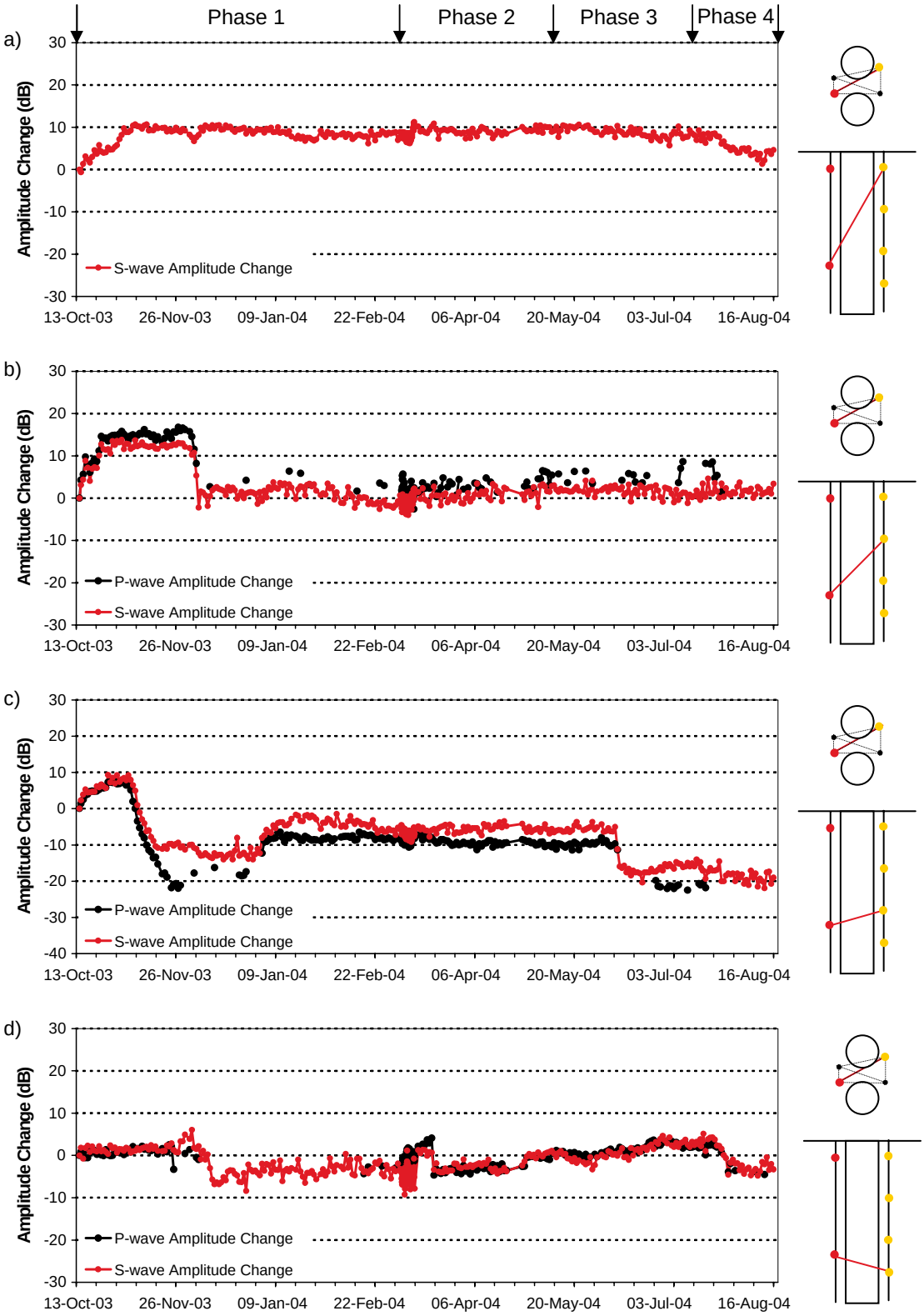

Boreholes KQ0064G02 and KQ0066G01 **a)** t_n=4, r_n=13; **b)** t_n=4, r_n=14; **c)** t_n=4, r_n=15; **d)** t_n=4, r_n=16

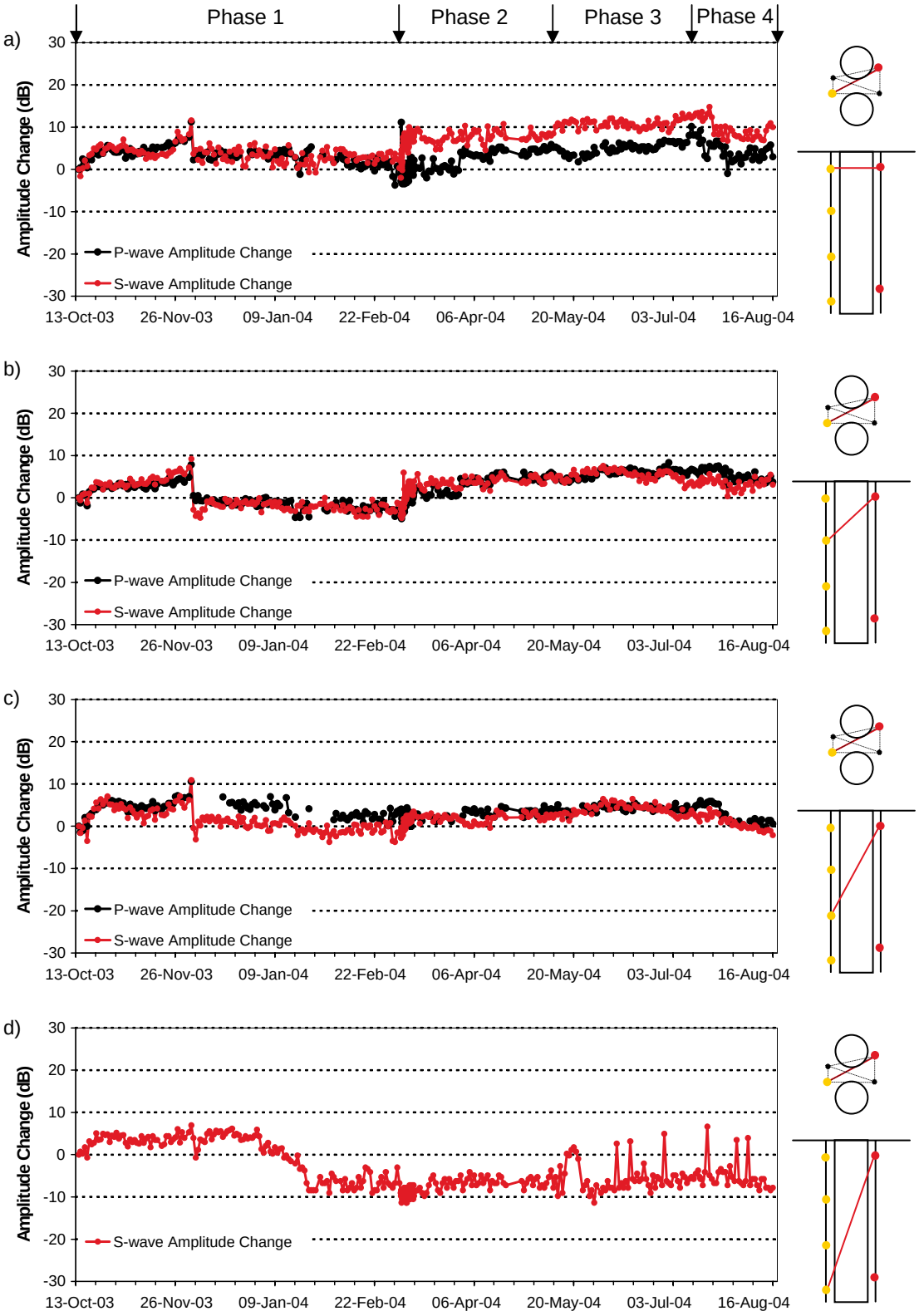

Boreholes KQ0064G02 and KQ0066G01 **a)** t_n=7, r_n=5; **b)** t_n=7, r_n=6; **c)** t_n=7, r_n=7; **d)** t_n=7, r_n=8

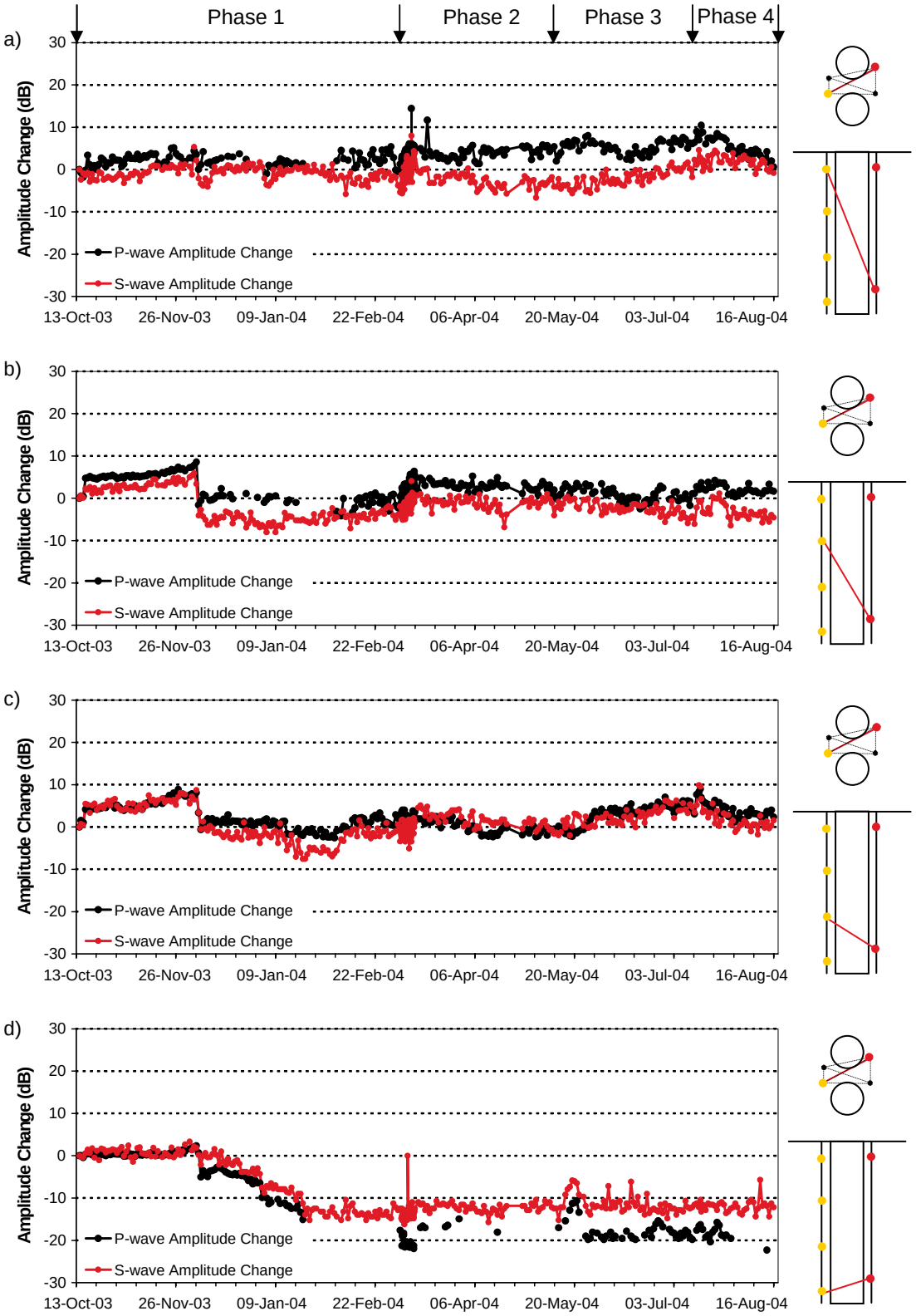

Boreholes KQ0064G02 and KQ0066G01 **a)** t_n=8, r_n=5; **b)** t_n=8, r_n=6; **c)** t_n=8, r_n=7; **d)** t_n=8, r_n=8